Process Control and Instrumentation Methods for Biomass Fluidized Bed Gasifier Operation

A Thesis Submitted to the College of Graduate Studies and Research

in Partial Fulfillment of the Requirements for the Degree of

Master of Science

in the Department of

Agricultural and Bioresource Engineering

University of Saskatchewan

Saskatoon, Saskatchewan

By

William Allan Campbell P.ENG.

PERMISSION TO USE

In presenting this thesis in partial fulfillment of the requirements for a Postgraduate degree from the University of Saskatchewan, I agree that the Libraries of this University may make it freely available for inspection. I further agree that permission for copying of this thesis/dissertation in any manner, in whole or in part, for scholarly purposes may be granted by the professor or professors who supervised my thesis/dissertation work or, in their absence, by the Head of the Department or the Dean of the College in which my thesis work was done. It is understood that any copying or publication or use of this thesis/dissertation or parts thereof for financial gain shall not be allowed without my written permission. It is also understood that due recognition shall be given to me and to the University of Saskatchewan in any scholarly use which may be made of any material in my thesis/dissertation.

DISCLAIMER

Reference in this thesis/dissertation to any specific commercial products, process, or service by trade name, trademark, manufacturer, or otherwise, does not constitute or imply its endorsement, recommendation, or favoring by the University of Saskatchewan. The views and opinions of the author expressed herein do not state or reflect those of the University of Saskatchewan, and shall not be used for advertising or product endorsement purposes.

Requests for permission to copy or to make other uses of materials in this thesis/dissertation in whole or part should be addressed to:

Head of the Department of Agricultural & Bioresource Engineering
College of Engineering
University of Saskatchewan
57 Campus Drive
Saskatoon, Saskatchewan, Canada
S7N 5A2

ABSTRACT

A fluidized bed gasification (FBG) pilot plant was designed and constructed at the University of Saskatchewan Chemical Engineering Department Fluidization Laboratory. FBG is a thermo-chemical method for converting solid biomass to a gaseous fuel, termed syngas. Several instrumentation and control issues were particularly challenging with this pilot plant, including development of the fuel feeding system, pressure measurement of high temperature fluids, and metering of steam as a process reactant.

The fuel feeding system was tested using MBM (meat and bone meal) to determine the output rate stability, and predictability and measurability of the system as the components in the fuel feeding system were integrated. The fuel feeding system that was tested included a 150 mm primary metering screw conveyor, a 150 mm rotary airlock, and a 50 mm secondary injection screw conveyor. Each component of the system was fitted with a 3-phase electric motor and a variable speed drive to allow for a variable output rate. The weighing system that was integral to the metering conveyor was tested as well, but upon pressurizing the metering conveyor and hopper, the weighing system sustained an unreasonable amount of noise. Integrating a pneumatic injection nozzle with the injection conveyor was found to work effectively both under ambient temperatures and hot FBG conditions up to 725^{o}C. Above 725^{o}C, it was found that the test fuel would char and coat the nozzle, causing it to plug. Testing of the feeding system with the injection nozzle removed illustrated that the system could work well without it. It was determined that the injection conveyor speed to metering conveyor speed ratio that should be used for this system was 1:110 for absolute rotational speeds, or 1:1 of the full conveyor speeds. The complete system, including the injection nozzle, was analyzed and determined to produce a fuel output rate (FS) for % speeds from 5-25%, which roughly corresponded to the desired plant fuel feed rate of 1-5 g/s.

Techniques for remote pressure measurement of fluidized beds were examined as well, including the use of long tubes to cool hot gases and filters for blocking solid particles. The pressure measurement delay of these techniques was examined in comparison to a direct local measurement. This was conducted by comparing the pressure readings from two

identical sensors; one mounted directly to a manifold, and the other mounted via a variable assembly (comprised of a variable length of 6.35 mm (1/4") PE tubing and a porous plate filter). Assemblies without a porous plate were found to have a minimal delay of up to 0.303 seconds for 30 m length of PE impulse tubing. More significant delays were found for systems using both a 10 media grade porous plate filter and impulse tubing; a 3 m tube length with filter has a delay of up to 0.221 s, and a 30 m impulse tube combined with the filter has a measurement delay of up to 1.915 s, a significant delay in cases where high-frequency analysis of pressure is used for bed agglomeration prediction, or systems where fast response is required to changing pressure conditions.

Additionally, a steam flow measurement system using an orifice plate and differential pressure sensor was installed and calibrated. By collecting time-based steam samples and process data, the physical system coefficients were determined for this system, allowing for steam flow measurement, accurate within 5% over a flow range of 0.5 to 2.0 g/s.

ACKNOWLEDGEMENTS

I would like to state my appreciation to the Government of Saskatchewan Ministry of Agriculture and Food, as well as Nexen INC. for the funding provided to the fluidized bed gasification pilot plant, upon which my research was based.

I would also like to thank Dr. Todd Pugsley, Dr. Terry Fonstad and Dr. Ajay Dalai for involving me with this project, and providing me with this excellent work and learning opportunity.

I would also like to thank Dr. Zhiguo Wang and Regan Gerspacher, whom I worked with on the FBG pilot plant project, for all of the help provided in procuring and setting up equipment, as well as commissioning the plant and for the great deal of help from Regan in collecting much of the data presented and analyzed here.

I would also like to thank Randy Lorenz, Louis Roth and Mike Miller, all with the Dept. of Ag/Bio Shops, who procured and fabricated the fuel feeding system components for the pilot plant, and a major component of the subject matter presented here.

I would like to thank Bruce King at Saskatoon Processing Co. for supplying samples of both cracklings and MBM for system testing and plant operation.

I would also like to thank Elizabeth Gusta, who assisted with review and editing of this thesis.

I would also like to thank my GAC committee, Dr. Scott Noble, Dr. Huiquing Guo (Chair), Dr. Terry Fonstad, and also Dr. Satya Panagrahi, who stood in as Chair while Dr. Guo was on sabbatical. Thanks to all committee members for their past and continuing support and assistance with meeting my research goals and deadlines, and for their technical and procedural advice.

And finally, special thanks to my advisor, Dr. Terry Fonstad for helping me to pursue my interest in bioenergy research, providing me with an exciting project to work on, continued financial support throughout, and his invaluable assistance with all aspects of my graduate education.

DEDICATION

To my wife and partner,

Joanna Smith

TABLE OF CONTENTS

LIST OF TABLES

LIST OF FIGURES

MAIN ABBREVIATIONS

FBG	fluidized bed gasifier (or gasification)
MBM	meat and bone meal
SRM	specified risk material
kW	kilowatts
kPa	kilopascals
kPaa	kilopascals (absolute)
kPag	kilopascals (gage)
PPH	pounds per hour
lpm	liters per minute
PE	polyethylene
Pa	Pascals
kg	kilograms
s	seconds
min	minute
g/s	grams/second

LIST OF SYMBOLS

β	Diameter ratio
ε	Expansion factor
ρ	gas density
C	Discharge coefficient
q_m	gas mass flow-rate
Cv	Valve coefficient (liquid)
Cg	Valve coefficient (gas)

LIST OF FORMULAE

1.0 INTRODUCTION

Fluidized bed gasification (FBG) is a thermo-chemical process for efficiently converting bulk solid or liquid organic feedstocks to syngas, a combustible gas mixture which can be used as fuel for electricity and heat production (Mckendry, 2002). In simple terms, gasification is the thermal decomposition of large complex molecules (hydrocarbons, lignin, cellulose, protein and fats) to produce high heating value gases such as hydrogen (H_2) and methane (CH_4), and the lower heating value gas carbon monoxide (CO) (Mckendry, 2002). This syngas can be used to replace natural gas in certain applications (Prenma, 2008), potentially decreasing feedstock costs and net CO_2 emissions (if renewable fuels are used to produce the syngas). Energy production from organic, residual, and renewable sources is a growing and evolving field, and FBG is a very active area of research for development of 'green' energy infrastructure. It was as part of the overall goal of developing this technology for use in Saskatchewan, Saskatoon in particular, that a FBG pilot plant was designed and constructed at the University of Saskatchewan to examine gasification of biomass and meat and bone meal (MBM). This follows the work done at other universities, including Iowa State University examining switchgrass gasification (Smeenk et al, 2002), University of Utah's work with black liquor gasification (Whitty et al, 2005), and the University of Seville's work with co-gasification of Orujillo (olive oil processing residue) and MBM (Gomez-Barea et al, 2006). The work herein explores the process of designing, testing and operating three key process control and instrumentation systems for the University of Saskatchewan pilot plant.

Gaseous fuels are much easier to work with and can be used to produce electricity and heat with much higher efficiency than solid fuels. In part this is due to the higher energy density (by mass) of gaseous fuels: for example methane has 55.7 Mj/kg (Dorin et al, 1987) energy density vs. 24 Mj/kg for black coal (Woodgas.com, 2010). As well, deriving mechanical and electrical energy from gaseous fuels is generally more efficient than from solid fuels, due the fewer number of stages (process/phase changes) required to convert the fuel to electrical energy. It is theoretically possible to design a gasification-incorporating electrical generating plant that could economically achieve up to 52% electrical efficiency, as compared to less than 40% efficiency for a conventional coal-fired thermal combustion power plant (Basu, 2006). Additionally, where FBG

can be applied to combined heat and power plants, efficiencies as high as 70-80% overall can be achieved (DOE, 2009). Application of this technology to replace fossil fuels with biomass is also of interest because of the potential to reduce greenhouse gas emissions from electrical generation (Klimantos, 2009).

Gasification is achieved through thermal cracking (pyrolysis) of the carbonaceous material to release volatile organic compounds, which then undergo partial oxidation with a source of oxygen such as gaseous O_2, or steam (Wang, 2008). Partial oxidation is achieved by maintaining a gaseous medium which has only 20-30% of the oxygen required for complete combustion. At this combustion rate, the heat generated can sustain the gasification reactions, yet still produce a gas with significant heating value.

Fluidized bed gasification (FBG) is a specific implementation of gasification, in which the reactions occur in a composite medium of both solid and gaseous matter. The medium is typically comprised of small solid particles such as sand, and a stream of gas, containing oxygen or steam which is injected into the sand from below (through a distributor plate), such that the sand particles take on the behavior of a fluid (Basu, 2006). The distributor plate acts to retain the bed particles when the reactor is inactive, and also provides a balanced distribution of gas through the particle bed when in operation. The gas/solid mixture is heated by combustion of natural gas or other gas/liquid fuel, or external electrical heating. Once gasification temperatures are reached, fuel is then added to the hot fluidized bed. A simplified illustration of this method is shown in Figure 1. The benefit of this type of gasification is the improved heat distribution through the fluid bed vs. other gasifier types, resulting in more consistent temperature, thus greater predictability and controllability of the reaction profile. The product gases that are extracted from an FBG contain some quantity of solid particles (fuel ash & bed particles), as well as tars (large complex hydrocarbons) and inert gases, in the case of air-blown gasification. Once the solids and tars are removed from the gas stream, the produced gas can then be used in a similar fashion to natural gas, as fuel for an internal combustion engine, gas turbine engine, or gas heater (Basu, 2006).

Depending upon the carbon and water content of the utilized fuel, gasification can generally

produce enough thermal energy to maintain its reactions (isothermal operation). This makes gasification generally an efficient process for converting solid fuel to gaseous fuel, with cold gas efficiency of up to 89% [Basu, 2006]. Further upgrading of this gas, through removal of nitrogen and/or carbon dioxide, further increases the energy density of the gas, increasing its HHV and its fuel value.

Efficient operation of fluidized bed gasification systems requires that operational conditions be closely and accurately measured, and that inputs to the system be effectively controlled.

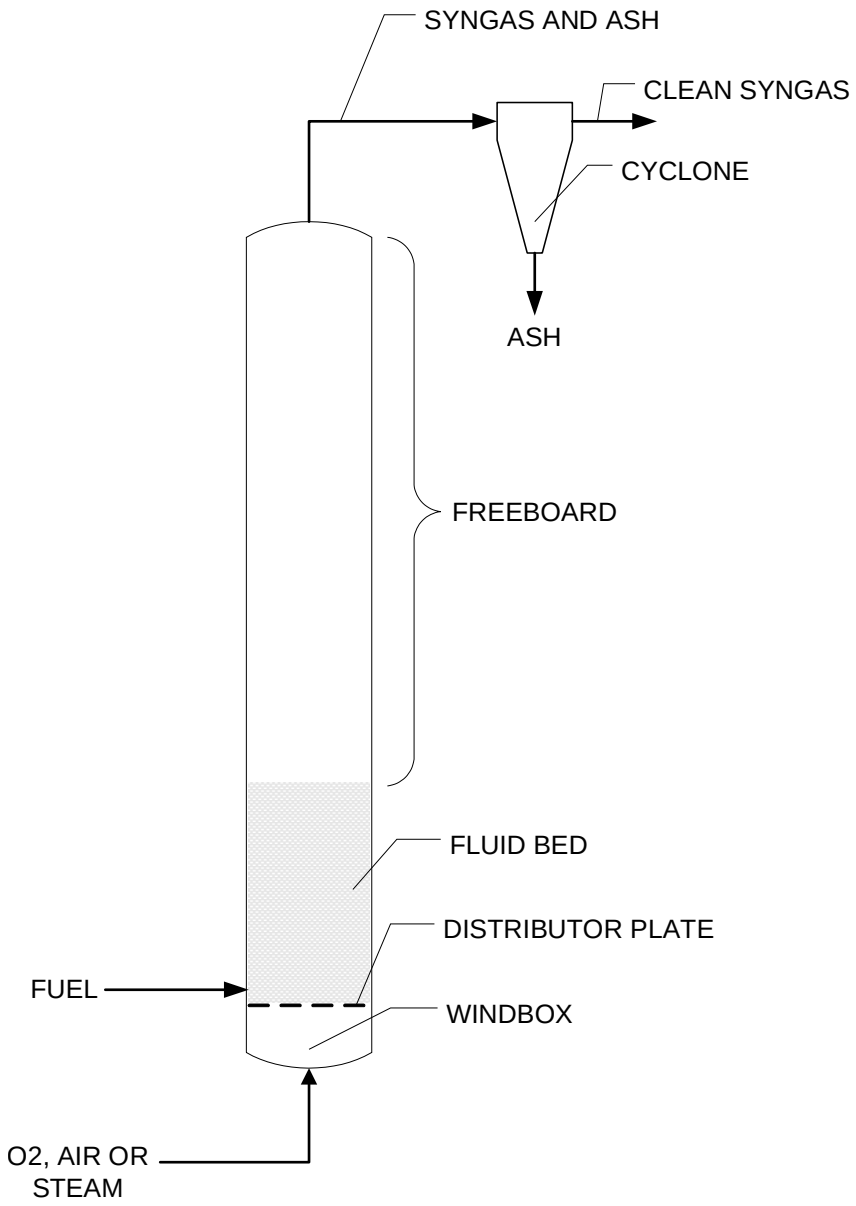

Figure 1: Simplified FBG schematic

Fluidized bed system conditions which are important to monitor and control include fuel feed flowrate and oxidizing medium flowrate, which can include air, oxygen, or steam. Reactor pressure values are also important, including distributor pressure drop, static bed pressure, and bed pressure drop. Measurement and analysis of the bed pressure drop can provide insight as to how fluidized the bed is, also known as the bed regime.

A fluidized bed gasification pilot plant was designed and constructed for the University of Saskatchewan Chemical Engineering department. This pilot plant was funded by the Ministry of Agriculture, Government of Saskatchewan, as well as Nexen Inc. A primary goal of this FBG pilot plant was to examine the potential for meat and bone meal (MBM) as a fuel for a commercial scale FBG unit. The reason for this particular focus was that a specific class of MBM, termed specified risk material (SRM) was in 2007 (CFIA, 2010) deemed to be unsafe for industrial or agricultural purposes. This was due to the understanding that this class of material was most at risk for carrying prions, the protein believed responsible for the spread of bovine spongiform encephalopathy (BSE), also known as “mad cow disease”. MBM is a valuable solid byproduct of rendering, the process of separating tallow (fat) from the inedible/low value parts of animals. MBM, though of less value than tallow, still was considered to be a valuable material due to its high protein content (as much as 50%), making it an attractive feed additive for the growing of livestock for meat, as an enriched protein diet will cause such stock to grow faster, and thus be ready for slaughter sooner. The recent outbreak of this disease in Canada in 2003 led to a re-examination of the practice of using MBM as feed for agricultural production, resulting in a ban on feeding proteins derived from most mammals to ruminant animals such as cattle, sheep and elk, and a total ban on the use of SRM in any feed products (CFIA, 2009).

SRM includes parts of ruminants including the brain, skull, and spinal column among others. Gasification is an attractive option for dealing with SRM, as it can both convert this waste material to a gaseous fuel, and submit it to the requisite temperature of 850°C (believed to destroy the prion pathogens), as required by the Canadian Food Inspection Agency (CFIA) for thermal treatment of this material (CFIA, 2010). MBM does pose some difficulty for its use a fuel source, however, as it can be sticky when heated due to its high fat content, and has significant ash when combusted due to the calcium, potassium and phosphorous from the bone

component of its makeup. In using this fuel with the pilot plant, this ash is retained in the fluidized bed until such time as the system is shutdown, and the entire mass of bed particles removed for filtration/replacement. Full scale FBG reactors generally have systems for continuous bed filtration, in order to maintain a consistent bed mass and avoid the difficulties associated with high retained ash content.

Several areas of control and instrumentation for this pilot plant posed significant challenges to its successful design and operation, those challenges being the subjects to be examined herein. Areas of focus will include three different process systems/parameters for FBG operation. These will include biomass fuel metering, high temperature fluidized bed pressure measurement, and steam metering for use as a reactant in FBG. The fundamental theory and developmental history of FBG and these specific systems will be examined next in order to provide a background of understanding for more detailed examination.

1.1 FBG PILOT PLANT DESIGN & CONSTRUCTION

The biomass FBG pilot plant that has been constructed at the University of Saskatchewan (U of S) department of Chemical Engineering was built in cooperation with the U of S department of Agricultural and Bioresource Engineering. Project originators and facilitators for the pilot plant included Dr. T. Pugsley, Dr. T. Fonstad, and Dr. A. Dalai. Process development, mechanical design and assembly were primarily the responsibility of Dr. Z. Wang, while electrical, instrumentation and automation design and installation were that of W. Campbell P.Eng. (Author). Fuel chemistry analysis and testing were completed by C. Soni, and plant operations and commissioning by R. Gerspacher.

1.2 PLANT DESCRIPTION

The pilot plant mechanical component schematic diagram is illustrated in Figure 2. This FBG converter consists of a 0.2 meter diameter, 6 meter high reaction column, to support a bubbling fluidized bed of approximately 0.3m height. The primary reactor components are constructed of Inconel 600, a nickel-based alloy which has higher tensile strength than stainless or carbon steel at higher temperatures up to (and above) 850°C (Ulrich, 2004), which is near the desired operating range for an efficient biomass gasifier (Basu, 2006).

The distributor plate, which disperses the fluidization air into the fluid bed, was fabricated from grade 10 Inconel porous-plate, and supported by an Inconel 600 rigid frame. The bed catalyst used in this case is ordinary sand. Steam is supplied from a dedicated 6kW electric steam generator (Figure 3) capable of supplying up to 7.2 kg/hour of steam at an adjustable pressure (temperature) from 200 to 600 kPa.

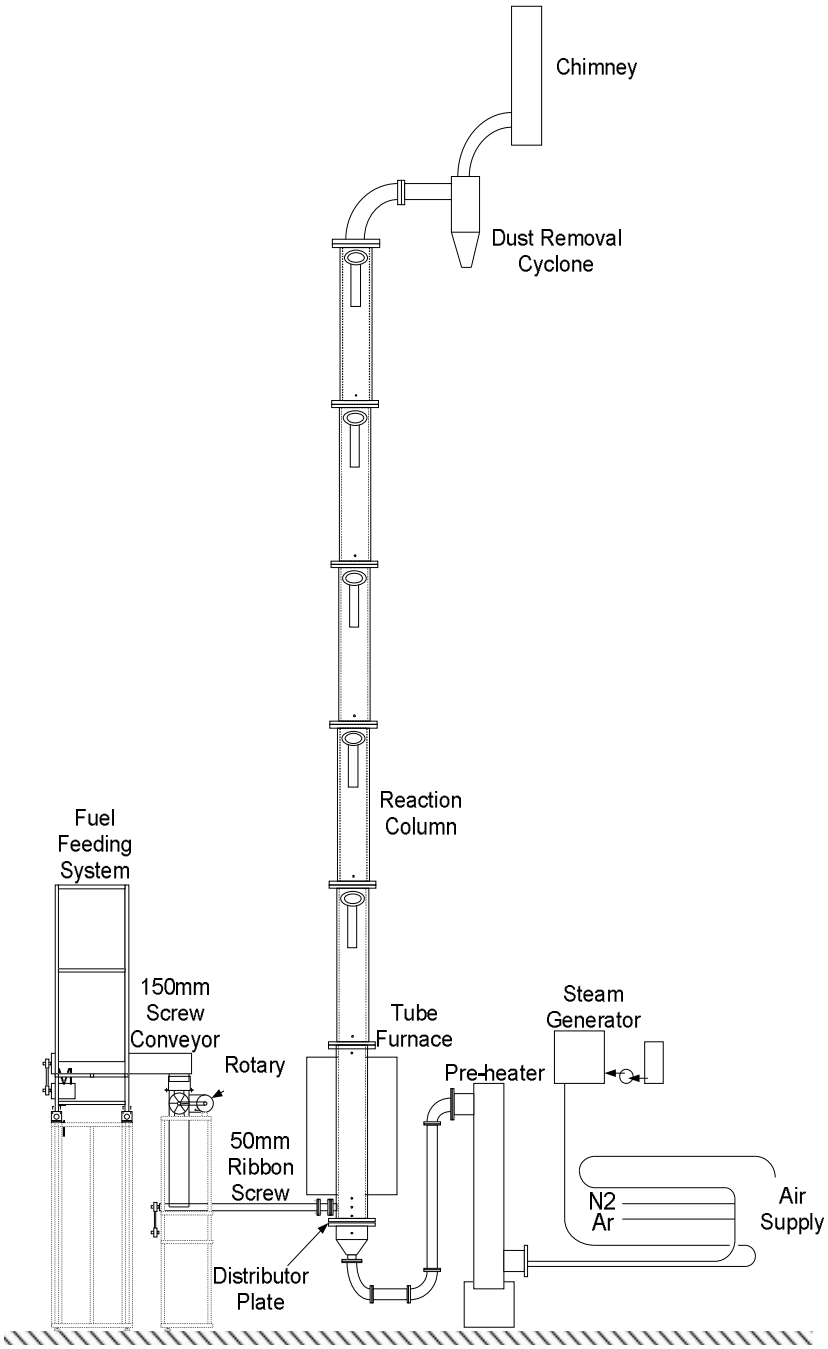

Figure 2: FBG pilot plant schematic

The fluidization gases, which may include varying quantities of air, steam, nitrogen, and argon, are preheated by an inline 90kW electric heater to temperatures of up to 500°C. They are then passed through the distributor to fluidize the particle bed, and provide oxidation media for the fuel.

Air is supplied from either the local building compressed air supply, or a dedicated compressor in the adjacent utility room. The fluidized bed mass can be pre-heated or continuously heated by a 24kW electric clamshell style tube furnace (Figure 4), up to as hot as 850 to 900°C.

Figure 3: FBG pilot plant steam generator.

Figure 4: FBG pilot plant fluid bed tube furnace and reactor

Biomass is injected laterally into the hot fluidized bed (at a rate of 1-5 g/s) at approximately 0.11 meters above the distributor plate, via the fuel conveying system. The conveying system consists of several stages, starting with a 150 mm diameter screw conveyor, drawing from a 0.15 m^3 hopper (Figure 5). Full speed of this conveyor is approximately 1.0 rpm. This conveyor discharges into a 150 mm rotary airlock, which has a full speed of 100 rpm. The airlock then

discharges into another hopper, with a volume of 0.01 m^3. This hopper feeds a 50 mm ribbon screw, with a full speed of 110 rpm. The entire fuel feeding system is indicated in Figure 6.

The 50 mm ribbon screw conveyor discharges into the FBG reactor at 0.11 m above the distributor plate. Backflow of the fluidized bed and gases is prevented by pressurization of the fuel feeding system slightly above the pressure of the fluidized bed. Each motor in the conveying system operates at 208VAC 3 phase 60Hz, operated by variable frequency drives, with each conveying system motor running at only a fraction of its full speed during plant operation.

Figure 5: FBG pilot plant fuel feeding system metering screw conveyor

Figure 6: FBG pilot plant fuel feeding system

Gases produced in the fluid bed pass upwards through the freeboard, and then through a cyclone, where ash and other heavy particles are separated from the gas stream. Gas sampling occurs via ports located above the cyclone (Figure 7), where manual samples can be drawn from the gas stream. The gas stream is then vented to atmosphere through a chimney (Figure 8) atop the building roof (produced gas is not retained).

Figure 7: FBG pilot plant chimney connection point and gas sample point

Figure 8: FBG pilot plant chimney

1.3 SUBJECT WORK OF PILOT PLANT

The work that was completed in conjunction with the construction of this pilot plant included the design and testing of several key mechanical and control systems. Included in this testing were the fuel feeding system, data acquisition system wiring panel, specification of several different instruments including the steam measurement and control system, implementation of various safety systems including emergency shutoff switches for heating systems and conveyors, and a high-temperature shutdown system. Figure A-1 (Appendix A) illustrates the major mechanical and control components, in the form of a P&ID diagram, a standard drawing for illustrating the physical and control connections within a processing plant. The command interface for the pilot plant was also developed, using National Instruments Labview 6.2. Access to fluidization gas volumetric flowrate measurement and control, steam system activation and flowrate control, fuel

feeding system activation and speed control were all integrated into the Labview computer interface.

The pilot plant control system included mass flow controllers for fluidization and injection gases, thermocouple probes for reactor temperature monitoring, and pressure sensors along the reactor. Gas sensors for combustible gases and CO are located in the vicinity of the system, to detect leaks in the reactor and discharge piping. All instruments are wired to a windows PC-based data acquisition system. The fluidization gas pre-heater and fluid bed clamshell heater (which surrounds the fluidized bed) both have temperature controllers, which measure the process temperature via thermocouple probe, and have an operator setpoint that can be input from the controller front panel. Both heater controllers can be activated or deactivated from the Labview Interface.

The primary interface screen is shown in Figure A-2 (Appendix A). This graphical interface attempts to illustrate the physical connections in the system, with material streams entering on the left, and exiting on the right, in standard PFD format (Ulrich, 2004). The reactor is shown at center, indicated as a tall column, comprised of six 1 meter sections, representing the physical construction of the reactor. On the left hand side of this interface screen, 4 boxes are shown to represent the gas mass-flow controllers, with actual flowrate, as well as the operating setpoint for each, which can be set from the Labview interface.

At the top of this operating screen, alarm setpoints (and bypasses) are available for each temperature sensor, pressure sensor, and gas sensor. When any of these alarm conditions is met, a system alarm indicator and audible alert are activated. This alert can be disabled through a "silence" button. The upper right of this screen also has indicators for the plant operator, to assist in starting equipment and achieving process setpoints in the correct order, to safeguard equipment. Start/stop controllers are available for fuel feeding system conveyors, steam generator, pre-heating and bed heater units. The rotational speeds for the 150 mm and 50 mm screw conveyors can also be set from this operating page, from 5-100%.

Electrical system design began with assessment of loads for the new 208VAC 3phase supply. This assessment is summarized is a single-line diagram, as shown in Figure 9. A single line diagram such as this illustrates the loads and breaker sizes on an electrical panel. The 208 VAC 3 phase Loads on this panel included the 24 kW fluid bed heater, fuel feeding system motors 0.19 kW (0.25 hp), 0.37 kW (0.5 hp), 0.75 kW (1.0 hp), and the steam generator (6 kW). 120 VAC single phase loads include data acquisition panel, relay panel, weight meter panel, high temperature interrupt panel, and steam controller. This diagram illustrates the complexity of simply supplying electricity, even to such a small pilot plant.

After the size of each electrical load was determined, in terms of its steady state current and breaker size, the location of each load in the plant (and the required cable length) was determined. This allowed for sizing of the feeder cables for each piece of equipment.
The cable information, as well as the wiring schematic for each major electrical load is indicated

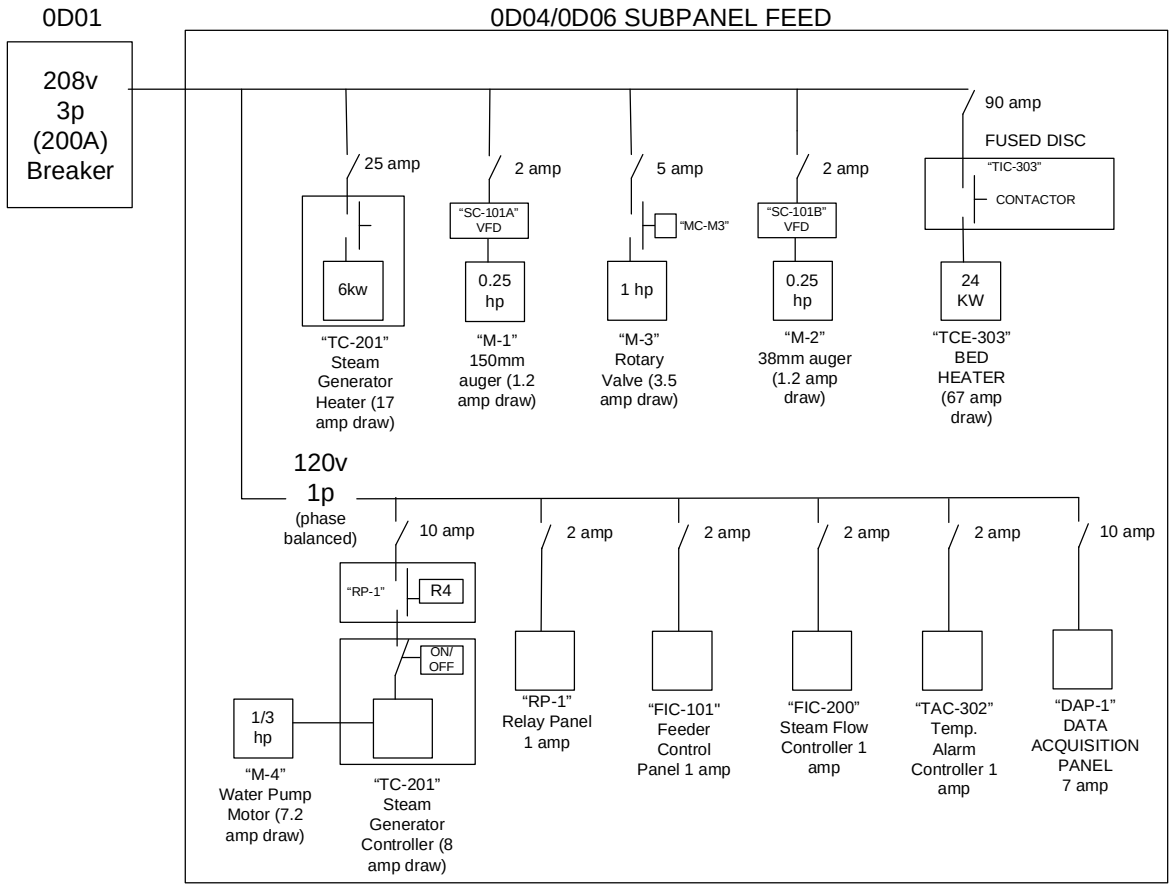

Figure 9: FBG pilot plant single line diagram

in a schematic and wiring diagram, such as Figure A-4 (Appendix A), which illustrates this information for the fluidized bed heater. The schematic, on the left hand side of the drawing, illustrates how the control equipment within the heater controller is integrated with the data acquisition and control system, and the other fail safe devices such as the high-temperature controller and emergency stop switches. The right-hand side of the diagram shows all cabling connecting the heater and controller to the power supply, and related control devices, as well as the wire gauge, and conductor quantity for each cable.

Instrument system design included wiring and schematic diagrams for thermocouples, mass flow controllers, pressure sensors, gas level monitors, load cells, and steam measurement and flow control system. For each of these devices, cabling was selected and purchased, and for some of the devices, DC power at specific levels was required, requiring purchase of 8V DC and 24V DC power supplies. A typical schematic is shown in Figure 10, illustrating the wiring for three of the mass flow controllers.

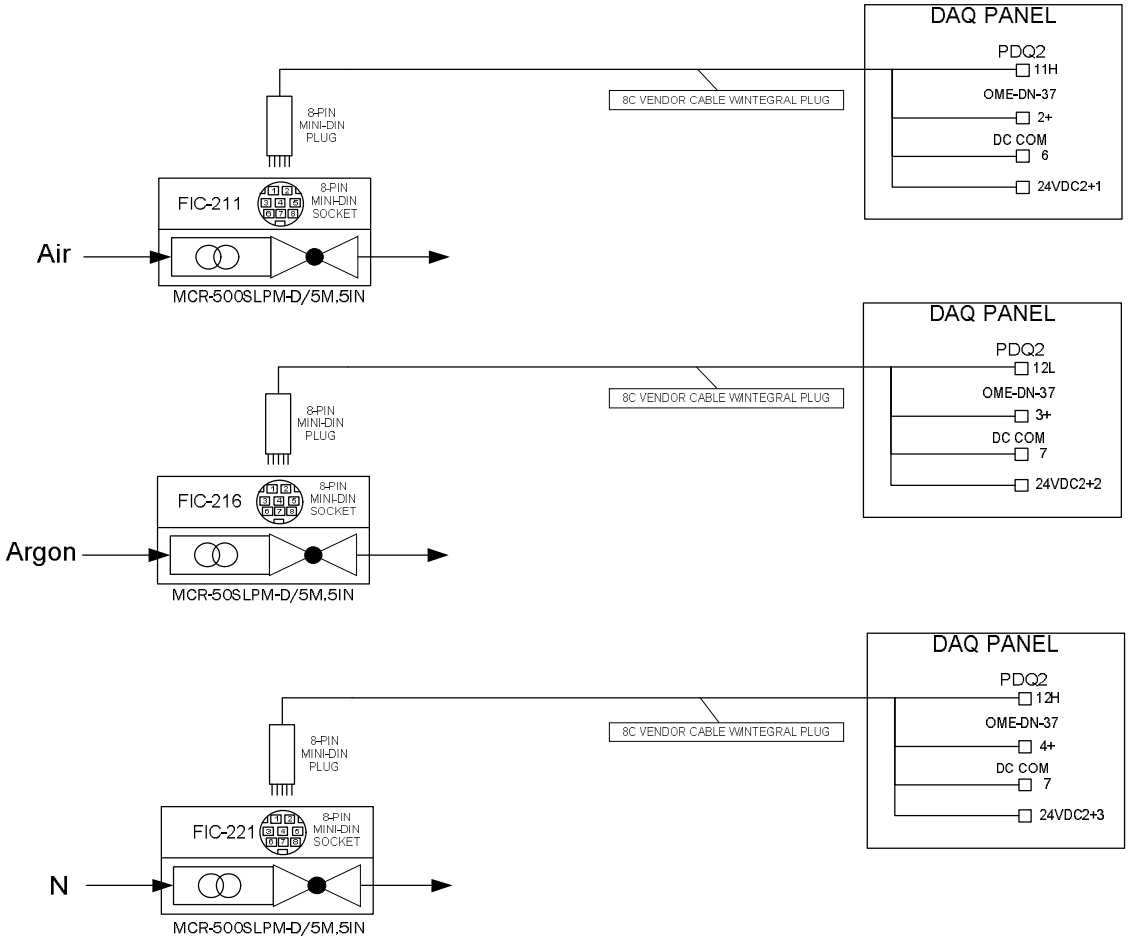

Figure 10. FBG pilot plant gas mass-flow controller loop diagrams

A steam generator was installed, for addition of H_2O to the gasification reaction, which could potentially increase the amount of hydrogen produced in the product syngas. A system for measurement and control of steam mass-flow was therefore purchased for this pilot plant, with the system components selected by the vendor based on the provided mass flowrate range, pressure and temperature. The system that was purchased included an orifice plate, an electronic differential pressure sensor for measurement of flow, and a Flowtek 13 mm ball valve with a 15 degree v-port for flow control. A process controller was also purchased separately, a Red Lion loop controller, with RS-485 communication capability. This controller communicates the orifice plate differential pressure (measured as a 4-20 mA current signal) to the data acquisition system through the RS-485 communication port. The control valve position setpoint from the Labview interface is received by the controller via this communication port as well, and transmits this value to the valve positioner (also as a 4-20 mA signal). The steam mass flow rate is proportional to the square root of the orifice pressure drop (in addition to other factors discussed later), with this calculation being performed by a Labview subroutine.

Setpoint deviation alarms were implemented for each of the gas mass-flow controllers. If the mass-flow controller was unable to achieve the setpoint within 5% of the actual flowrate, an audible and visual indicator would alert the operator that either that flowrate could not be supplied, or that the process conditions were limiting the flow.

The fuel feeding system for the pilot plant was designed partially based on previous work with MBM flow testing and partially based on the physical install location of the pilot plant and other factors. A mass flow measurement system was also designed into the feed system, and was evaluated during this testing as well. This system consisted of strain-gauge type load cells located under each support member of the 150 mm screw conveyor and hopper, connected to a weight transmitter, which transmits the feeder weight continuously to the data acquisition system. Mass flowrate of discharged fuel is calculated by the change in weight of the storage hopper/conveyor over time (rate of loss calculation).

All instruments and controllers were interconnected to the data acquisition desktop PC through a marshalling and acquisition panel, indicated in Figure 11.

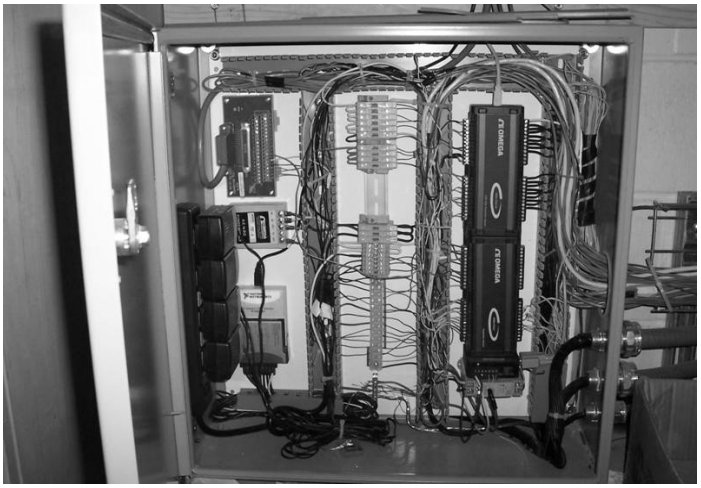

Figure 11. Data acquisition panel, installed

Three separate acquisition modules were connected to the Labview PC, with input module (Omega DAQ-56) for both analog and discrete inputs connected via USB, as well as USB Relay output module (National Instruments NI-9472), and PCI Card based analog output module (Omega OME-PIO-DA16).

Mass flow controllers were installed for each gas flow, with controllers installed for fluidization gas flowrate, injection air flowrate, fluidization Nitrogen (N_2), and fluidization Argon (Ar). The manifold which these controllers are installed within is indicated in Figure 12.

Figure 12. Gas supply manifold

1.4 OBJECTIVES

Three key problems encountered in design of the measuring and control systems for the FBG pilot plant were examined for this thesis. These were the fuel feeding system, pressure measurement of dusty, high temperature fluids, and steam flow measurement and control.

1.4.1 FBG FUEL FEEDING SYSTEM DESIGN AND EVALUATION

Difficulties with fuel feeding system design for a FBG are related to the high temperatures in the FBG reactor, as well as the need to contain and maintain the pressure of the fluidized bed. Control and measurement of the fuel flowrate is very important, to ensure that the fluidized bed does not receive too much or too little fuel; this rate must be carefully ratioed with the oxidization media provided to the fluidized bed. Feedrate control is particularly difficult for rates as slow as are required for this reactor, 1-5 g/s. Measurement of solids flow is also difficult. There are only a few methods available, and those are not easily implemented for such low flowrates. The design process of the fuel feeding system is examined here, as well as experimental evaluation of the operation of the feeding system, fuel output measurement system, conveyor speed control system, equipment synchronization, flowability, and output stability.

1.4.2 FBG PRESSURE MEASUREMENT

Pressure is a key measurement for control of fluidized bed gasification. Pressure measurement at various points in fluidized beds, including below and above the fluid media distributor plate and above the fluidized bed (Figure 13), can be used to calculate the air velocity and thus determine and confirm the fluidization regime for the fluidized bed (Basu, 2006).

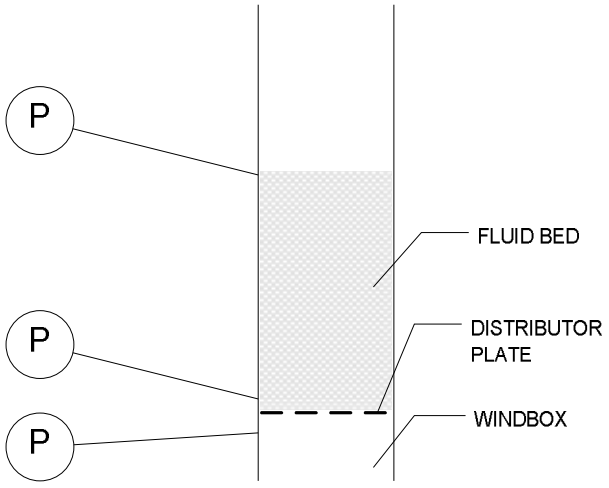

Figure 13: Typical FBG pressure sensor installation

Pressure measurement of the fluidized bed at high sample rates (>100Hz) can also be used to predict agglomeration conditions in the fluid bed. Procurement of pressure sensors which would meet the temperature range of this FBG was found to be difficult, however, with the highest temperature sensors having a limit of only 300°C, far below the FBG operating temp of 850°C. An examination of techniques for measuring high-temperature dusty fluids was therefore undertaken, with the simplest and easiest method found being sensor isolation using metallic tubing (which acts as a cooling fin) to reduce fluid temperatures to near-ambient temperatures (Kane, 2002), and the use of filter media to block dust particles from entering pressure measuring tubes and measuring devices. The principle area of investigation for these techniques was an assessment of the delay effect that these methods have upon the pressure sensor transmitting the correct pressure value to the data acquisition system.

1.4.3 STEAM FLOWRATE MEASUREMENT AND CONTROL

Control of fluidization gas flow is straightforward for air, as integral flowmeter/controllers can be purchased, such as the Alicat MCR series. However, measurement and control of steam for fluidization was found to be a more complex matter. Steam flow measurement requires a combination of multiple sensors, including pressure and temperature sensors, and installation-specific calibration procedures. A typical setup for steam flow measurement includes an orifice plate to create a pressure drop, a differential pressure sensor to measure that drop, as well as temperature and pressure sensors downstream of the orifice plate. The required steam flow rate must be known within a fairly close tolerance as well, in addition to the supply pressure and temperature at that flowrate. The differential pressure sensor installation is quite complex, requiring very specific orientation of components, block and bleed valves, and regular filling of water capillary tubing. A calibration procedure for collecting samples of flowing steam was developed in order to determine several physical system constants required for the complex flow calculation. Control of steam flowrate was found to be difficult as well. The automatic control valve as supplied by the vendor, which was supplied based on the predicted process conditions, did not function as it was supposed to, with very poor control of the flowrate. Proper flowrate control was further examined using different valves, including the same valve body with a slot-type ball, and a manual needle valve.

1.4.4 APPROACH TO OBJECTIVES

The approach to achieving the objectives of this thesis shall include:

1. Design, testing and calibration process for biomass fuel feeding system.

   This procedure will begin by examination of the results from earlier fuel feeding system testing, followed by a design process that incorporates an examination of the FBG pilot plant reactor design, and the install location. Testing will be performed on individual feeding system components as they are assembled, and installed. Testing will be performed sequentially, in order to evaluate the addition of further components. Evaluation of system performance will be performed through collection of mass flow data, either through the pilot plant weight meter, or an external electronic balance scale. This data will be subsequently statistically analyzed to allow for quantitative comparison between system components.

2. Illustrate functionality of using isolating sensing lines and filters for pressure measurement of hot dusty gases (as in FBG pressure measurement)

   Pressure sensor response will be evaluated using a cold (room temperature) test system, allowing for comparison of two sensors, a control sensor that is directly coupled to the disturbed system, and a second that is connected through a sensing tube and/or filter. The signals from each sensor will be compared to determine the effect that tube length and filtering have upon measurement delay.

3. Steam metering apparatus evaluation and calibration for FBG operation

   The steam metering system will be evaluated and calibrated through a two step process. Initially, the steam flow control meter will be evaluated simply by startup of the steam generator, then sequentially opening the control valve by fixed amounts, and venting the produced steam into a receptacle/atmosphere. The flow rate, as measured ostensibly by the orifice plate and differential pressure sensor will be logged electronically. The

functional operating range of the control valve will be determined from this test, as well as the response resolution of the valve/DP sensor.

Secondly, the flow measurement system will be calibrated, beginning with a similar procedure to the first step, except that the mass of steam that is discharged will be measured, and the time interval of its production will be recorded. The temperature and pressure of the steam with respect to the orifice plate will also be electronically recorded. Calibration will be performed by deconstruction of published steam mass flow formulae, and determination of its component coefficients. Calculation of the unknown calibration coefficients will be accomplished by sample flowrate calculation, known physical system characteristics, and steam density lookup tables. Several samples will be taken over the required flowrate range in order to calculate a system calibration coefficient that results in the most accurate flowrate for at least 10 samples over the flow range.

2.0 LITERATURE REVIEW

The path of human civilization has depended on reliable sources of combustible fuels for thousands of years, for purposes as varied as home heating, food and materials processing, water sterilization, and industrial processes. Wood was the earliest of these fuels, and was predominant up until the industrial age; beginning in the 1800's when coal came into wide use. The modern era followed with the widespread discovery and use of petroleum and natural gas in the 1900's (Kunstler, 2005), followed by the transition into nuclear fuels, which are also used for heat and electricity generation, but through controlled thermo-nuclear reactions rather than combustion. Each of these fuels, over the course of its use, has obvious and less obvious costs both to the local environment and human health. Now, in the modern technological age, with a human population that covers nearly every land surface of the earth, the impacts of energy use take on global impacts, with human induced climate change becoming a very likely and significant reality. In facing this, human civilization must re-evaluate how we interact with our planet, and how we derive, capture and utilize energy. Additionally, the fossil fuels oil and natural gas are predicted to run out completely within the next 40 years (Kunstler, 2005), necessitating innovation and research in all energy sectors. In the process of this evaluation, it becomes obvious that waste and inefficiency are one area to focus, in terms of reducing the impacts of existing and future energy production, and extending energy production from existing systems and sources. Gasification technology comes into play in improving energy efficiency, as this method can be used to convert many different types of solid or liquid carbon based materials and residues to gaseous base combustible fuels. These gaseous fuels can be utilized with greater efficiency and reduced overall environmental impact than their solid fuel counterparts.

2.1 FLUIDIZED BED GASIFICATION

Fluidized bed gasification is the type of gasification that is most suited for conversion of biomass (Basu, 2006), therefore this is the type of system which has been implemented at the U of S and will be the system under analysis by this thesis. The next area of discussion will include key aspects of gasification, and the design and operation of bubbling fluidized bed gasifier systems.

Gasification is best described as a set of reactions that occur between the products of pyrolysis and partial combustion in an oxygen reduced gaseous medium. Pyrolysis is the breaking apart of organic matter that occurs when it is exposed to high temperatures (Table 1, Formula 1), starting from at least 230°C (Basu, 2006). Pyrolysis produces ash (composed of elements too heavy to vaporize), char (carbon that remains in solid form), as well as gaseous CO, CH_4, CO_2, H_2, and H_2O, as well as many heavier gaseous/vaporized hydrocarbons (though these decrease in concentration at high reaction temperatures). Pyrolysis is of course an endothermic (energy absorbing) reaction, so a continuous energy source is required to perpetuate pyrolysis. A normal wood fire, for example, is initiated by an external heat source, such as a match, which heats up the wood until pyrolysis begins to occur, releasing combustible gases, including hydrogen, methane and carbon monoxide. When an oxidation medium such as oxygen is available, those gases will combust, releasing energy from these combustion reactions (Table 1, Formulae 2, 3), thus providing heat for continued pyrolysis. Gasification works in much the same way; some of the gases produced by pyrolysis of the fuel source are combusted, producing the energy to maintain pyrolysis of added fuel. This percentage of combustion is controlled by carefully metering the amount of oxygen added to the fluidization medium.

Table 1: Chemical Reactions of Gasification Process

Formula #	Formula Name	Formula	Energy Balance	Ref
1	Pyrolysis	Coal or Biomass + energy → Char + Gases + Vapors	Endothermic	(Basu, 2006)
2	Partial Combustion	C + ½ O2 ↔ CO + 268MJ/kg-mole	Exothermic	(Mckendry, 2002)
3	Complete Combustion	C + O2 ↔ CO2 + 393 MJ/kg-mole	Exothermic	(Mckendry, 2002)
4	Hydrogen Combustion	H2 + O2 ↔ H2O + 742 MJ/kg-mole	Exothermic	(Basu, 2006)
5	Water Gas Reaction	C + H2O + 131.4 MJ/kg-mole ↔ CO + H2	Endothermic	(Mckendry, 2002)
6	Shift Conversion	CO + H2O + 42 MJ/kg-mole ↔ CO2 + H2	Endothermic	(Basu, 2006)
7	Methane Formation	CO + 3H2 ↔ CH4 + H2O + 74.9 MJ/kg-mole	Exothermic	(Basu, 2006)
8	Boudouard Reaction	CO2 + C + 172.6 MJ/kg-mole ↔ CO + CO	Endothermic	(Basu, 2006)

Where pyrolysis and combustion can be maintained in an oxygen deprived medium, CO and H_2 gases will remain. The reactions that occur between these gases and H_2O comprise what is termed gasification (Table 1, Formulae 5-7). The occurrence of these reactions is dependent upon the relative concentration of the available reactants and energy, with the exact prediction of how these reactions balance out being a fairly complex matter. By adding any of these constituent components, however, the reaction ratios can be shifted. Water, in the form of steam for example, can be added to the fluid medium to promote the water gas reaction and the water gas shift reaction, which will increase hydrogen concentration in the produced syngas.

Fluidized Bed Gasification is a reaction process that uses a special type of gas/solid contactor (a type of process equipment (Ulrich, 2002)), called a fluidized bed, to improve mixing and distribution during the gasification process. This contactor has the gas medium flowing upward through a distributing grate into a bed of inert solid particles such as sand, whereby those particles take on the behavior of a turbulent gas-solid fluid mixture. If that fluid is then heated to above approximately 300°C, and organic (or carbonaceous) material is added, gasification reactions will begin to occur if there is some oxygen present in the gas fluid medium to promote combustion. The syngas produced by these reactions is then displaced upwards through and out of the reactor by the inflowing gas medium. The benefit of using a fluidized bed for the gasification process is that it has a very even and controllable temperature, due to the mixing action that occurs in the bed from the inflowing gas medium. The reaction temperature is critical for maintaining correct reaction equilibrium between the reactions in Table 1. Additionally, the agitation occurring in a fluidized bed is very helpful in breaking down organic matter that is added, and in providing a place for any produced char to break down over time, providing additional fuel for the reactions. These characteristics make fluid bed gasification a very suitable gasification method for organic material that is constituted by relatively small dimensional components, such as powders, grains, pellets and similar substances.

The components of a fluid bed gasification system will each have specific design constraints to ensure that the overall system can operate efficiently as possible. Optimization of the design and operation of each component will allow the gasifier to waste as little energy as possible while at producing syngas with the highest possible heating value. Figure 14 illustrates the key components of a FBG system, including biomass, solid media and conditioner feeding systems, feed injection point, air delivery and heating system, gasification chamber, which itself includes the windbox, distributor plate, particle bed material, and freeboard. Solid media such as sand can be added through the fuel conveying system, or in some systems, through dedicated conveyors. Bed ash removal systems are also required on larger and commercial units, to ensure solid waste accumulation does not occur. Equipment downstream of the reactor can include heat recovery apparatus, dust removal system, gas cleaning and upgrading systems, and gas storage / use equipment.

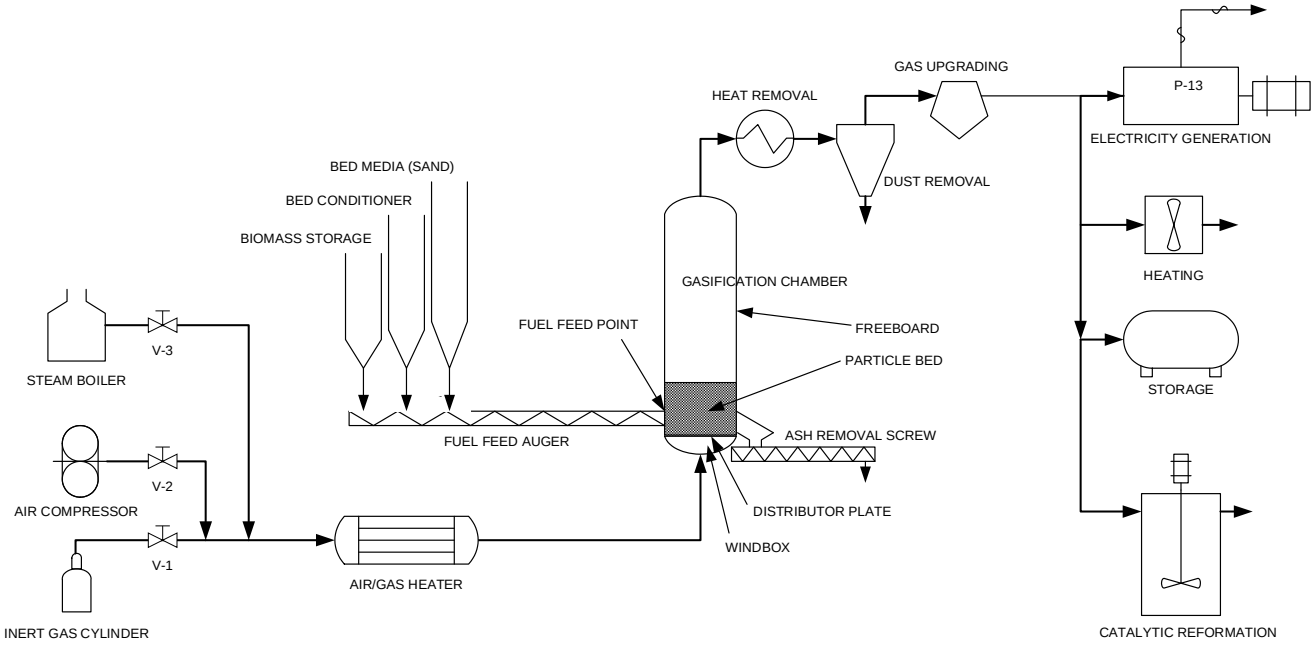

Figure 14: Overview of fluid bed gasification system components

The choice of gas medium for use in an FBG is significant to how the system will operate, as the composition and flowrate of this medium will in large part dictate what gases are produced by an FBG. Oxygen present in the fluidization medium will be consumed in combustion reactions with the fuel in an FBG, and any water vapor (steam) will react in water gas and water gas shift reactions, shifting their balance. Inert carrier gases will flow through the FBG, essentially reducing the combustion value of any produced syngas. A certain range of gas flow will be required to maintain adequate gas velocity in the fluidized bed, at least exceeding what is termed the "minimum fluidization velocity". This velocity must be met in order to maintain a bed regime which is either "bubbling" or "turbulent", but not faster, or the inert particles will be ejected from the bed, and then become entrained in the product gas stream. If too much oxygen is supplied there will be too little H_2 and CO remaining to be of value due to excess combustion. Too little oxygen is supplied there will be insufficient heat from combustion to maintain pyrolysis efficiently. If air is used as the gas medium, then gaseous nitrogen will be mixed with the produced syngas, lowering the heating value of the syngas. Steam can be added to the gas medium to promote the gasification reactions further, which can enhance hydrogen production. These reactions are on balance endothermic, however, consuming more heat from the reaction mixture, lowering the temperature, requiring additional oxygen for more combustion, or external heating. Knowing all these issues that influence the gas medium, it becomes important to know

in advance what is available, what product gases are desired, and control and measurement over the flowrates of each component become critical to balance the reaction appropriately.

2.2 FBG FUEL FEEDING SYSTEM DESIGN

With regard to the equipment for feeding fuel into an FBG, both the fuel properties and the reactor capacity must be taken into account. The fuel type, composition, physical dimensions and properties must be considered, as well as the required energy output of the reactor and the physical limitations of the installation location. Specific limitations with regard to fuel feeding into FBG's must be considered as well, including isolating the stored fuel from the hot reactor, preventing the pressurized fluid bed from infiltrating the fuel feeding system, and ensuring that fuel is added at a consistent and regular rate. Storage of the fuel must be considered as well, in addition to methods for controlling and measuring the throughput of the system.

2.2.1 FUEL PROPERTIES

In considering different fuels for use with FBG, the physical and chemical properties of those fuels must be evaluated, to determine their suitability for gasification by this method. The key elemental constituents of fuel relevant to gasification include carbon, hydrogen, oxygen, nitrogen and sulfur. Greater proportions of carbon and hydrogen in the fuel will increase the available components for producing CH_4, H_2, and CO. Additionally, the proportion of fixed carbon, volatile matter, and water content are important considerations, and can be determined from proximate analysis of the fuel. The fixed carbon in biomass will remain in the fluid bed for some time after the volatile matter and water have been released through pyrolysis. Fixed carbon will eventually combust, or otherwise react out, as it is agitated in the fluidized bed. Ash must also be considered; this material will remain in the fluid bed after the biomass has reacted. When using a fuel with high ash content with FBG, accommodations must be made for removal of this ash from the fluid bed, such as periodic removal and filtering of the bed media. When examining biomass, it may also be useful to know quantities of lignin, cellulose, lipids and protein, as these different types of biological structures may require specific equipment for preprocessing and handling. The fuel that was used specifically with the U of S pilot plant, meat and bone meal, will now be examined in greater detail.

2.2.2 MEAT AND BONE MEAL

Meat and bone meal (MBM) is a product of the rendering process, an industrial process that separates non-consumable animal products (typically bones and organs) into tallow (animal fat) and MBM (EPA, 1995). Non-consumable animal products may also include the complete remains of downers (cattle/animals which are too sick to slaughter for meat, or which have died on farm/in transit). In North America, MBM is primarily sourced from cattle (50%), swine (35%), and poultry (10%), with aquatic animals, wild game and exotic animals making up the remaining 5% (Garcia et al, 2006). MBM is composed of protein, lipids, solid minerals, and water, with typical concentrations of 55%, 10%, 30%, and 5% respectively (Garcia et al, 2006). The solid mineral content (what would resolve as ash in a FBG) is primarily calcium, with smaller amounts of phosphorous, sodium, potassium, and magnesium (Dalai et al, 2006). Typical MBM produced in North America has a mean particle size of 387 μm, and has the appearance of a light yellow to dark brown powder. The bulk density of MBM varies somewhat, but generally has a median loose fill density of 0.50 g/mL, and a tapped density of 0.68 g/mL. Due to the lipid content, MBM typically will have a sticky, agglomerative behavior when exposed to mechanical action. MBM has a lower heating value (LHV) and higher heating value (HHV) of 5 MJ/kg and 15-17 MJ/kg respectively (Garcia et al, 2006). By way of comparison, brown coal (Hambach, Germany) has an LHV of 24.6 MJ/kg, and HHV of 25.6 MJ/kg (Energy Centre of the Netherlands, 2010). Higher heating value (HHV) is defined as the heat produced by complete combustion of a defined quantity of fuel, assuming that the products of combustion are cooled down to the original fuel temperature. The lower heating value (LHV) on the other hand is defined as the heat produced by combustion assuming that water vapor formed by combustion is not condensed (thus this heating value lacks the latent heat energy of that phase change), and is closer to the actual energy that can be derived from fuel. (Engineering Toolbox (2), 2010)

MBM, under CHNS (Carbon, Hydrogen, Nitrogen and Sulfur) combustion analysis, is composed of approximately 46% Carbon, 6.5% hydrogen, 9.8% Nitrogen, and 0.5-1% sulfur (by mass). This high composition of carbon, as well as low concentration of water, makes this a relatively rich potential fuel source. Mineral and metal analysis of MBM ash show CaO and P_2O_5 in

significant quantities (28.4% and 22.8% of ash respectively), with lower quantities of Na_2O, K_2O, and MgO (3.24%, 2.31%, 0.96%) (Dalai et al, 2006).

In terms of its commercial value, MBM had been used widely up until the 1990's in Europe, UK, and North America as a protein and mineral supplement for all types of livestock, including beef and dairy cattle, swine, poultry, as well as pets and zoo animals. A severe outbreak of the disease BSE (mad cow disease) in Britain, culminated in 1989 with the ban of MBM in ruminant animal feed in that country, followed by bans in Europe (1990), Canada and U.S. (1997) (The BSE Inquiry, 2000). As the MBM feed bans for ruminants were widely ignored, Europe subsequently (in 2001) banned MBM from all feed supplements for animals for human consumption, pending being able to enforce the ban effectively (Forge, 2005).

As a result of the discovery of several cases of BSE in Canada in 2003, the Canadian Food Inspection Agency (CFIA) imposed additional restrictions on the animal materials most at risk for containing prions, the infectious agents which may spread BSE. These materials, deemed specified risk materials (SRM), which include the skull, brain, spinal cord, vertebrae and distal ileum, subsequently must be separated from other cattle remains before those other materials can be rendered to tallow and MBM. SRM are not allowed for commercial use in Canada at all, and must be either buried (where the prions will decompose over time), composted, or heated to 850°C until nothing but ash remains (CFIA [2], 2007).

Prions, the infectious agents which spread BSE, are proteins which cause misfolding of other proteins in the neural tissues of different animals, including cattle, sheep, humans, and deer, resulting what are called transmissible spongiform encephalopathies (TSE's) in these animals (Prusiner, 1997). Accumulation of misfolded proteins in animal neural tissues results in the symptoms of TSE's such as loss of motor control, confusion, and death. Prions are normally only transmitted between animals when infected neural tissues are consumed, from parent to offspring in some cases, and from prions passed through digestive tract in other cases (Anderson et al, 1996). Because prions are proteins, normal sterilization procedures cannot destroy them, and they must be destroyed at a molecular level to be fully deactivated, such as incineration, or a combination of heat and pressure (The BSE Inquiry, 2000). The combination of having

significant heating value (near that of coal), low moisture content, and the requirement for thermal destruction make SRM in particular a good candidate for FBG fuel, and it has been proven an effective fuel for gasification in several instances (Cummins et al, 2005; Fryda et al, 2006). In fact, gasification is one of few methods that can bring SRM materials to the required temperatures of 850°C (EU) or 900°C (CFIA, 2007) to ensure prion destruction, while at the same time producing energy rich syngas (AARI, 2005).

MBM is a suitable candidate for further exploration as an alternative energy source, due to both its chemical energy content in the form of carbon and its low (and decreasing) market value. In total, approximately 2.1 million tonnes of MBM are produced in North America per year (Garcia et al, 2006), and 3.0 million tonnes in the E.U. per year (Fryda et al, 2006), making this a widely available fuel in these regions. (In total these two regions produce enough MBM to fuel an 800MW power plant (conventional), enough to supply electricity to approximately 1 million homes – assumes LHV = 5MJ/kg, 40% electrical efficiency, home average electricity consumption = 0.8kw) In the E.U., MBM has no legal commercial value; therefore all of the MBM produced there must be destroyed at cost to the processors there, making it an attractive option as fuel. In North America MBM produced from SRM would be of particular use, as this material in particular is considered pathenogenic in this region and significant cost is incurred to destroy or isolate this material. The physical particle size and high energy content make MBM very suitable for use as a fuel for FBG, and will be tested here as a fuel for that purpose. Due to the solid mineral content of MBM, one would expect up to 30% of its mass to remain as ash, which would remain in the fluid bed. This would either be removed from the fluid bed, or carried out as fly ash which would be removed during gas cleaning. MBM has significant volatile content, which can result in significant tar production during gasification (Fryda et al, 2006); therefore consideration must be made for either thermal or catalytic treatment or removal of these tars. Heating syngas to 1100-1200°C for example is one method of breaking tars down to gaseous hydrocarbons (Basu, 2006).

This material provides a combination of challenging properties, including significant lipid content, heat-induced denaturation, a tendency to bridge and compact, and an angle of repose

(AOR) of 48 to 50 degrees (Garcia et al, 2005). A high angle of repose such as this means that this material will have poor flowability, and will tend to form high, steep piles.

2.2.3 FEEDING SYSTEM

Because the optimum fuel particle size for use with FBG is between 0.03 to 3 mm (Basu, 2006) MBM is a suitable fuel candidate for FBG, with a mean particle size of 0.387 mm. Because MBM is typically in this fine, powdered form, equipment used for conveying powders and small granular materials were examined for MBM fuel handling applications. When considering fuel feeding systems for FBG reactors, accommodation must be made for the high temperatures in and near the reactor chamber, the pressures and gases present in the bed itself, and the need for controllable and stable output rate when evaluating feeding methods and equipment (Maxwell, 2005).

Typical systems for fuel feeding into FBG's consist of screw conveyors in multiple stages (Smeenk et al, 2005, Goransson et al, 2008), with a primary material handling stage (a metering stage) drawing fuel from a reservoir, producing a measured and carefully controlled fuel output rate. The secondary stage of feeding (injection stage) will typically be separated from the primary stage by an airlock, and will inject the fuel in a consistent and predictable fashion into the reactor, aided by air or other pressurized fluid, to overcome or balance the pressure within the fluidized bed (Basu, 2006).

Several types of fuel feeding systems are typically used for fluid bed gasifiers, including gravity feeding chutes, screw conveyors, and pneumatic injection systems, among others (Basu, 2006). Gravity feeding systems involve an electromechanical conveyor that moves the fuel to a certain point, after which it falls into the feed chute, and down into the reactor. This method requires that the feed chute be slightly pressurized, to ensure that the pressure within the combustion chamber be slightly below the pressure in the feed chute, in order that hot gases are not able to flow back into the feed system. Another difficulty with this type of feed system is that due to the low velocity of fuel entering the bed, the fuel tends to concentrate in that area, causing corrosion, and higher pressure to accumulate in this area (Basu, 2006). Mass flow metering would be

required upstream from the gravity chute, in order to control the rate of fuel addition. This method is also not well suited to low throughput systems, as the fuel would tend to build up in a small chute, without the impact of falling fuel to keep it flowing.

Belt conveyors can be used for conveying powders and grains as well (Ulrich, 2002), but the matter of enclosing belt conveyors in sealed containment systems to enable pressurization makes them an expensive and complex option for feeding gasification systems. This method has been shown to work on large scale, however, having been successfully integrated with continuous mass-flow weighing systems for a production gasifier gas turbine power plant (Maxwell et al, 2005).

Screw conveying of fuel into the fluidized bed is another suitable feeding method, but is also subject to the condition that the secondary stage screw casing be isolated or pressurized at or above the fluidized bed pressure. This pressurization will prevent upsurge of hot gases from the fluidized bed into the screw conveyor. Plugging can be an issue in screw conveyors if the fuels used tend to denature and become tacky at high temperature, or if they have high moisture content (Basu, 2006). This can occur, because the screw conveyor near the reactor would be exposed to temperatures ranging from 700 to 900°C, potentially causing the fuel to denature and stick to the screw casing and flighting. In cases where the fuel is discharged downward from the end of the screw conveyor, the fuel can compact and stick to the end plate of the conveyor. Shaftless screw conveyors, such as is illustrated in Figure 15, are very suited to wet and sticky solids conveying. This type of conveyor is much more able to resist plugging and compacting, and they do not require a fixed bearing on the discharge end, allowing for direct horizontal conveying (Spirac, 2009).

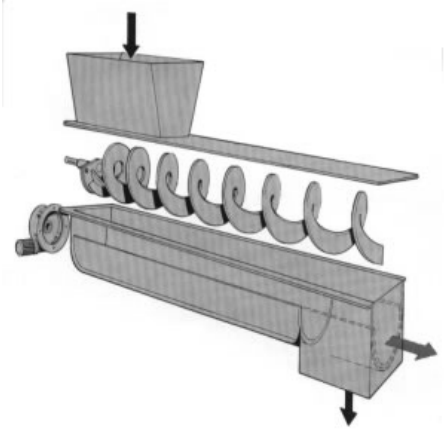

Figure 15. Screw conveyor (shaftless) construction (Spirac, 2009)

Pneumatic injection of fuel into the bed is another option, used especially in cases where the fuel is a very fine dry powder that can be completely suspended in an air stream.

In coal-fired fluidized beds, powdered coal is often pneumatically injected from below the fluidized bed, combining the fuel with the combustion air (Basu, 2006). This method would not be well suited to biomass, however, except for very dry, finely ground materials. A typical example of a fuel feeding system for an FBG is the switchgrass feeding system used by Iowa State University (Smeenk et al, 2005). This system is comprised of an injection screw conveyor, rotary airlock, and metering screw conveyor and bin (Figure 16). The ISU system was operated at an average input rate of 180 kg/hour, or about 10 times the fuel mass-flow rate required for the U of S pilot plant.

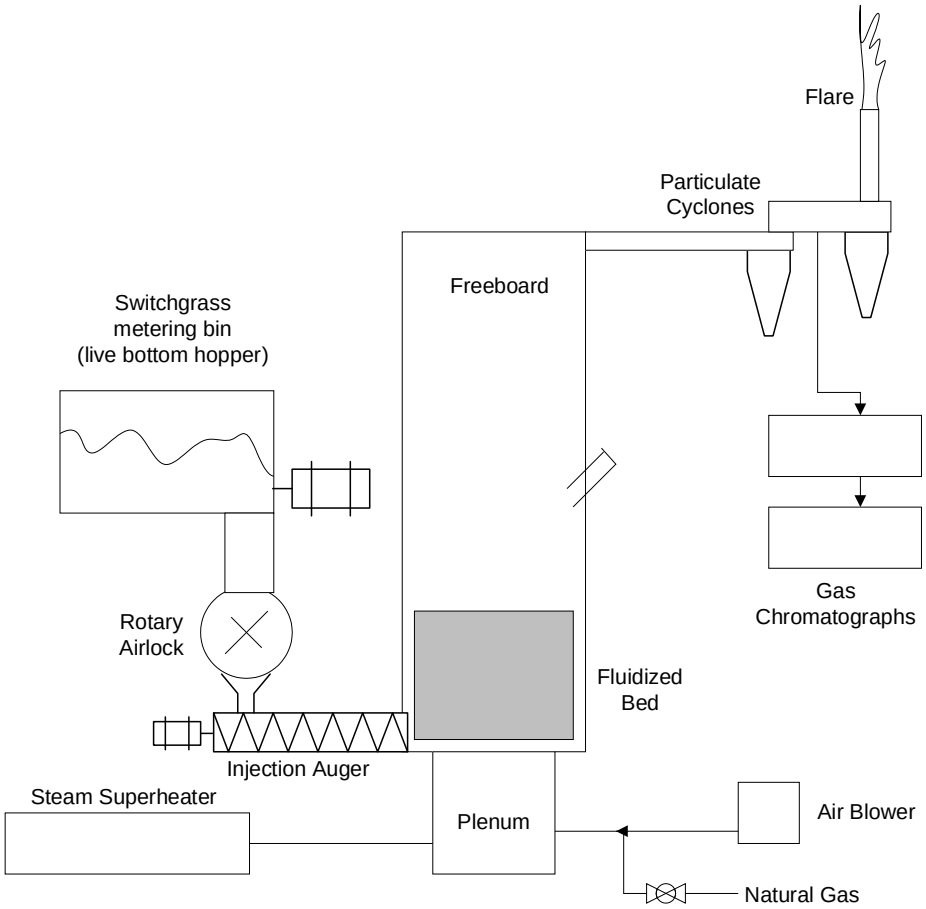

Figure 16: ISU fluidized bed reactor schematic (After Smeenk et al, 2005)

A practical examination of fuel feeding methods for conveying MBM into gasifier pilot plant at the U of S in 2007 had shown that a two-stage system was suitable for this material as well. For

the required fuel rate for the proposed pilot plant, a suitable system would consist of a 150 mm metering conveyor, a 50 mm injection conveyor, and a pneumatic injection nozzle, which is mounted on the end of the injection conveyor (Figure 17). This arrangement was the result of extensive testing of MBM conveying methods in 2007. This conveying method helps to direct the MBM into the reactor, prevents plugging of the discharge nozzle, and prevents the hot combustion gases from traveling up the screw conveyor (Albietz and Fonstad, 2007).

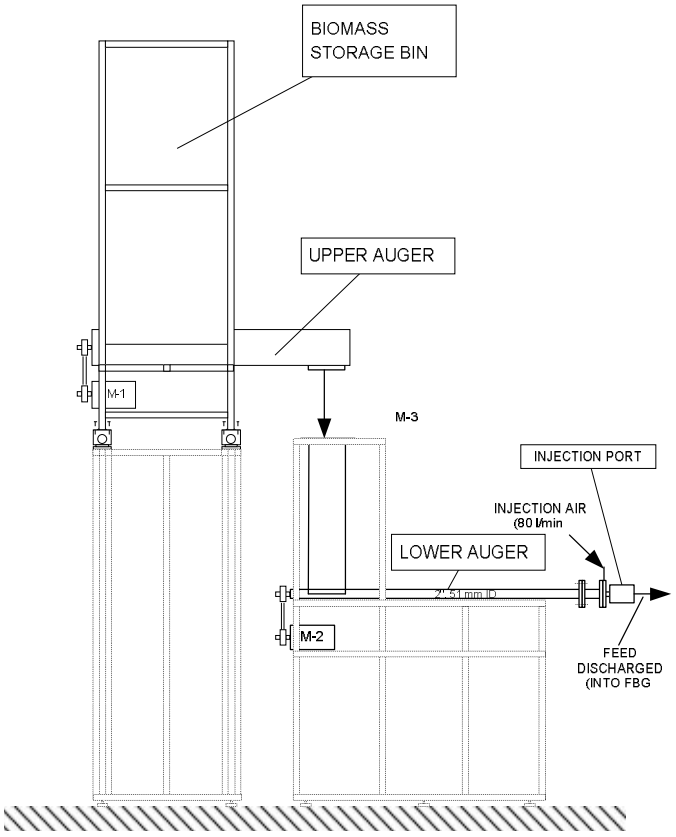

Figure 17: FBG pilot plant fuel feeding apparatus design

The principal areas of difficulty with this type of system include the practicality and method for measuring and controlling the fuel output rate, isolation of the fuel feeding system from destructive/denaturing reactor temperatures, and the ability to maintain a consistent, regular output rate. These problems were examined in this research, and comprise one of the three components of this thesis.

2.2.4 FUEL STORAGE

Because FBG utilizes fuels with particle sizes between 0.03 to 3 mm (Basu, 2006), storage methods used for bulk powder and granular solids can generally be used, including hopper-bottom silos, bins, and chutes. MBM, however, is a sticky material due to its high lipid content, with an angle of repose of approximately 48-50 degrees. With a normal particle size less than 1 mm, this material will tend to agglomerate into larger particles if compressed due to its moisture and lipid content (Garcia, 2005). MBM will also tend to bridge across shallow, low angled or narrow hoppers over time due to its angle of repose and the tendency of its particles to stick together (Figure 18). A hopper to store MBM will therefore need to have a very high sidewall angle, to ensure continuous feeding at low rates and to ensure that hoppers are emptied completely. Additionally, any points in a flow system with significant geometric transitions may be susceptible to bridging and plugging, necessitating measures to counter these difficulties.

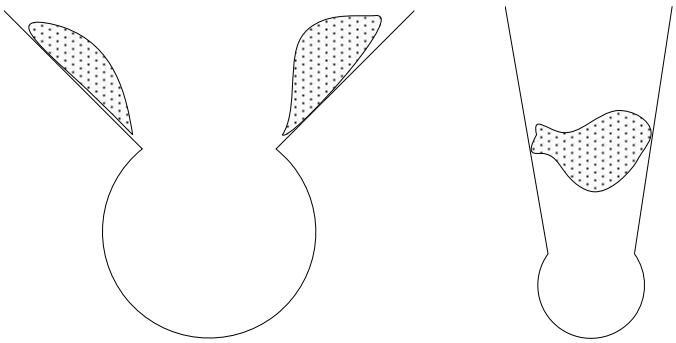

Figure 18: Typical plugging and flow issues with MBM

2.2.5 AIRLOCKS

A significant problem for fuel feeding systems for FBG's is the transition from atmospheric pressure to the fluidized bed pressure in FBG reactors. This can be accomplished simply by entirely sealing and pressurizing the fuel feeding systems, resulting in a batch type system, or by incorporating an active airlock, as in Figure 19, into the flowing stream of the system.

Rotary airlocks are electromechanical devices, typically used to isolate high and low pressure zones in solids feeding systems (U.S. Air Filtration, 2009). The ISU system described in section 2.2.4 utilizes this method for separating low and high pressure zones for gasification. Rotary airlocks function by having a rotating multi-vane paddle which is sealed against housing. Material falls into the top of a rotary airlock, and is conveyed around a central axis by the moving vanes, and then is conveyed out of the airlock through the bottom.

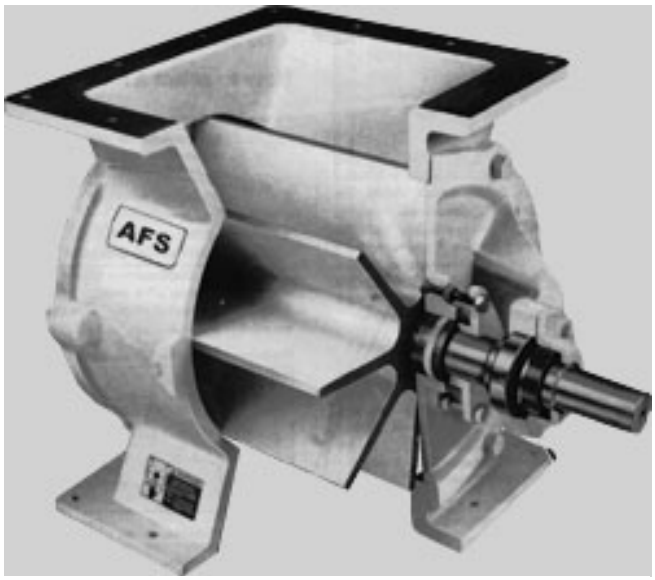

Figure 19. Rotary airlock construction
(Advanced Fil-Tech, 2009)

As only the pockets of air between vanes move between the pressure zones, it is possible to maintain a pressure differential across the airlock with only minimal leakage (from high to low pressure zones). The ability of an airlock to function with minimal losses depends on the seal that is created by the fins against the housing, and also depends upon the rotational speed of the airlock, as the airlock will exchange more air between zones as it operates faster.

2.2.6 VARIABLE SPEED DRIVES

In order to vary the mass-output rate of a fuel feeding system, a method for varying the motorized conveyor speed is required. Because the FBG pilot plant will operate at a varying fuel-feed rate from 1-5 g/s, and because several motorized conveyors will be interacting, this method must be applied for each motorized device. Variable speed drives are electrical / electronic devices that are able to modulate the rotational rate of an alternating current (AC) motor. A typical installation will have supplied 3 phase electrical line voltage as an input to a

VFD, along with control signals, and 3 phase electrical output to the motor, or load. A VFD achieves speed control of its attached motor through shifting of the ac frequency and applied RMS voltage to the motor, from the base frequency of 60Hz (or 50Hz) to higher or lower values. As the ac frequency is reduced from the base value, the action of the rotor (moving part of a motor) slows relative to the stator (fixed part of a motor), thus the rotational speed of the motor is reduced (Figure 20).

A VFD such as that in Figure 21 achieves control over the frequency of its output voltage by re-creating the three phases electronically. The VFD first converts the supplied line AC voltage to DC voltage using a rectifier bridge and a bank of capacitors, referred to as a DC Bus. The drive then recreates the required voltage and frequency levels digitally from the DC bus using an inverter switching circuit, producing a quasi-ac voltage signal (Joliet Technologies, 2009). By varying the frequency of the transmitted voltage on the three phases, a VFD is able to modulate the speed of a motor, according to the following formula (for a 60Hz 3phase motor):

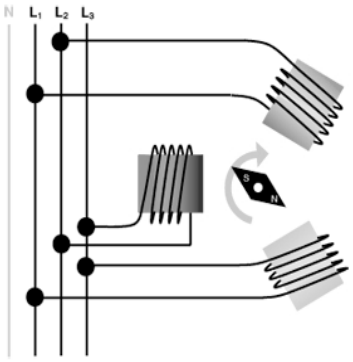

Figure 20: Three phase motor wiring diagram (Zeitlauf, 2009)

Figure 21. VFD - typical (Automation Direct, 2009)

$$N = \frac{120 \times f}{p} \tag{9}$$

Where:

N = RPM speed of motor

f = frequency of applied voltage

p = # of pole pairs for the motor

Variable frequency drives are typically applied to fuel feeding systems where rate control is required, as their speed control capability allows also for rate control of conveying equipment. Effective control of fuel output rate typically involves an electrically operated conveyor using a VFD and some type of mass flow measuring device. This is the method applied for fuel-feedrate control in the FBG pilot plant. VFD's were implemented on each conveyor as well as the rotary airlock and controlled from the Labview interface interacting with a mass-flow measuring system.

2.2.7 SOLIDS MASS FLOW MEASUREMENT

Instruments for mass flow measurement of solid materials generally take the form of weigh belt tables (Thermo Scientific, 2009), impact flowmeters (Eastern Instruments, 2009), or load cells utilizing loss-in-weight computation (BLH, 2009). Each of these devices utilizes strain gauges in one way or another to measure either continuous force (moving or fixed weight), or instantaneous force (from the impact of falling material).

Weigh belt tables are very common in both mining and mineral processing, and are well suited to measuring mass flows measured in tonnes/hour from several tonnes per hour to several hundred tonnes per hour. This type of measuring system involves a belt conveyor, which has rolling idlers that are mounted on load cells (weighing cells) that continuously measure the mass of solid material resting on the belt, as well as speed sensors mounted on the end rollers to determine the linear speed of the moving belt (Figure 22).

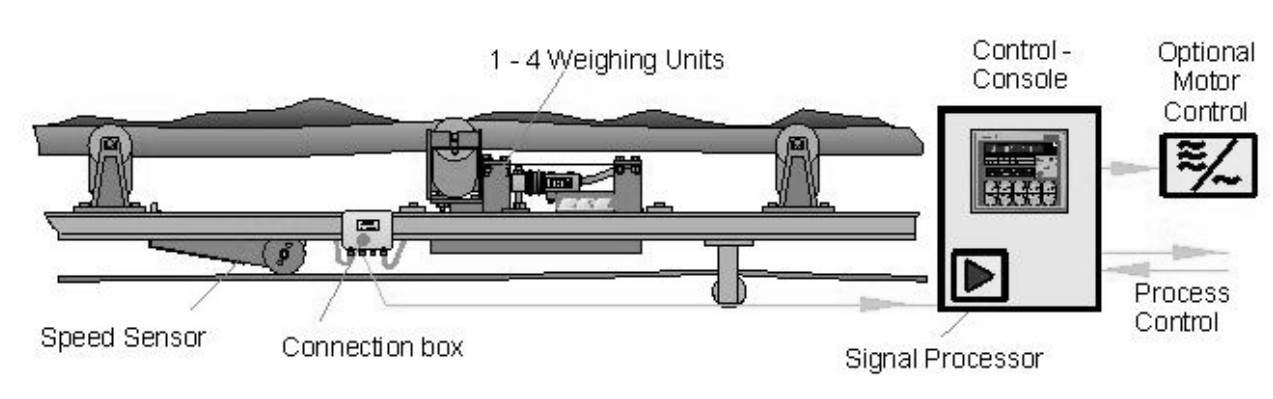

Figure 22: Belt scale mass flow measuring system (SEG, 2009)

A flow computer then uses these values to compute an output reading in mass/time, according to Equation X. (Thermo-Scientific, 2009).

$$Q = S \times C \times L \quad (10)$$

Where:

Q = Mass flow rate (kg/min)

S = Belt speed sensor rotational speed (rpm)

C = Belt speed sensor circumference (m/rotation)

L = Load cell measured mass for a given belt length (kg/m)

Because belt conveyors are more suited to larger mass-flow rates as are used in mineral processing, they may have significant applicability for biomass FBG's that are also large in scale, where they can either be sealed entirely and pressurized (Maxwell et al, 2009), or operated at atmospheric pressure and separated from the pressurized injection conveyor by an airlock.

Impact flowmeters operate through the translation of the force from falling solid materials as they hit a solid plate. That plate is bonded to a strain gauge, which is calibrated to convert the measured impact force into a mass flowrate (by flowing a known mass-flow rate of material through the meter). Impact flowmeters consist of an integral chute, which is constructed to direct the flow of falling materials onto the measuring plate and then allow those materials to flow down and out of the chute (Figure 23).

Figure 23: Impact flowmeter - typical (Belt-way Scales, 2009)

Impact flowmeters again are more suited to large flowrates from several tonnes hour up to hundreds of tonnes per hour, and steady, continuous flow profiles (Omega, 2009). The use of this type of system may be appropriate for biomass flow measurement for larger capacity systems, measured in tonnes/hour rather than kg/hour.

The dominant instruments for weight measurement and for mass flowrate measurement of solids are load cells. Load cells (such as in Figure 24) are devices which convert mechanical force into an electrical output, using an electrical element such as a strain gauge (Omega [2], 2009). Load cells are constructed by bonding a strain gauge to the deforming component of a structural support for a storage vessel. As load is applied to/removed from the support, the resistance of the strain gauge will change in some proportion to the force, or weight applied. By continuously monitoring the mechanical force exerted by the storage bin and feeder on the platform which it rests upon, the average loss of weight from the bin can be calculated (BLH, 2009). By installing a load cell on each structural support of such a bin, and adding the output of each load cell together, the most accurate measurement of the vessel's weight can be achieved.

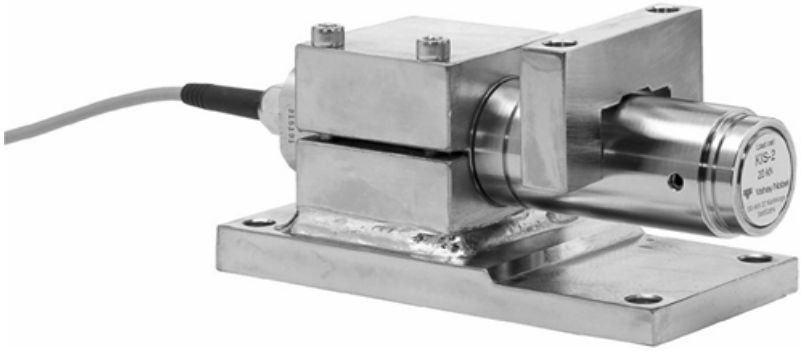

Fig 24: Load cell - KIS-2 series (Vishay-Nobel, 2009)

2.3 FBG PRESSURE MEASUREMENT

Pressure is one of the key process control variables for FBG's, as this property is used to assess the ability of the fluid media (fluidization & oxidation media, and product gas) to flow through the system. Gas flow rate is inferred through the pressure drop across each key component. Figure 25 illustrates the key points of pressure measurement on a FBG system, indicated with a "P".

Pressure is typically measured at the windbox (below distributor plate, point P1), just above the distributor plate (at the base of the fluid bed; point P2), and at some point above the fluid bed (P3 or P4). Pressure measurement of points before and after cyclones (P5) and any other post-processing equipment may also be required, to assess the efficacy of such equipment, as each of these devices will have a rated pressure drop at a given flowrate and temperature, for proper operation. Aside from bed temperature, pressure is the most important process property with respect to FBG monitoring and control, as the pressure drop across the distributor plate, and across the fluidized bed will allow for the best performance analysis of these system components (Basu, 2006).

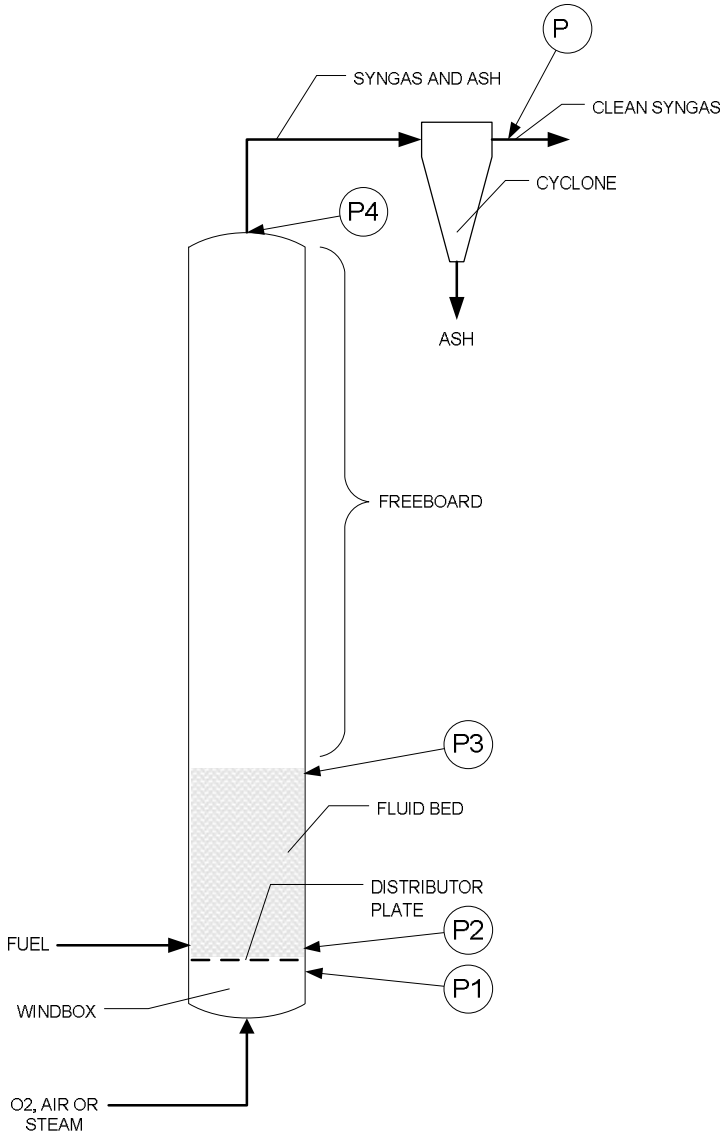

Figure 25: Typical FBG pressure sensor locations

Measurement of pressure at the base of and above the fluidized bed can be used to infer whether or not minimum fluidization velocity (U_{mf}) has been reached. This information can be inferred from the bed pressure drop. The fluid bed pressure drop will increase only until that minimum fluidization velocity has been reached (Figure 26), then it will remain relatively constant (Rhodes, 2007). The minimum fluidization velocity is exactly as it sounds, that is, the minimum fluid media velocity required to mobilize the solid bed particles into a fluidized state, conferring the mixing, temperature distribution and reaction benefits therein. As is indicated in Figure 27, minimum fluidization velocity is the point where a static bed begins to fluidize, and transitions into bubbling, turbulent and fast "regimes". Voidage in this diagram refers to the total percentage of solids relative to the total bed volume.

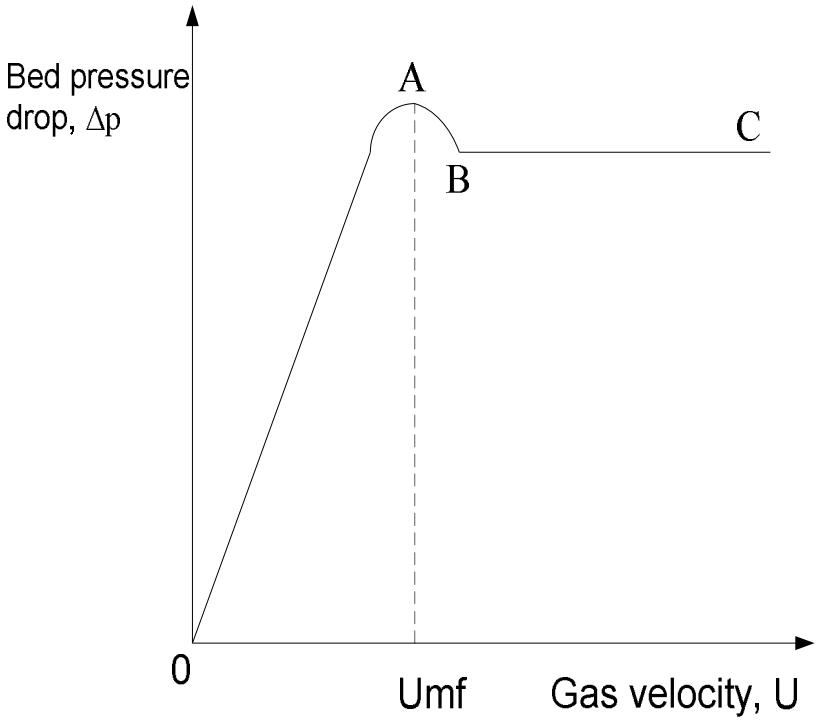

Figure 26: Press. drop vs. gas velocity for fluid bed (After Rhodes, 2007)

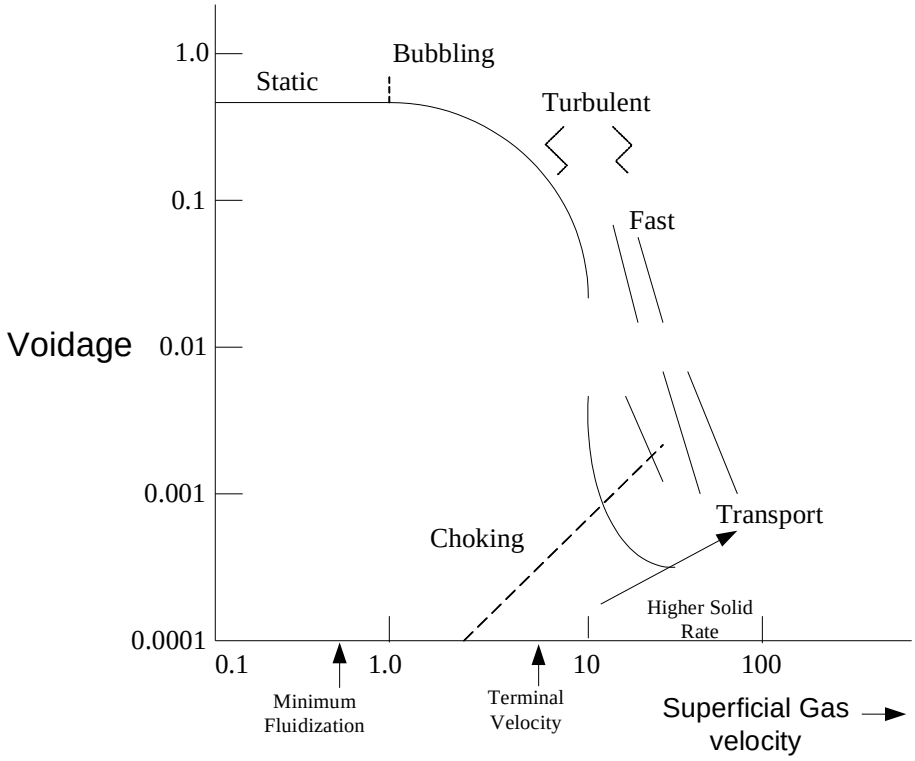

Figure 27: Voidage vs. superficial velocity
(After Basu, 2006)

Pressure measurement can also be used to predict when a bed may be about to enter into an agglomeration condition. Agglomeration occurs when residual biomass ash in a fluidized bed begins to stick together and to the solid media particles (such as sand), increasing the particle size and mass such that the particles are no longer able to fluidize. The pressure drop across the fluidized bed can indicate when agglomeration has occurred (when fluidization has failed) by an increase in bed base pressure, and bed pressure drop. However, by analyzing fluctuations in the bed pressure drop using advanced computational and statistical techniques agglomeration conditions can be predicted, detected early, and possibly averted by addition of conditioning material or initiating ash removal (Nijenhuis et al, 2007). To be able to do this, the fluidized bed pressure measurement must be accurate, fast, and high frequency, with at least 200 Hz sample rate (Korbee et al, 2006).

2.3.1 PRESSURE MEASUREMENT

Pressure is measured using several different principles, including strain gauge, capacitive, piezoelectric, magnetic and optical. Strain gauge sensors are quite common and inexpensive, and work based on the principle that the force applied (by liquid or other fluid) will be

proportional to the pressure. Figure 28 illustrates the operational principle for a strain gauge based pressure sensor. By connecting to both ports (P1 and P2), this can be used as a differential sensor, gauge pressure sensor if P2 is left open to atmosphere, or as an absolute pressure sensor if the low side is connected to a vacuum reference (Omega [3], 2009).

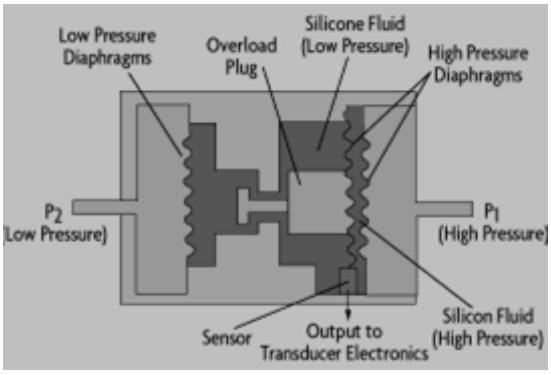

Figure 28: Strain gauge pressure sensor (Omega, 2009)

Pressure can be measured using many different units, including Pascals (SI units), bar gage (SI units, equivalent to 100 000 Pa or 100 kPa), psi (imperial units), and for measuring much smaller pressures, inches of water (inH_2O) or inches of mercury (inHg) are used. Typically when measuring properties of steam using imperial units, psi units will be used to measure the static pressure of the steam, and inches H_2O will be used for measuring pressure drops across orifice plates, as for typical systems, the measured values using these units will conveniently be between 0-500 in the case of each. S.I. measurements are much simpler, generally using Pascals or kiloPascals for all units, reducing the complexity of conversion calculations.

Absolute pressure can be described as the pressure of a fluid relative to vacuum. Gage pressure is the pressure of a fluid measured above the local atmospheric pressure. Atmospheric pressure at mean sea level is 101.35 kPa, while in Saskatoon, SK which is at 501m above sea level (The Weather Network, 2009) the atmospheric pressure is 95.63 kPa (Turblex, 2009). Differential pressure is the pressure of one fluid measured relative to the pressure of a second fluid. In the case of gas flow measurement using an orifice plate, the differential pressure is measured, that being the pressure of the gas downstream of the orifice relative to the gas pressure upstream of the orifice.

Because strain gauges are limited in their temperature range, commonly having temperature limits below 100°C, care must be taken in measuring fluids which are hotter than these limits. Steam, particularly, can be damaging to pressure measuring elements, as it can have temperatures above 150°C, and as high as several hundred degrees. Fortunately, water can be used as a capillary fluid for steam pressure measurement, as it combines several properties which work well for this purpose. Capillary fluids are used in pressure sensing apparatus' for mechanical transmission of pressure signals from hot, abrasive, corrosive or otherwise difficult media, to electronic signal generating surfaces. This is the method used in the FBG pilot plant to protect the pressure sensing surfaces from the high temperature steam.

2.3.2 TEMPERATURE ABATEMENT FOR PROCESS INSTRUMENTS

In cases where pressure measurement is required, but the fluid to be measured has a temperature which exceeds the physical limitations of the sensor, tubing or pipe can be used to cool the process fluid down to a level which is within the sensor limits. This is often referred to as "impulse" tubing, as it is used to relay pressure impulses from the fluid source to the sensor, using the same fluid media as being measured. In the case of FBG pressure measurement, the fluid that will be measured will be a gas, composed of nitrogen, oxygen, carbon monoxide, hydrogen, carbon dioxide, and methane, in addition to other hydrocarbon gases and vapors. The tubing or pipe that connects the pressure sensor to the process will itself contribute much more to the temperature of the sensor than the gas itself, as any metal will have a thermal conductivity of 100x or more than the gases in question (Kane, 2002).

The connecting tube will therefore be considered the primary heat conductor, where the sensor is concerned. Using this assumption, the following formula can be used to calculate the cooling effect of a length (L) of tubing;

$$\frac{(T - T_\infty)}{(T_o - T_\infty)} = \frac{1}{\cosh\left(\sqrt{\frac{4 \times h \times D_1}{12 \times K \times (D_1^{\,2} - D_2^{\,2})}} \times L \times 6.26\right)} \qquad (11)$$

where:

T = temperature of point of interest on tubing (°C)

T_∞ = temperature of ambient air (°C)

T_o = temperature of pressurized (hot) fluid (°C)

L = length of tubing (m)

h = thermal conductivity from tube to still air (assumed to be 8.18 W/m^2*K)

K = thermal conductivity in W/m^2*K

D_1 = outside diameter of tube (m)

D_2 = inside diameter of tube (m)

For Inconel 625, K = 31.8, and for 316 SS, K = 53.4

(From Kane, 2002, converted to S.I. units by Author)

For a 316SS 6.4mm diameter impulse tubing, measuring air at 850°C source temperature, the cooling effect is illustrated in Figure 29. As is indicated, very little length of tubing is required to achieve safe temperatures for pressure sensing, with only 0.2 m required to achieve temperatures below 50°C.

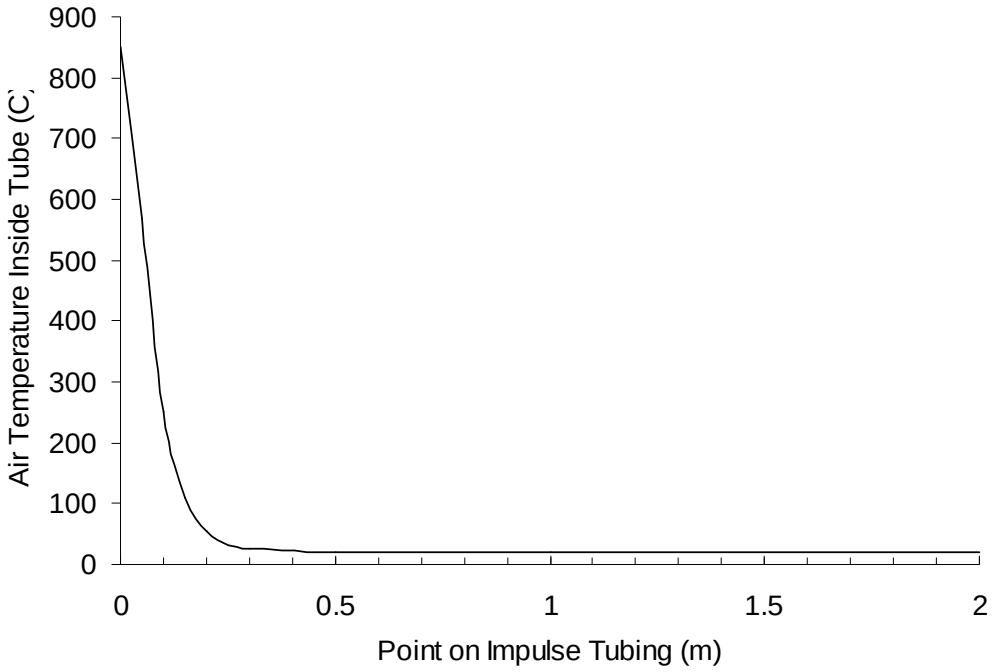

Figure 29. Cooling effect of 6.4mm SS impulse tube
(effect on air, with 850C source temperature, 20C ambient temperature, 2 m max length)

2.4 STEAM FLOW MEASUREMENT AND CONTROL

Steam, also known as vaporized water, exists at temperatures above 100°C at standard atmospheric pressure. Saturated steam represents the boundary between wet steam and superheated steam, and is steam that is at the temperature which corresponds to the boiling temperature for the given pressure that the steam has. Superheated steam is steam which has been heated above the boiling temperature for the given steam pressure (Spirax Sarco, 2010).

2.4.1 STEAM FLOW MEASUREMENT

Measurement of flowing gases or vapors, including steam, can be accomplished through use of an orifice plate, which will impose a small pressure drop on the flowing gas (or vapor) (ASME, 1990). This is a very typical method for steam flow measurement, as used in the gasification plant at the BTL laboratory - Mid Sweden University (Goransson et al, 2008). An orifice plate is simply a metal disc with a hole through its center, that hole having a diameter that is a fraction of the diameter of the pipe which the gas is flowing through. The orifice plate is installed between tapped flanges, which are installed as in Figure 30.

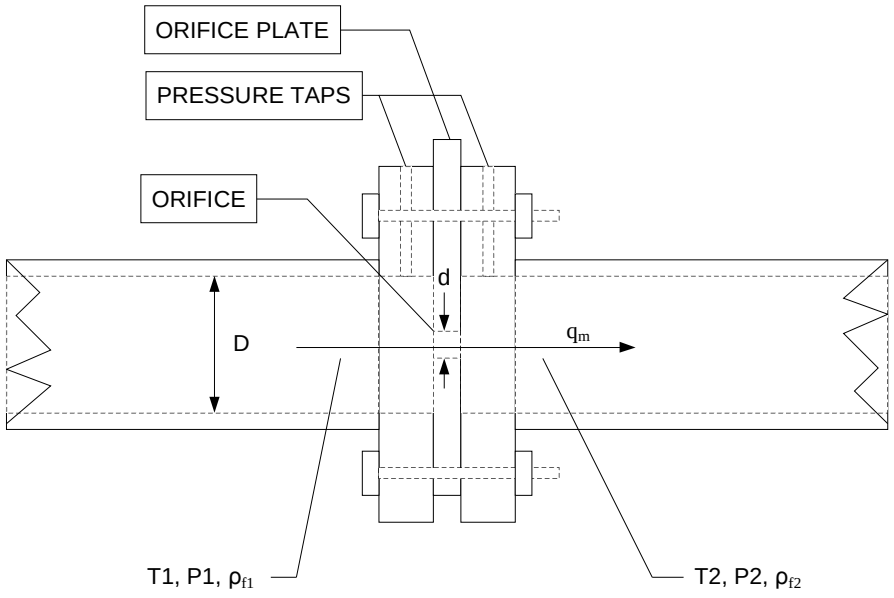

Figure 30: Pipeline orifice plate installation - typical
(with relevant points for measurement of the mass flow rate)

The tapped flanges allow for direct access to the pressurized gases both before and after the orifice, and are connected to pressure sensor(s) for measurement and transmission of the pressure loss across the orifice plate.

Measurement of steam mass-flowrate can be implemented via the use of the orifice plate to create a pressure drop, and a differential pressure sensor which transmits the pressure drop across the orifice plate to the data acquisition system. The relationship between this pressure drop (Δp) and the mass flow rate of steam (q_m) are given by Formula 11 (ASME, 1990. Volumetric flowrate of steam would be calculated by dividing q_m by the steam density (ρ_{f2}):

$$q_m = \frac{\pi}{4} \times C \times \varepsilon_2 \times d^2 \times \sqrt{\frac{2 \times \Delta p \times \rho_{f2}}{1 - \beta^4}} \qquad (12)$$

where:

q_m	=	Mass Flow Rate	(kg/s)
C	=	Discharge Coefficient	(dimensionless)
ε_2	=	Expansion Factor	(dimensionless)
D	=	Upstream Pipe Diameter	(m)
p	=	Orifice Pressure Drop	(Pa)
ρ_{f2}	=	Fluid Density after Orifice	(kg/m^3)
β	=	Ratio of diameters d/D	(dimensionless)
d	=	Orifice Diameter	(m)

ρ_{f2} being derived from standard steam tables using P_2, and T_2, where:

P_2	=	Static (Downstream of orifice) Pressure of Fluid	(Pa)
T_2	=	Temperature of Fluid (Downstream of orifice)	(degrees Kelvin)

Discharge coefficient C is a dimensionless number, defined by Formula 12, and is dependent on the Reynolds number, and the geometry of the piping system. C is normally determined through calibration using an incompressible fluid (liquid), where $\rho_f = \rho_{f1} = \rho_{f2}$ (ASME, 1990), and ε (expansion factor) is equal to 1.

$$C = \frac{q}{\frac{\pi}{4} \times d^2 \times \sqrt{\frac{2 \times \Delta p \times \rho_f}{1 - \beta^4}}} \tag{13}$$

The expansion factor ε represents the "variations in the isentropic exponent" of the flowing gas (ASME, 1990), and can be determined to represent that value for the gas both upstream (ε_1) and downstream (ε_2) of the primary element (orifice), where the difference between these values is dependent upon the changing steam density as it loses pressure passing through the orifice:

$$\varepsilon_1 = \frac{q_m}{C \times \frac{\pi}{4} \times d^2 \times \sqrt{\frac{2 \times \Delta p \times \rho_{f1}}{1 - \beta^4}}} \tag{14}$$

$$\varepsilon_2 = \frac{q_m}{C \times \frac{\pi}{4} \times d^2 \times \sqrt{\frac{2 \times \Delta p \times \rho_{f2}}{1 - \beta^4}}} \tag{15}$$

The calculation of steam mass-flow therefore depends upon the ability to measure or determine the orifice pressure drop, the steam density (which can be determined from steam tables), and the ability to determine or estimate the discharge coefficient, and expansion factor. Calibration of the steam flow measuring system will allow for reverse calculation of estimated values for discharge coefficient and the expansion factor. With these system characteristics accurately determined, real-time measurement of the pressure drop and steam density will allow for continuous calculation of the mass-flow rate.

2.4.2 STEAM FLOW CONTROL

Steam can be a difficult medium to control, as it is often generated at much higher pressures than it is utilized at, as is the case of using it as a combustion/fluidization medium for atmospheric gasification. Controlling the flow of media from low to higher pressures over a wide control range can be difficult, and requires a control valve with very low Cv or Cg values. Cv or cg is

the short form for the flow coefficient (Cv for liquid, Cg for gas) for a control valve, and for steam in particular, can be calculated using equation 15:

$$Cg = \frac{7.21 * m}{\sqrt{(p_i - p_o) * p_o}} \quad (16)$$

where:

Cg = Flow Coefficient (gas) (dimensionless)

m= steam flow (kg/hr)

p_i = inlet steam absolute pressure (kPa)

p_o = outlet steam absolute pressure (kPa)

For the steam supply for FBG pilot plant, a steam flow rate of 4.5 kg/hr is assumed, as well as supply pressure of 480 kPa, and a discharge pressure of 10 kPa. This yields a valve coefficient of 0.16 (See sample Calculation D-2).

To specify a valve for controlling over a certain range, one must calculate this value over a range of flowrates/pressures, to ensure that the valve installed performs over a range. Generally a valve will be specified by its Cv value at increments of 10 degrees or 10% of its range.

An example of a valve that works with the Cv calculated above is the Fisher Baumann 24000 ½" valve with series 102 plug, as indicated in Figure 31. Meeting the relatively low steam flow control requirements of the FBG pilot plant would require a globe valve with a trim selected from among those with the smallest Cv range for the 102 series plug.

Table 4. **Cv VALUES @ 100 PERCENT PLUG OPENING (Kv = 0.86 x Cv)**

VALVE SIZE	ORIFICE DIA.	PLUG TRAVEL	PLUG SERIES				
			102	577	548 / 588	677	648 / 688
NPS	in	in	Cv	Cv	Cv	Cv	Cv
1/2 3/4 1	0.25	0.50	0.02,0.05 0.1,0.2	---	0.2, 0.5, 1.0	---	0.5 1.0
	0.375	0.50	---	1.0, 1.5 2.5	1.5 2.5	0.1, 0.2, 0.5 1.0, 2.5	1.5 2.5
1/2	0.8125	0.50	---	4, 6	4, 6	5	4, 6
3/4	0.8125	0.50	---	4, 7.5	4, 8	5	4, 8
1	0.8125	0.50	---	4, 8.5	4, 9	5	4, 9
	1.0625	0.50	---	13	13	---	13
1-1/2	1.25	0.75	---	20	10, 20	20	10, 20
	1.5	0.75	---	10, 17, 28	10, 17, 28	10, 17	10, 17, 28
2	1.5	0.75	---	10, 17, 28	10, 17, 28	10, 17	10, 17, 28
	2.0	0.75	---	30	30, 50	30, 50	30, 50

Figure 31. Excerpt from Fisher Baumann globe valve bulletin (24000 series product bulletin) (Fisher, 2009)

3.0 FUEL FEEDING SYSTEM EVALUATION

3.1 MATERIALS AND METHOD:

A fuel feeding system was developed for conveying MBM (meat and bone meal) into the atmospheric fluidized bed gasifier that was constructed for the University of Saskatchewan Chemical Engineering Department. This fuel feeding system was sequentially tested and analyzed to ensure adequate performance with regards to reliability and stability of flow, and prevention of material plugging within the feeding apparatus. MBM was used as the test feedstock for these experiments, and was sourced from Saskatoon Processing Co., a local rendering plant.

Initial feeding trials to determine the optimal method for conveying biomass into the FBG pilot plant, were performed using MBM as fuel, by Ben Albietz, a summer researcher working for Dr. T. Fonstad. The trials that were conducted included sequential testing of approximately 40 different specific apparatus setups (such as in Figure 22), which tested various permutations of feeding systems, including different diameters and combinations of screw conveyors, different types of conveyor flighting, vibratory feeders, and included development of a pneumatic injection port for this purpose.

The final recommendation, as indicated in Figure 32, was a feeding system consisting of two screw conveyors connected in series, with a pneumatic injection port to discharge the MBM into the fluidized bed (Albietz and Fonstad, 2007).

Figure 32. MBM fuel feeding final test apparatus,
(Albietz and Fonstad, 2007)

The first screw conveyor would be of larger diameter, 150 mm, and would draw the MBM or other biomass from a storage hopper. This conveyor would be used to control the feeding rate of the fuel into the FBG, and would be equipped with a 3 phase electric motor and a variable speed drive for this purpose. Testing of similar conveyors yielded that the desired feed rate of 1-5 g/s could be achieved by operating a 150 mm conveyor within the range of 0 – 1 rpm. This main conveyor would discharge into the feed hopper of a second smaller screw conveyor of 45 mm to 55 mm diameter, with ribbon-screw type flighting. The benefit of this open type flighting was that it will resist the tendency for the MBM to compact and plug in the auger tube, as any resistance to flow would result in material remaining in place, rather than being compressed, as in a closed-flight conveyor. This second conveyor would be operated at a higher rotational rate, approximately 10-100 rpm depending on the feed rate. This conveyor was to be operated by 3-phase electric motor and variable speed drive as well. Finally, for interfacing these feeders with the FBG, a pneumatic injection port was designed (Figure 33), which would narrow the 50 mm opening of the injection screw to 12-17 mm, and force the fuel through this narrow opening with the addition of compressed air at approximately 550 kPa and 80 lpm flowrate.

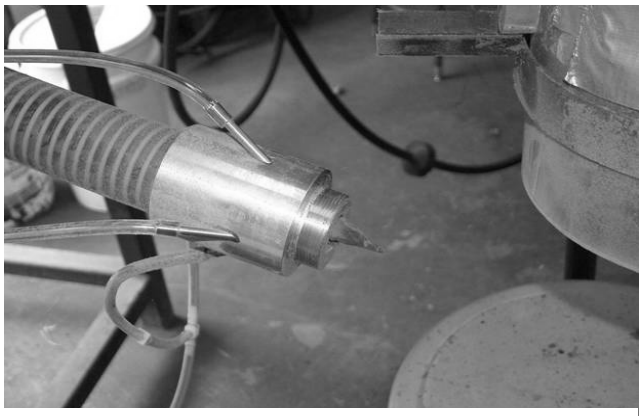

Figure 33: Pneumatic injection nozzle prototype
(Albietz and Fonstad, 2007)

The purpose of this nozzle was to provide as small an opening between the feeding system and the fluidized bed as possible, to minimize intrusion of the bed material into the fuel conveyor. Additionally, the addition of pressurized air to the fuel would result in a spraying of the powdered fuel into the fluidized bed, and hopefully result in improved fuel dispersion within the bed.

Based on these recommendations, and on the designed layout of the FBG pilot plant, design of the plant fuel feeding system was undertaken. The recommendations were taken, and adapted to the physical layout (Fig A-3 – Appendix A) and desired fuel storage capacity (0.15 m^3) of the pilot plant, which affected the footprint dimensions of the conveyors, as well as the structural supports required for the equipment. In addition, it was a requirement that the fuel discharge rate from the system be measured during operation; therefore an examination of methods to perform this was undertaken. Two basic methods were evaluated which would be applicable to this installation, including impact type flowmeters, and load cell based loss-of-weight systems. Based on practical applicability to this pilot plant, due to its specific flow rate range, load cells were selected as the method for calculation of mass flow rate for this system.

The fuel feeding system for the FBG pilot plant that was developed, included a 0.150m^3 storage hopper, the recommended 150 mm metering screw, 150 mm rotary airlock, injection surge hopper and 50 mm shaftless injection screw, and 4-port pneumatic injection nozzle (Figure 34).

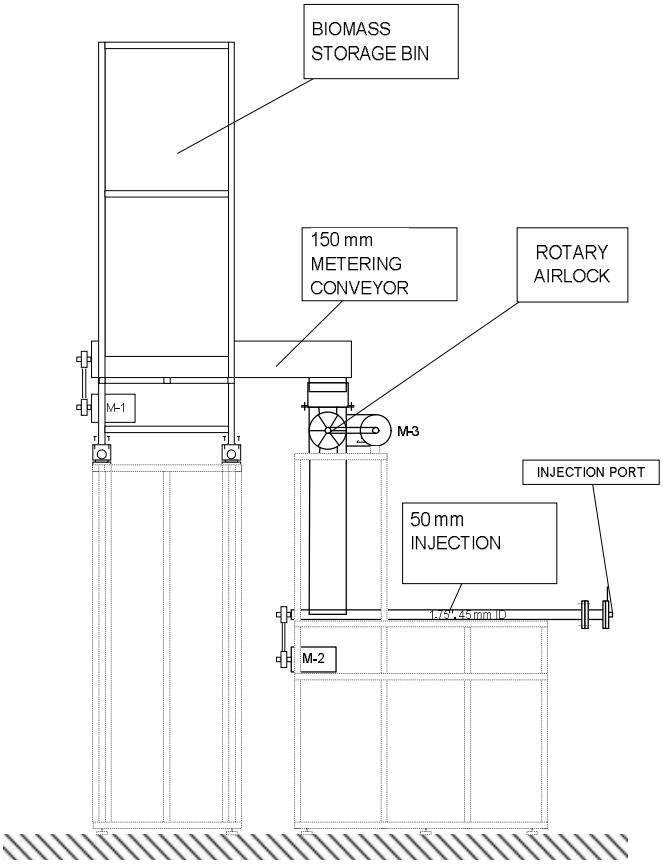

Figure 34: Fuel feeding system final design

The dual conveyor system was developed, as this is a typical method for FBG fuel feeding. This method has the advantage of isolated storage and injection points, finely controlled metering (slow metering conveyor), and regular output rate (fast injection conveyor). The 150 mm metering conveyor will draw fuel slowly from the storage hopper, discharging into an isolating rotary airlock, between the two conveyors. Injection of MBM into the reaction chamber on the other hand, required a smaller conveyor and end nozzle so as to maintain containment of the fluid bed material within the reaction chamber. This is also a very common type of arrangement used in biomass FBG pilot and larger scale plants, such as the air-blown BFBR gasifying orujillo and MBM at the University of Seville (Gomez-barea, 2006), and the air-blown FBR at Iowa State University (Smeenk et al, 2009). The motorized screw conveyors utilize variable frequency drives and inverter duty motors operating at 230VAC 3 phase and 60 Hz, so as to be able to adjust their rotational rate, and thus the fuel mass-flowrate into the FBG.

Prior to testing of any motorized equipment, the correct rotational rate range for the 150 mm screw conveyor had to be determined. The system at this point consisted of only the 0.150 m^3 hopper, the integral 150 mm screw conveyor tube, and flighting. The motor that had been procured for this conveyor was a 0.19 kW (0.25 HP) 208 VAC 3p motor, with 1800 rpm speed at 60Hz, though it was not installed at that point. Determination of the rate range would allow for correct sizing of the gearbox and additional chain drive gear reducers. The desired rate for the system was to be 1-5 g/s, therefore a rate range which encompassed this flowrate was desired. This rate range was determined by manual rotation of the conveyor flighting, when filled with MBM, onto a digital balance scale, until a preset mass was achieved, then converting that mass to the output rate of the conveyor, using the following formula:

$$R = \frac{M}{Cr}(\text{grams}/\text{rotation}) \qquad (17)$$

Where: M = sample mass (grams), Cr = # of Rotations

This value R was used to determine the maximum and minimum required rotational speeds (S_{min}, S_{max}) to achieve the desired 1-5 g/s flowrate (F_{min} to F_{max}).

$$S_{(min/\ max)} = \frac{F_{(min/\ max)} \times 60}{R} (rotations/min) \quad (18)$$

Once the correct speed for the metering conveyor was determined, the gearbox and additional gear reduction would be determined. Once the individual components were completed, the two conveyors and the rotary airlock were installed in the pilot plant, and connected to the variable speed drives and to the voltage supply panel. At this point, full testing of the motorized equipment commenced.

Testing of the fuel feeding system consisted of operation and data collection for 3 different assemblies. The three assemblies represented the sequential and linear construction of the complete fuel feeding system, beginning at the top end with just the metering conveyor (Assembly 1), and then adding the rotary airlock and injection screw (Assembly 2), with finally the attachment of the injection nozzle (Assembly 3). By operating and collecting data for each assembly, the impact of added equipment could be assessed with regard to the output rate and the deviation of that rate.

3.1.1 ASSEMBLY 1

Assembly 1 included only the metering screw conveyor (150 mm), feeding MBM from its 0.15m^3 storage hopper, and discharging into a sample container positioned on top of a Mettler Toledo 3.8kg digital balance scale (Figure 35). The balance scale was connected to the pilot plant PC (DAQ-PC), through the data acquisition system via a serial (9-pin) cable. A Labview subroutine was created to continuously sample and log the scale reading using the Modbus protocol to communicate with the scale. Other data that were collected at the same time were the conveyor speed setpoint and weight transmitter reading. Assembly 1 was operated at 7 different speeds, including 5, 10, 15, 20, 25, 50 and 100% of full speed rotation.

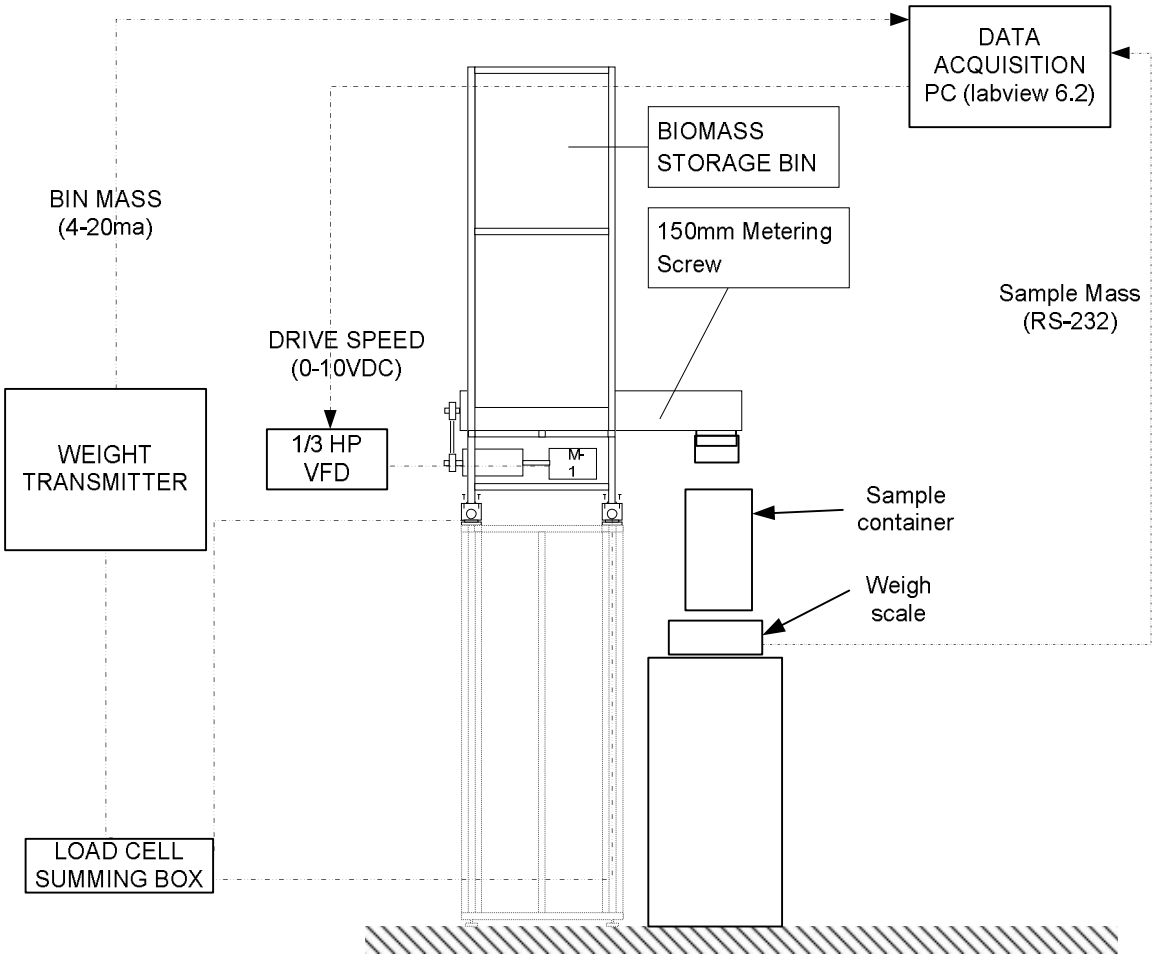

Figure 35: Fuel feeding system testing Assembly 1

3.1.2 ASSEMBLY 2

Assembly 2 included the metering screw (Assembly 1), 150 mm rotary airlock, and 50 mm injection screw, with the injection screw conveyor discharging into the sample container on the transmitting balance scale, as in Assembly 1. This is illustrated in Figure 36. An optimal speed for the rotary airlock was determined first, that is the minimum speed which allows for unimpeded flow of MBM. Faster speeds would be less desirable, as they would result in greater air leakage through the airlock from the pressurized side to the unpressurized side.

The two conveyors were then operated at different percentage of full speed speeds to determine the optimum rotational rate or rate relationship between these mechanisms to produce the most consistent, regular and predictable output as measured by the continuous scale reading.

Additionally, fuel movement was observed through the system to ensure that no bottlenecks or plugging points interrupt or restrict flow.

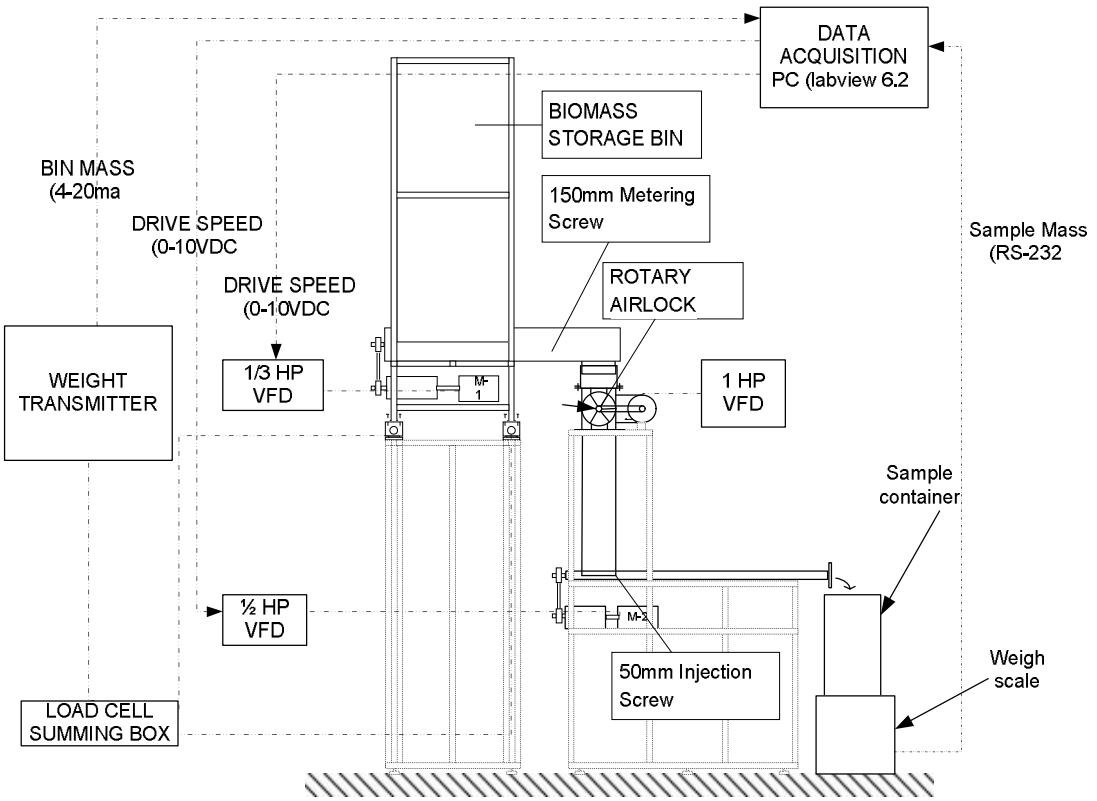

Figure 36: Fuel feeding system testing Assembly 2

3.1.3 ASSEMBLY 3

Assembly 3 included the components of Assembly 2, in addition to the pneumatic injection nozzle (Figure 37). This Assembly was tested in the same method as Assembly 2, with the addition of testing different injection nozzle air flowrates, to both minimize the required air flow rate, and optimize the system fuel flowrate stability. Injection air flowrate would begin with 80 lpm, the recommended rate from preliminary testing, and the impact of increasing and reducing this flowrate would be examined.

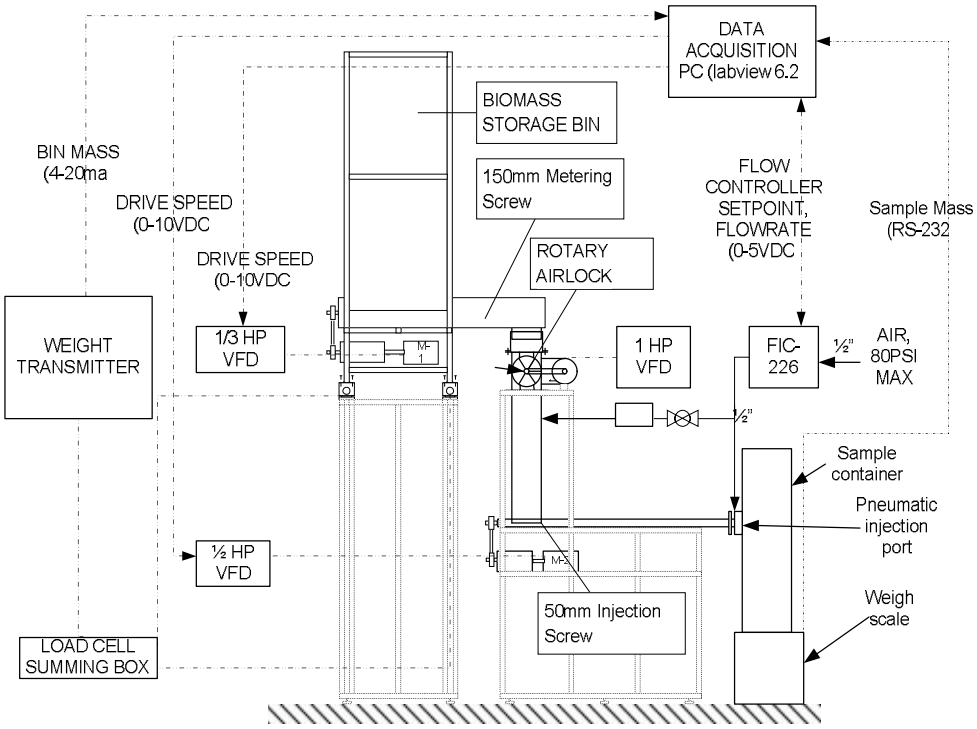

Figure 37: Fuel feeding system testing Assembly 3

For testing of each of these assemblies, the trials were conducted in short time frames of several days. It should be also mentioned that the same fuel supply was reused several times in this period, due to the small supply available at the time. Repeated tests using the same sample could be subject to some error due to the possibility of density change to the fuel during the time period. Subsequent fuel supplies also could have somewhat different densities, due to the inherent variation in feedstock supply for MBM production. System output characteristics that are determined, therefore, may be subject to change for these reasons, and results may not necessarily be repeated. However, continued operation of the system does rely on the system characteristic determined, and this characteristic is recalibrated periodically, and it is also checked against the recorded weight signal from the weight meter system.

3.1.4 DATA ANALYSIS METHOD

Each Assembly (1-3) was evaluated and characterized by logging of output feed rate, captured by a Mettler Toledo scale connected to a Windows PC, using Labview software. A sample of approx 3000-3500 grams was received by the container on the scale, as 4.0 kg was the measuring limit of the balance used. The storage hopper also provided an instantaneous mass output via 4

load cells installed beneath each primary support member. Each load cell was a 50 kg (max) Vishay-Nobel model #(KIS-2-0.5KN, connected to an electronic summing box (Vishay-Nobel Model #306), combining their voltage output signals The summing box transmitted the total weight signal to the weight transmitter (Vishay-Nobel Model#LCp-200), which in turn transmitted a 4-20mA signal to the data acquisition system, proportional to a 0-200kg value. The metering conveyor/hopper weight was sampled by the data acquisition system with an interval of Ts=0.5s, and was subsequently plotted using MS Excel©. The average rate of change R(t) for the scale was then plotted for intervals of 60 seconds, to characterize the smoothness and fluctuation of the output rate. This rate was calculated using the following Formula:

$$R(t) = \frac{m_t - m_{t-60}}{60\,\text{seconds}} \ (\text{g/s}) \qquad (19)$$

Where: m_t = metering conveyor mass at current time (0 seconds)

m_{t-60} = metering conveyor mass at time t-60 seconds

This mass flow rate was calculated for each dataset, which was sampled every 0.5 seconds. The continuous mass flow reading was then statistically analyzed to determine the mean value, median, mode, standard deviation, range, minimum and maximum values, and the data count. A data range from each test was selected for analysis that represented the steady state operation of the feeding system, after any initial output deviations.

3.1.5 HOT SYSTEM COMMISSIONING

Once an optimum combination of conditions and controls were achieved, the feeding Assembly 3 was coupled to the hot fluidized bed, and combustion/gasification of the fuel material was carried out. At this point, the fuel feeding rate was estimated, based on the conveyor speeds during operation, and the characteristic equation determined in the previous testing. The flow throughput was confirmed by checking the estimated output rate against the metering hopper mass from before and after the test. In addition, the effect of fuel being added to the hot fluidized bed was assessed through the temperature fluctuation of the fluidized bed, both during fuel addition and the observed temperature change that occurs after cessation of fuel addition.

3.2 RESULTS AND DISCUSSTION

The metering conveyor flighting was manually turned and sampled, with the goal of assessing what its full speed should be, based on the requirement of a 1-5 g/s output rate range. With the aim of isolating the high end of this range (5 g/s), a 300 gram sample was collected, which would yield the number of rotations corresponding to 5 g/s for 60 s, which is 300 g.

Manual testing of the 150 mm flighting yielded the desired output of 300 g over approximately 0.25 rotations of the metering conveyor. This yielded an R (g/rotation) value of 1200 g/rotation, using Equation 16, setting M= 300 g, and Cr = 0.25. The variable speed drive that was purchased (Automation Direct GS1 series), was capable of operating the purchased motor from 3Hz to 120Hz, or from 5% to 200% of the motor's full speed.

$$R = \frac{300g}{0.25 rotations} = 1200 g/rotation \tag{20}$$

Using equation 17, and setting F_{min} = 1 and F_{max} = 5:

$$S_{min} = \frac{1.0 \times 60}{1200} = 0.05 RPM = 0.05(\text{VFD min rate}) \times FS \Rightarrow FS = 1.0 rpm \tag{21}$$

$$S_{max} = \frac{5.0 \times 60}{1200} = 0.25 RPM = 2.00(\text{VFD max rate}) \times FS \Rightarrow FS = 0.125 rpm \tag{22}$$

The full speed of the conveyor would therefore need to be at least 0.125 rpm, and as high as 1.0 rpm (see sample calculation D-3), to include the above output rate range within its rotational operating range. A full speed of 1.0 rpm was established as a target based on this calculation.

Investigation into gearbox systems revealed that a 600:1 unit was most economical, which would bring the 1800 rpm motor down to 3 rpm. Further reduction of this rate was to be accommodated via reducing chain gears, from the gearbox to the screw shaft. Gear reducers were installed to deliver a base full speed (100%) of FS=1rpm, or a reduction of 1800:1, meaning that the chain gear reducer ratio was 3:1. The desired maximum output range of 5 g/s could therefore be achieved by operating the conveyor at 25%FS using the VFD, and the minimum rate

of 1 gram/second could be achieved at 5% FS. Using the low end of the feeder range for this feedstock would allow for future use of lighter (less dense) feedstock, over the same mass flow range, using the upper portion of the feeder rotational rate range.

3.2.1 ASSEMBLY 1: METERING CONVEYOR

Testing of Assembly 1 concerned the output rate of the metering conveyor at 7 different drive control setpoints, from 5% to 100%, with the output rate calculated from the data collected by the Data Acquisition PC, transmitted from the digital balance. The scale derived flowrate result was checked against the received signal from the feeder weight transmitter, which also transmitted the metering hopper weight continuously to the data acquisition system.

For a metering conveyor drive setpoint of 25%, the scale reading and calculated flow rate for one trial are presented in Figure 28. Analysis of the flow rate data for this trial for Δt of 60 s yield a mean rate of 4.80 g/s, standard deviation of 2.22 g/s, and range of 7.66 g/s. What can be interpreted from this data is that over the short term, in time quantities of less than 5 minutes, there is a great deal of irregularity to the output rate. Over longer periods of time, such as 15 minutes or more, however, the average output rate will be regular and predictable, and the fuel feeding system should be utilized in this time frame. For example, the very extreme pulses in Figure 38 do recur every 250 seconds or so, in a fairly predictable manner.

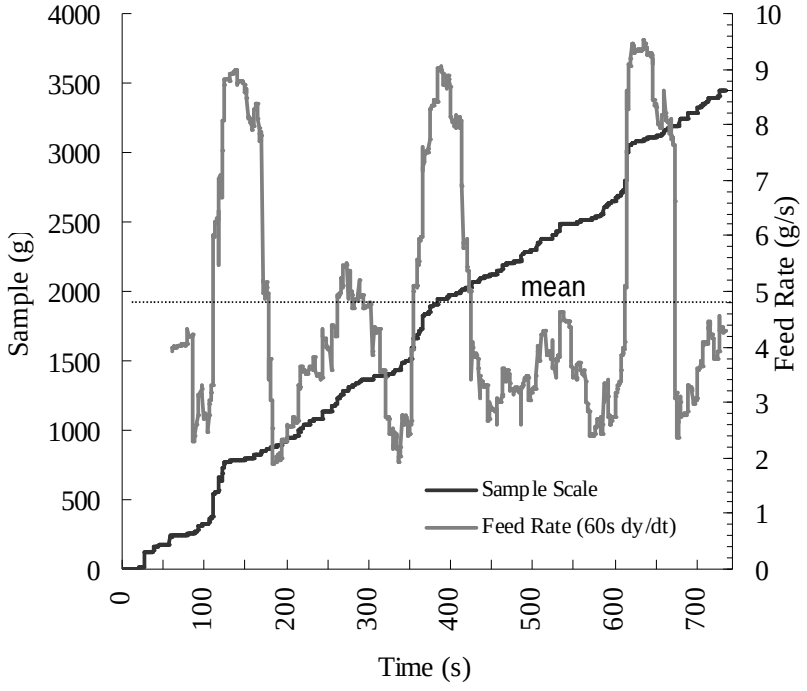

Figure 38: Assembly 1 results for 25% speed operation

These measurements were repeated for a wide range of feeder control rates, from 100%, with a calculated mean feed rate of 19.58 g/s, down to 5% output rate with a calculated feed rate of 0.77 g/s. These results are shown in Figure 39, where the plotted data points indicate the calculated mean discharge mass flow rate vs. the metering conveyor drive speed setpoint. Error bars plotted with these data points represent the flowrate standard deviation. The trend line plotted through these data points illustrates the linear relationship between the conveyor speed setpoint "S" and mean output flowrate "FM", and is summarized by equation 23.

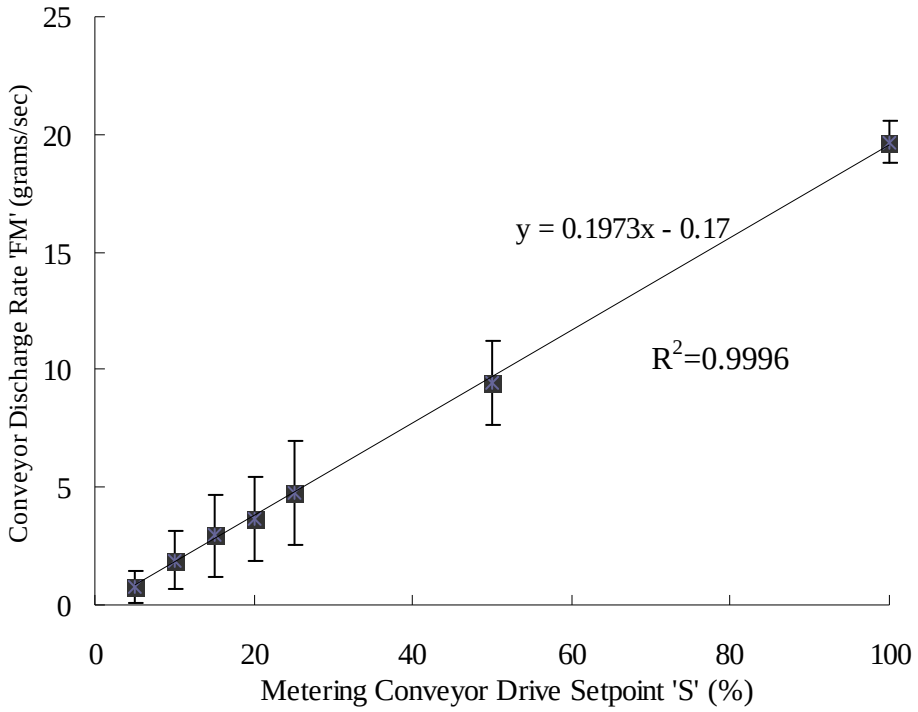

Fig 39: Assembly 1 results for 5-100% speed range
(Error bars are +/- 1SD)

$$FM = 0.197 \times S - 0.170 \quad (23)$$

The sum of squared errors was 0.9996 for this characteristic prediction, compared to the collected data. Because an output range of 1-5 g/s was desired, the conveyor control range from of 5% to 25% was isolated, and examined specifically for the subsequent tests of assemblies 2 and 3, as this roughly corresponded to that desired output range.

3.2.2 ASSEMBLY 2: COUPLED CONVEYORS

Assembly 2 was examined, which included the 150 mm metering conveyor that discharged into the 150 mm rotary airlock, and then from the airlock into the hopper of the 50 mm injection conveyor. The output of this assembly was measured and analyzed. For 25% (of full speed) metering conveyor and injection conveyor rates, and 15% airlock speed (~15 RPM), a feedrate of 5.37g/s was achieved with a standard deviation of 0.21, and range of 1.33 (Figure 40). The characteristic system relationship between conveyor VFD setpoint (%) and output rate (g/s) is illustrated in Figure 41, and is:

$$FM = 0.22 \times S - 0.36 \quad (24)$$

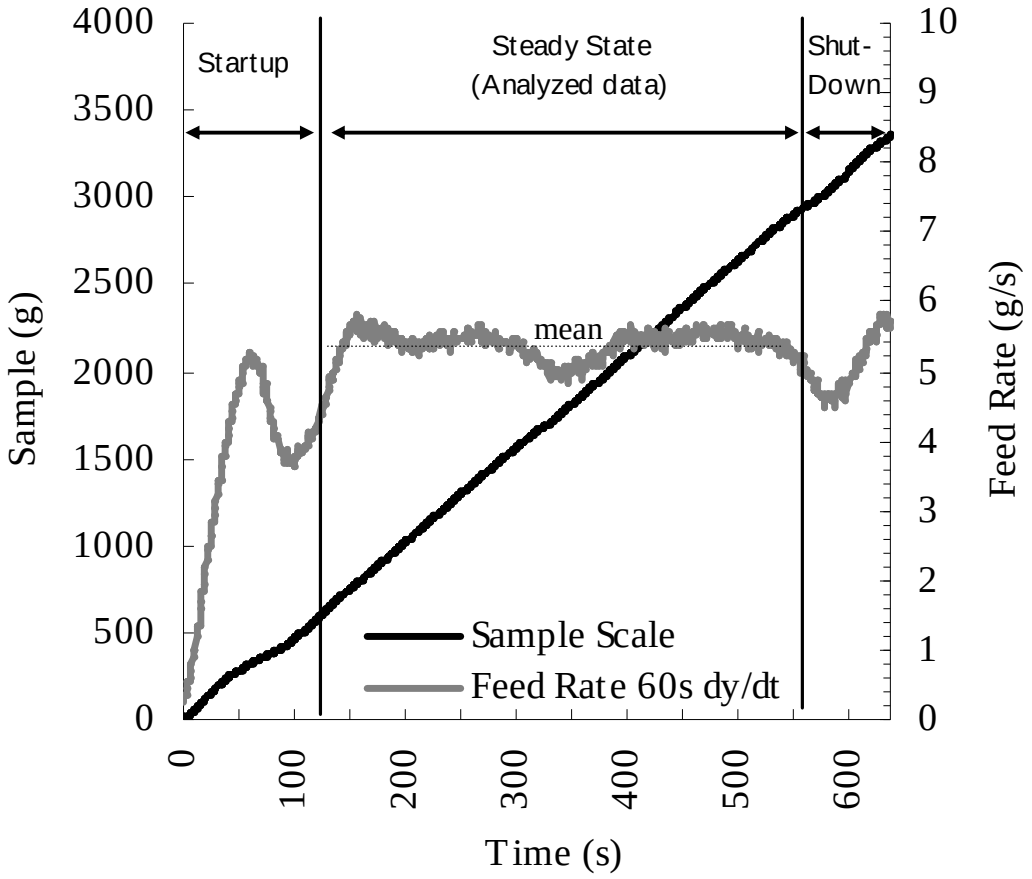

Figure 40: Assembly 2 results for 25%/25% speed operation
(Both conveyors running at 25% of full speed)

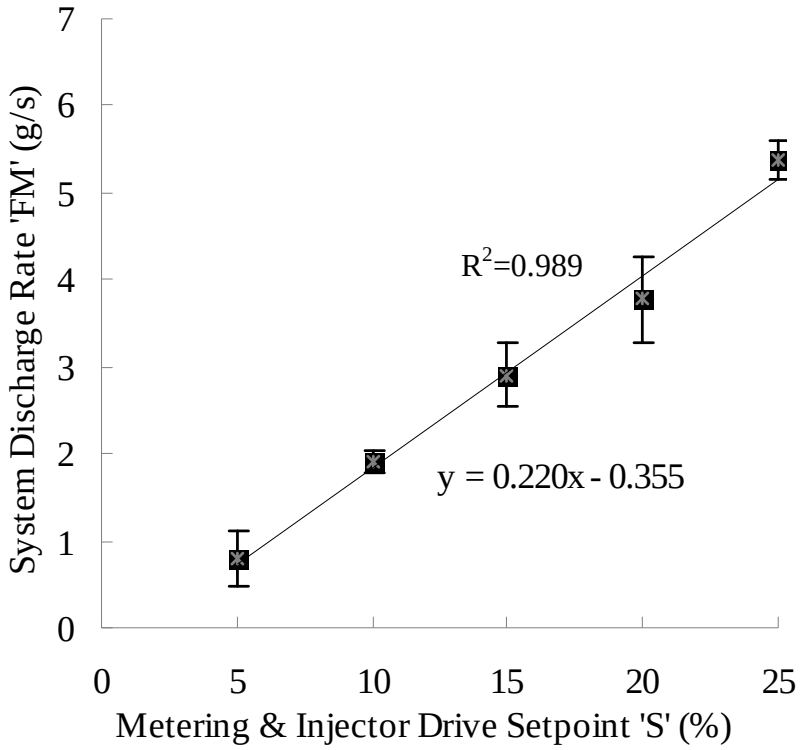

Figure 41: Assembly 2 results summary for 5-25% speed range

Operating at significantly lower injector speeds resulted in significant material accumulation in the injector hopper, as well as reduced overall output rate, although slightly slower injection conveyor speeds did result in somewhat less deviation. Higher speed ratios (injection speed vs. metering speed) were tested, and generally resulted in greater deviation in the output rate, as can be observed in Figure 42 and 43, where these results are compared for a higher ratio of 1.5 in Figure 42, and 1.0 in Figure 43.

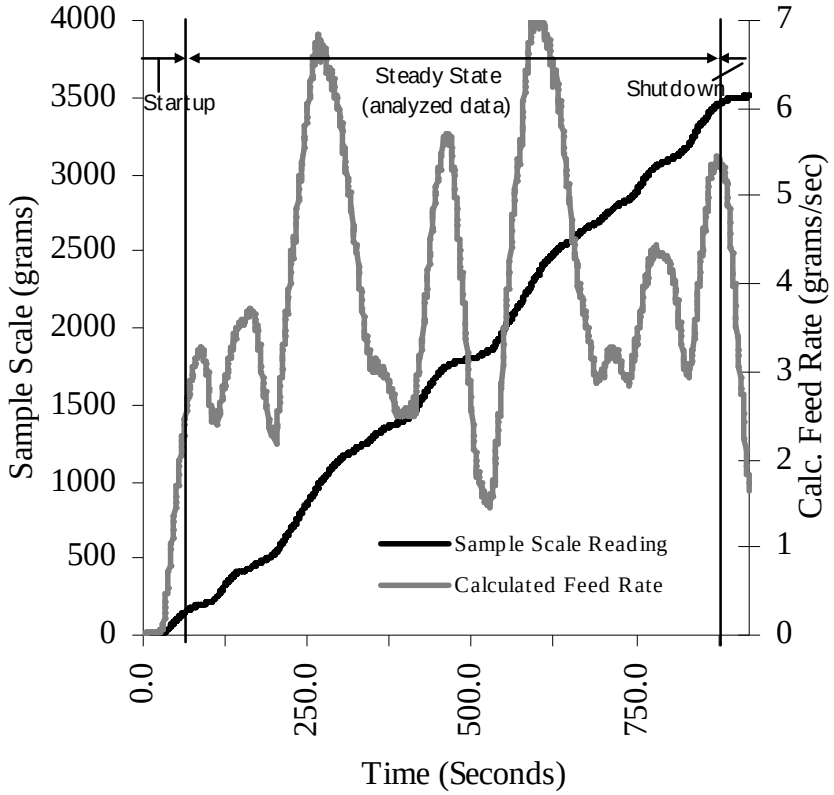

Figure 42: Assembly 2:
Injection conveyor at 1.5x speed rate of metering conveyor

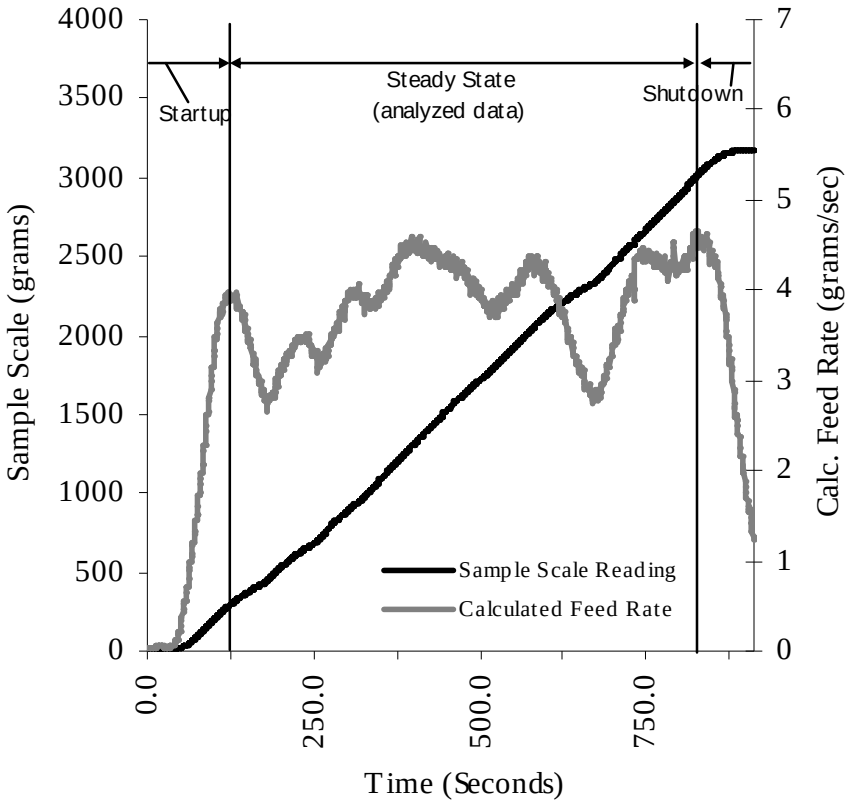

Figure 43: Assembly 2:
Injection conveyor at equal % rate to metering conveyor

It was generally found that matching the output speed of the metering conveyor to the injection conveyor produced an output rate with the lowest standard deviation, while allowing the injection conveyor to keep up with the output of the metering conveyor. Operation of the rotary airlock at 15 RPM (15% VFD setpoint) was found to be the slowest speed this airlock could be operated at, while still maintaining consistent flow through the system.

It was generally found that MBM would accumulate in the narrow hopper feeding the injection conveyor, resulting in bridging and plugging of this hopper. Several methods were implemented and examined to prevent this plugging, beginning with a bin vibrator mounted to the side of the injection hopper, which was not found to be effective. Next, an array of air injection ports was added to the base of the injection hopper, as well as a plexiglass observation window on the side of the injection hopper (Figure 44). A pair of solenoid valves were used to control the flow of air

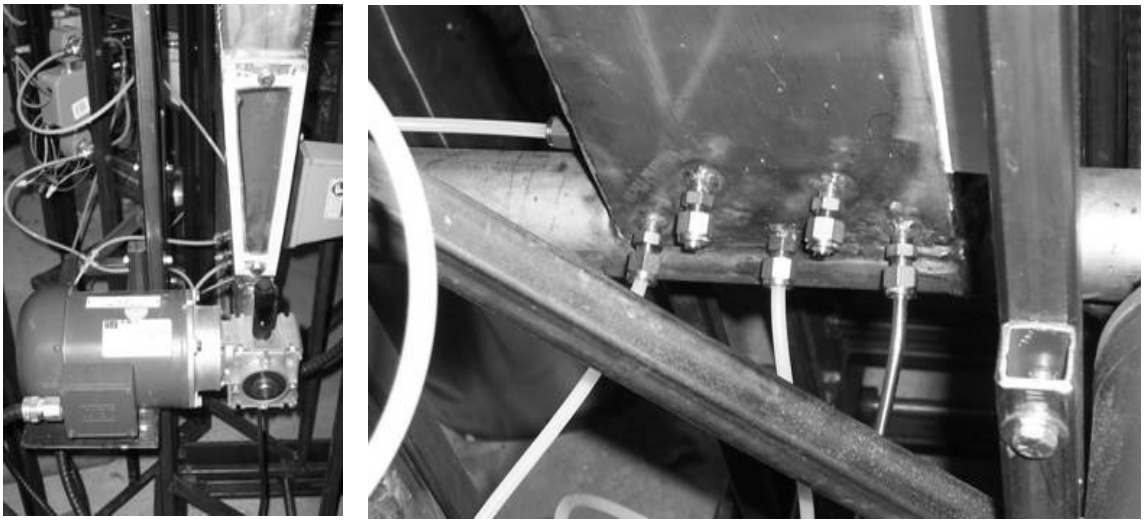

Figure 44: Injection hopper modifications
(plexiglass observation window - left, and air sparging ports - right)

to the sparging ports, and a programmable timing relay (Telemecanique Zelio-relay) was connected to the electric solenoid valves to control the duration of air pulses. Pulsing 1 second bursts of air into five 6.5 mm (1/4") ports in the injection hopper every 12 seconds was found to effectively prevent bridging of MBM in the injection hopper.

3.2.3 ASSEMBLY 3: CONVEYORS AND INJECTION NOZZLE

Testing of Assembly 3 was next, which included mounting the pneumatic injection port to the discharge end of the 50 mm injection conveyor. It was planned at this point to test the system, while pressurizing the injection conveyor and hopper slightly, using the rotary airlock to seal this pressurized system. A pressure of at least 7-10 kPa would be required (~1 psi) to exceed the expected pressure of the hot fluidized bed. However, when an attempt was made to pressurize the system, it was discovered that the rotary airlock did not seal well enough to contain the pressure, and leaked well in excess of 200 lpm of air without pressurizing. It was at this point that the metering conveyor and hopper were physically coupled to the rest of the system, to enable pressurization of the injection hopper and conveyor, while pressurizing the metering conveyor and hopper. The metering hopper was therefore pressure sealed, through installation of a hatch with a seal gasket, and coupling the metering conveyor to the rotary airlock with a rubber coupling (Figure 45).

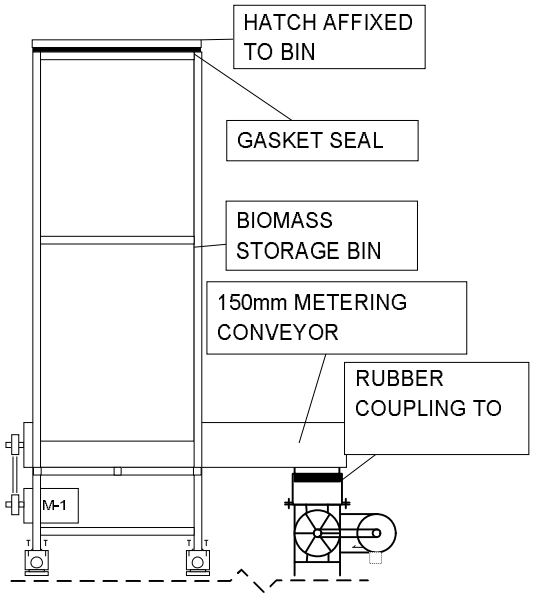

Figure 45: Illustration of metering conveyor sealing for pressurization

This unfortunately introduced a great deal of noise into the mass measurement of the feeder hopper, due to the pressure induced force on the discharge end of the metering conveyor.

At this point testing of Assembly 3 began, discharging MBM into a sample container, again on the digital balance. The output results from a combination of 25% feeder and injector conveyor speeds, 50 lpm injection air, and air sparging at 15 lpm are shown in Figure 46. Analysis of

these data was found to produce a mean output rate of 5.43 g/s at steady state, with a standard deviation of 0.155 g/s, and a value range of only 0.78 g/s. This combination resulted in the best overall output rate (least deviation) and no plugging events in the injection hopper. These results were equally satisfactory for lower feed rates at 10%, 15%, and 20%, though testing at 5% did result in some increased deviation. Figure 47 illustrates the conveyor speed to fuel output rate relationship for this final Assembly, for the speed range of 5-25% (same speed for metering and injection conveyors):

$$FS = 0.219 \times S - 0.42 \tag{25}$$

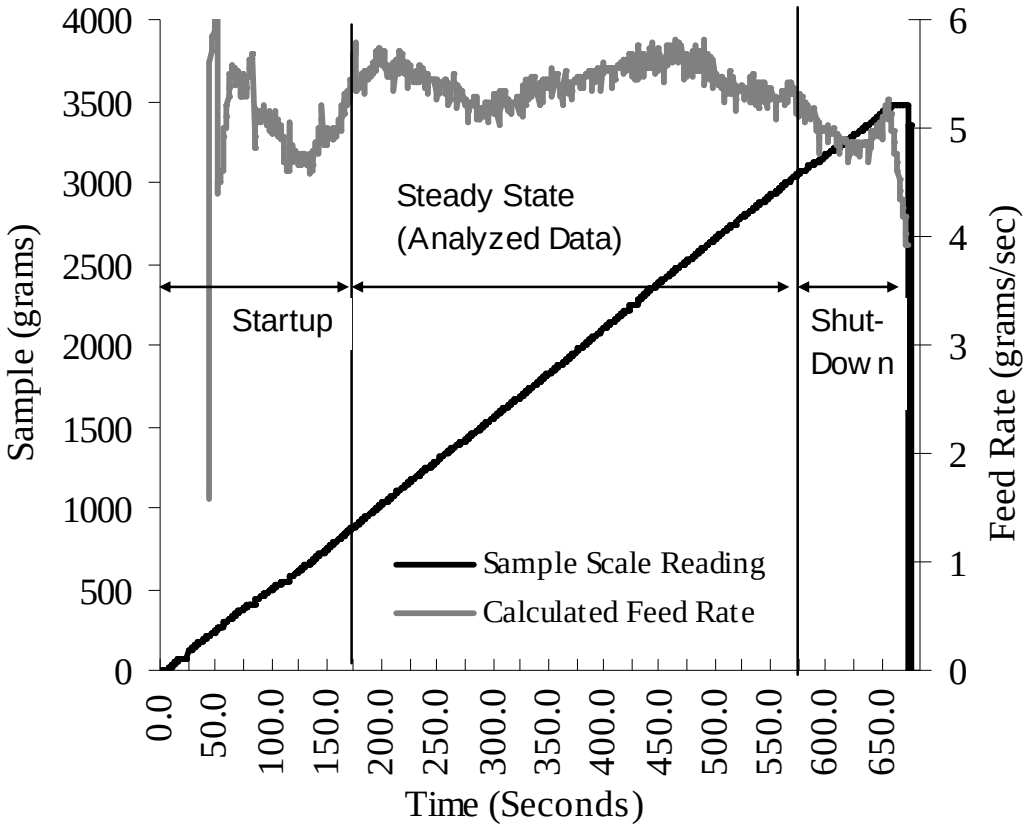

Figure 46: Assembly 3 results for 25%/25%/50 lpm operation

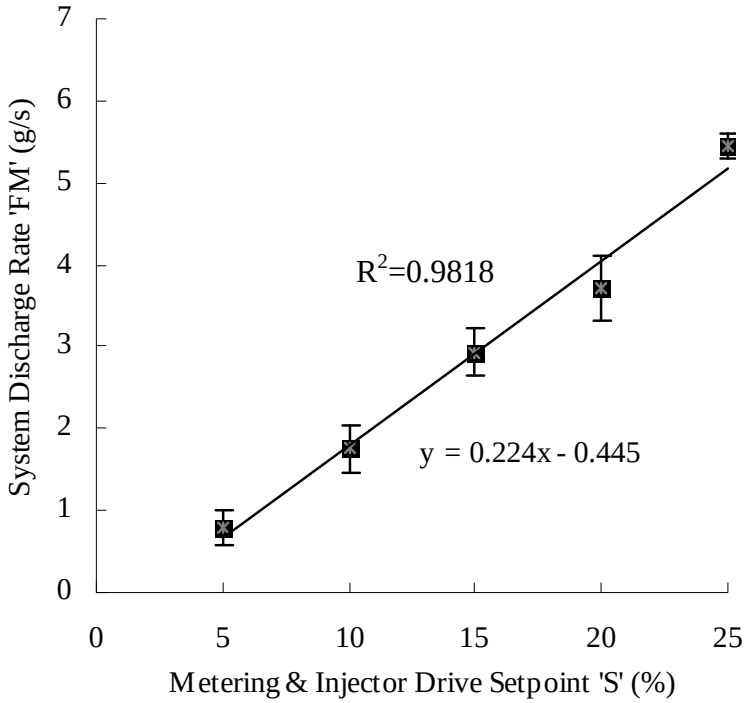

Figure 47: Assembly 3 results summary for 5-25% speed range

With regards to using the load-cell based weight meter to calculate the continuous fuel output rate of the coupled system, Figure 48 illustrates the difficulty with this procedure. The output rate, as calculated from the system weight meter using the same formula as used on the sample scale output has a great deal of noise. Though the load cell derived flowrate had a mean (average) value that is near the sample scale value (Table 2), its range (total span of analyzed values) and standard deviation (square root of variance) render the value and its calculation quite difficult and prone to error. Other descriptive statistics in this table include the standard error (standard deviation of the sampling distribution), median (the value dividing the probability distribution in half), minimum, maximum and count (the total number of sample points).

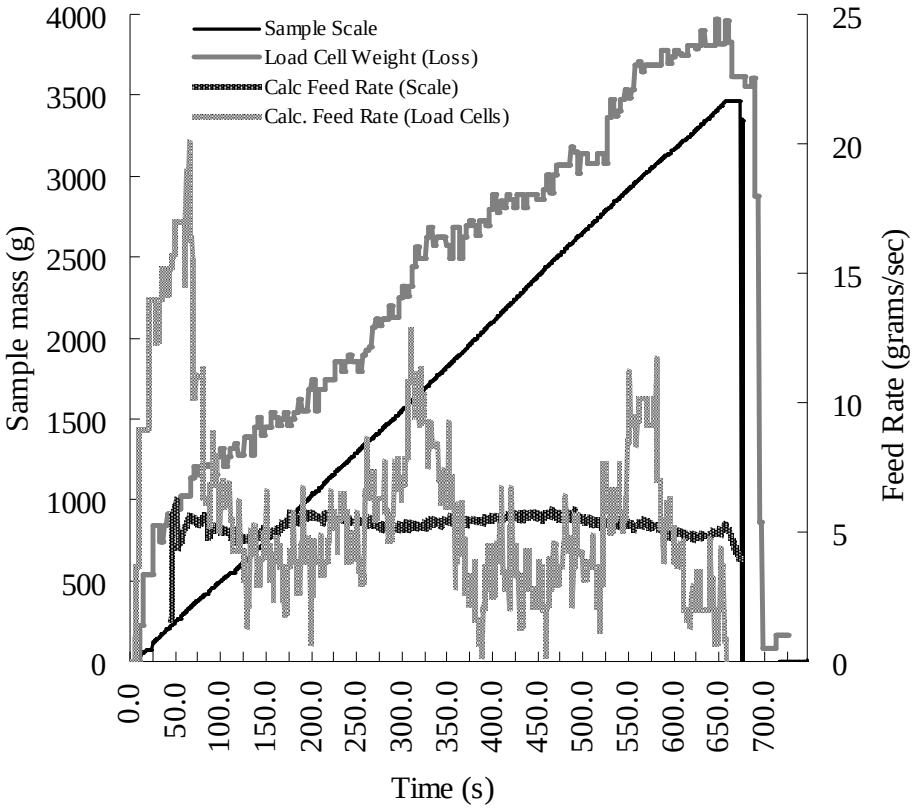

Figure 48: Assembly 3 - Comparison of Sample scale and Load cell flowrate for 25%/25%/50 slpm operation

Table 2: Comparison of Rate Calculations by Sample Scale weight, and load cell (weight meter)

	SAMPLE SCALE	WEIGHTOMETER
Mean	5.44	5.09
Standard Error	0.01	0.08
Median	5.44	4.5
Standard Deviation	0.16	2.37
Range	0.78	12.67
Minimum	5.04	0.17
Maximum	5.82	12.83
Count	801	801

3.2.4 FLUID BED GASIFICATION TESTING

The complete Assembly 3 was coupled to the fluidized bed gasifier reactor and the complete system was operated injecting MBM at approximately 1.75 g/s (10% conveyor rates) into a fluid bed heated to 250°C, fluidized with air flowing at 250 lpm. The temperature data collected from this commissioning run is indicated in Figure B-19 (Appendix B), along with key fuel addition points. After several short feed runs at this rate (1 min, 2 min, 5 min), feed was continuously

added to the hot fluidized bed for 55 minutes. Temperature of the fluid bed began to sharply increase at 20 min from start of this feed test, and achieved a warming rate of approximately 0.1 °C/s. Temperature continued to climb until reaching 640°C, at which point fluidization air was decreased to 150 lpm. Maximum temperature of 725°C was achieved at 50 minutes past cessation of biomass addition, after which point bed temperature began to sharply decrease, dropping to 500°C by 90 minutes past cessation of biomass addition.

Preliminary runs of the system using the injection nozzle were relatively successful, up to a bed operating temperature of approximately 750°C. At and beyond that operating temperature the air addition ports on the injection nozzle began to char and plug, resulting in plugging of the injection conveyor discharge (as the functioning air streams are required to clear the discharge point). As a result, for operation of the FBG above 750°C, the pneumatic injection nozzle was removed from the system, and system operation was attempted by injecting fuel directly from the discharge point of the injection conveyor.

Connecting the fuel feeding system to the fluidized bed without the pneumatic injection nozzle results in the fuel conveying system equalizing pressure with the fluidized bed. The effect of this is the ingress of fluidized bed particulate into the fuel feeding system. By continuously operating the injection conveyor however, it is found that the mechanical action of this conveyor effectively prevents ingress of those particles and Operation of the system without the injection nozzle was found to be satisfactory, with some ingression of silica sand from the fluidized bed into the injection nozzle during warm-up, but following start of the feeding system, the sand was discharged from the injector tube, with the tube maintaining a satisfactorily low operating temperature, below 150°C.

Continued operation of the gasifier using air as oxidant, and gradually increasing the peak temperature has produced very successful results using this feeding system. The feeding system continues to operate in a very satisfactory manner, but some problems have been encountered with the bed mass agglomerating (solidifying) at temperatures above 800°C. This may owe to the fact that small ash particles remain in the fluid bed over several runs, and may be binding to the sand particles at critical (melting) temperatures.

4.0 PRESSURE MEASUREMENT TECHNIQUES FOR HOT AND DUSTY GASES

4.1 MATERIALS AND METHOD

Pressure measurement at the high temperatures within a fluidized bed gasifier require special consideration, as the typical temperatures for a fluid bed gasifier, from 800°C to 850°C, are much higher than the typical temperature range for most industrial pressure transducers. For most pressure transducers, the upper functional temperature range is less than 100°C (Wika, 2009). Some specialized transducers may have temperature range of as high as 399°C (PCB Piezotronics, 2010), though this is still much lower than the temperatures of 800°C-900°C within a fluidized bed gasifier.

Two methods will be examined for isolating pressure transducers from hot and dusty gases, with particular focus on the delay effect that these methods have on the pressure measurement. The methods include the use of tubing to isolate and cool the gas medium, and the use of filters to block the flow of small particles into the measuring tube, or onto the transducer surfaces. These methods will be examined using a cold test apparatus, and using pressurized air as the gas medium.

4.1.1 EXPERIMENTAL APPARATUS

The apparatus for pressure sensor testing consisted of a small compressed air carry tank, with a 6.35 mm (1/4") manifold connected to the open port on the tank (Figure 49). To the manifold are connected two 6.35 mm (1/4") needle valves, one connected to the building air supply, the other vented to atmosphere. As well, a 6.35 mm (1/4") mechanical pressure gauge and the two pressure sensors are connected to the manifold. One pressure sensor (pressure sensor A) is mounted directly to the manifold, while the other (pressure sensor B) is connected to the manifold through the variable isolating system, consisting of a variable length of polyethylene tubing, and/or a porous plate filter. The pressure sensing isolating tube will have three possible lengths, 0m, 3m and 30m.

The pressure sensors used were Omega series PX142-015D5V sensors, 0-103 kPa (0-15 psi) range, transmitting the pressure via voltage signal 1-6 VDC, powered by 8 VDC power supply. This pressure sensor has hysteresis error of 0.15% FS (Omega, 2010).

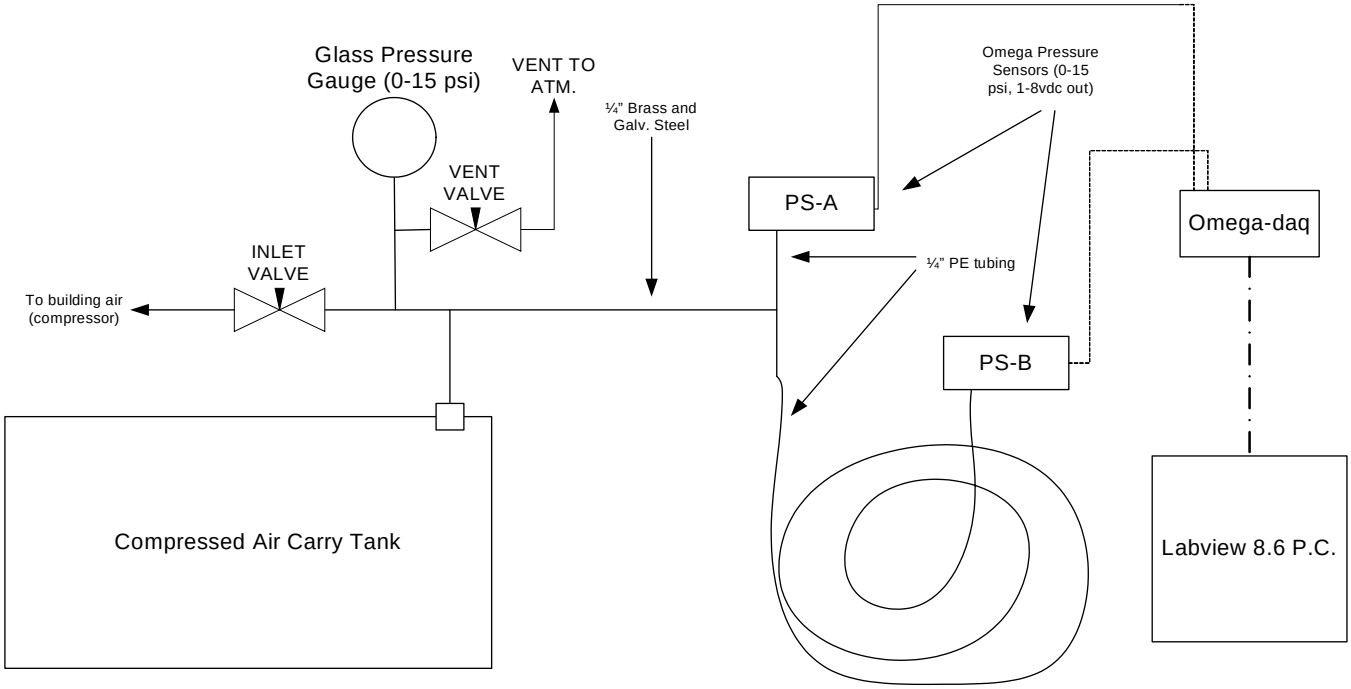

Figure 49: Pressure measuring fluid isolation methods testing apparatus

4.1.2 EXPERIMENTAL METHOD

The data acquisition system was set up to record the sensor pressure values five times/second. The experiment was started using both PS-A and PS-B sensors directly mounted to the manifold, using essentially zero length sensing tubes, without filtration. The pressure tank is filled with air from the local compressor by opening the needle valve slightly to achieve a pressure rise of approximately 0.5 to 3.0 kPa/s, up to a maximum pressure of approximately 100 kPa. This pressure is held briefly, then the venting needle valve is opened slightly to achieve pressure drop rate of about -1.0 kPa/s. This process is then repeated twice, for each setup.

This process is repeated, with the pressure sensing tube connecting sensor PS-B lengthened to 3.0 and 30 m. The procedure is repeated again, with the grade 10 media porous plate filter added in-line for each tubing length, including 0, 3.0, and 30 m. These lengths were selected in order to test the effect of changing tubing length by an order of magnitude, where the actual sensing line length would likely be from 3 to 5 meters in most cases.

After all five trials were complete; the data stream for Pressure sensors A and B was exported from Labview to an Excel-compatible file. For each trial period, the segment of data is isolated where the sensor readings cross 20 kPa. This data segment is then plotted, with the pressure value on the Y axis, and elapsed time on the X axis. For each trial, the time lag (TL) between pressure sensor A and sensor B (if any) will be determined through calculation of the rate of change ($PR_{S)}$ for 0.4 second portions of the isolated data segments, calculating the difference between the signal values, then dividing that difference by the rate of change for the leading signal, to determine the time lag between those signals. The average value of that lag (TL) will then be calculated for the isolated data segment using the following equations.

$$PR_S = \frac{P_{t+0.2} - P_{t-0.2}}{0.4\,\text{sec onds}} \ (\text{kPa/s}) \tag{26}$$

$$TL = \frac{PS.B(\text{kPa}) - PS.A(\text{kPa})}{PR_S(\text{kPa/sec})} \ (\text{s}) \tag{27}$$

TL_{avg} was then calculated for the time segment examined, that time segment encompassing 1-5 seconds of data which covered 1-2 kPa of pressure change, depending on the specific lag presented by the data. This TL average can also be confirmed by visual examination of the data segment.

4.2 RESULTS AND DISCUSSION

Data for the pressure measurement comparison tests is given as two discrete pressure signals for the duration of the test. One signal represents the control sensor, a pressure sensor with a very short sensing tube without any filtering. The second signal was the comparison measurement, transmitting the pressure signal from the variable sensing line. The sensing line in this case was of varying lengths, and may or may not have had a permeable plate filter. By examining the signals from these two sensors, the delay effect of the isolating methods on the signal could be observed and calculated.

Three different tube lengths were examined for the comparison signal, and each length was examined with and without the filter, resulting in five different comparison signals. Figure 50

illustrates the test, where the variable sensing apparatus was a 3 m PE tube. The pressure change rate for this test was 2.67 kPa/s, and the signal delay for PS-B was approximately 0.052 s.

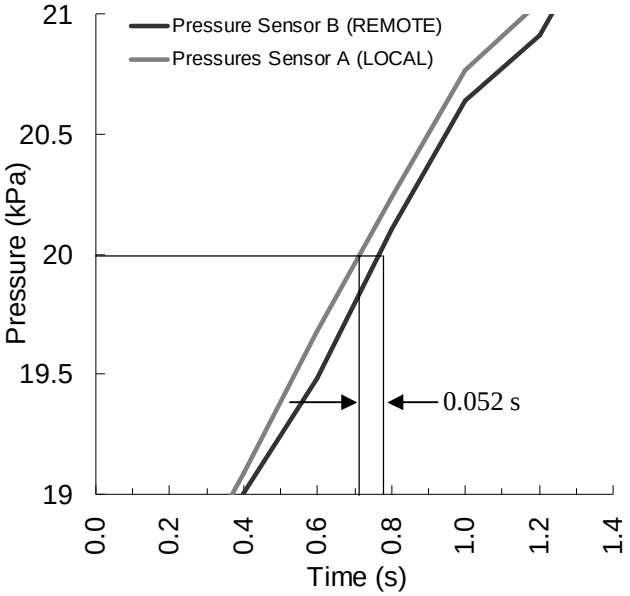

Figure 50: Pressure Sensor Reading Comparison - local vs. 3 m Tube

Figure 51 illustrates the results where a 30 m PE tube is used as the variable apparatus. The delay between the pressure signals at the 20 kPa crossing in this case increased to 0.303 s. The rate of change ΔP/t near the 20 kPa crossing for this test is 1.52 kPa/s.

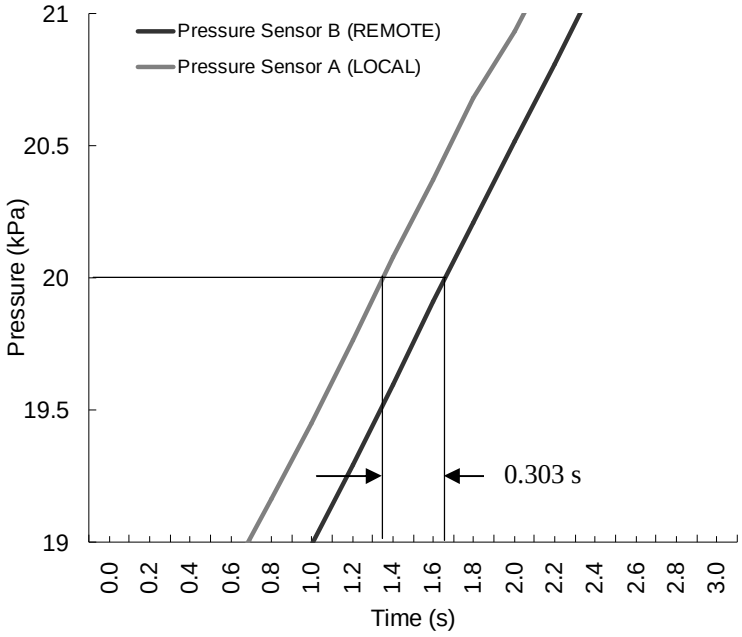

Figure 51: Pressure Sensor Reading Comparison - local vs. 30 m Tube

At this point, the porous plate filter is added to the variable apparatus, beginning with the filter only. Figure 52 illustrates a typical result for this apparatus, with a signal delay of 0.078 seconds, for a rate of change of 1.74 kPa/s.

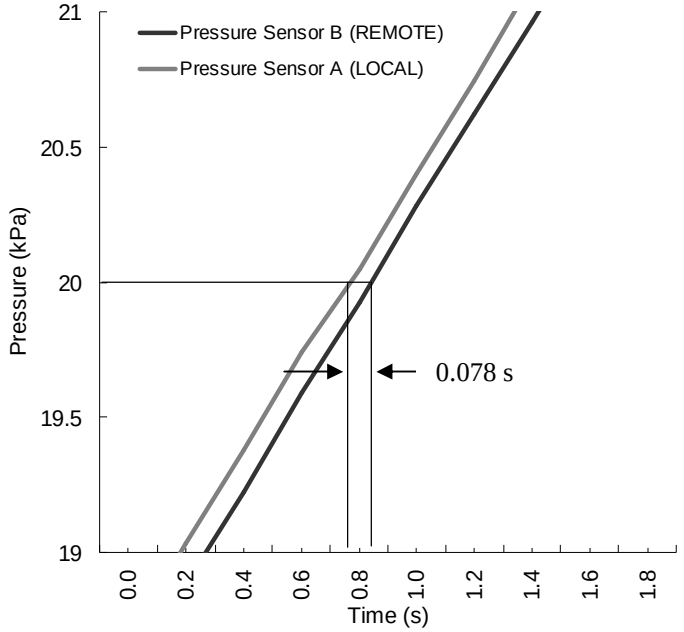

Figure 52: Pressure Sensor Reading Comparison - local vs. filter w/ 0 length tube

The filter is next added to the 3m tube, and this apparatus is tested. The resultant data is shown in Figure 53. Signal delay for this test is 0.20 s, for a pressure rate of change of 2.86 kPa/s, compared to the delay of 0.05 s for the trial of 3 m tube only, shown in figure 50.

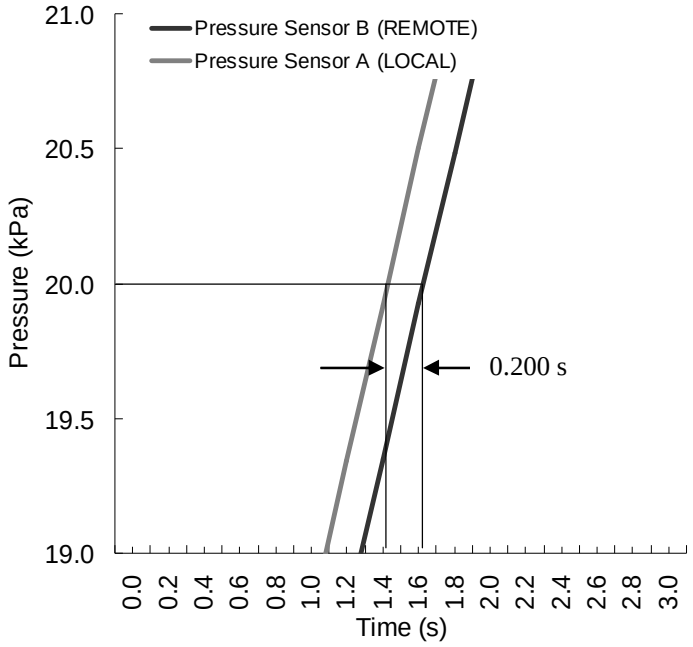

Figure 53: Pressure Sensor Reading Comparison - local vs. filter and 3m tube

Finally, the filter is tested with the 30 m PE tube, this being the test with the most notable result. For the data shown in Figure 54, a signal delay of 1.813 s is calculated, for a pressure rate of change of 2.34 kPa/s, compared to a delay of 0.303 s for the 30 m tube without filter, as shown in Figure 51.

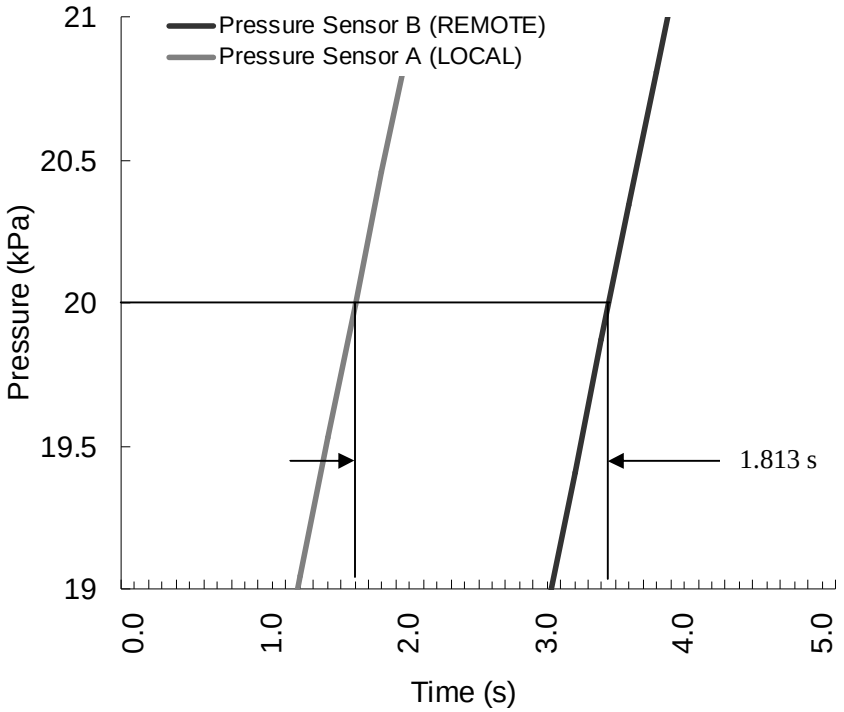

Figure 54: Pressure Sensor Reading Comparison - local vs. filter and 30m tube

Results for all pressure sensing apparatus test are summarized in Table 3. Generally, in a predictable fashion, longer sensing lines result in longer delays, the delay for 3m tube to 30m tube increasing from 0.052 s to 0.303 s. Additionally, for the tests using the filter plate, the delay increased from 0.078 s (for filter only), to 0.200 s (for filter and 3m tube), and finally to 1.813 s (for filter and 30 m tube).

Table 3: Pressure Sensor Isolation Methods Test Results

ΔP Rate (kPa/s)	TL (seconds)				
	3 m Tube	30 m Tube	Filter Only	Filter & 3 m Tube	Filter & 30 m Tube
2.28	0.056				
2.67	0.052				
0.52	0.129				
2.15		0.294			
1.52		0.303			
2.60		0.265			
2.14			0.076		
1.74			0.078		
1.86			0.084		
2.78				0.195	
2.86				0.200	
2.37				0.221	
2.35					1.813
1.95					1.888
2.24					1.915

While a pressure measurement delay of 0.2 s is not very significant for most control systems, a delay of 1.8 s or higher, as was observed with the filtered 30 m apparatus, could be very significant for process control systems where speed is important. Since very little length of impulse tubing is required to achieve safe temperatures (less than 0.2 m, see Figure 29), impulse tubing should be as short as practical to minimize this delay effect. In some cases, longer impulse tubes may simply be required to isolate the sensors themselves from locations that endure high ambient temperatures (which may adversely effect the electronics within), or where their location could be hazardous to maintenance personnel. Where such long isolation tubes are required, a liquid filled capillary tube sensing system could be used instead, which would have lower delay time, due to the faster speed of sound (pressure waves) in liquid vs. gas. For example, silicone oil has a speed of sound of 980 m/s vs. that for dry air which is 343 m/s (both at 20C). The delay effect of sealing diaphragms used with capillary tubing should be taken into account as well however, when comparing the delay effect of these different systems.

Pressure measurement delays could be especially significant where fluidized bed pressure measurements are used for predicting agglomeration behavior, and taking preventive action to stop agglomeration conditions. Investigation of the frequency response of similar isolation systems at frequencies of 200 Hz would give a much better idea of the effect of these systems for agglomeration early warning systems.

5.0 STEAM FLOW CONTROL AND MEASUREMENT FOR FBG PILOT PLANT

5.1 MATERIALS AND METHOD

A steam supply system (Figure 55) was designed for the fluidized bed gasifier in order to provide steam at up to a maximum 1.5 g/s as fluid media for fuel oxidation. Steam is provided from a dedicated 8.2 kg/hr, 6kW 208VAC 3phase electric Sussman generator. The steam is supplied from the generator to the reactor through a 13 mm (1/2") S.S. insulated tubing system. The required flowrate range for steam as oxidation media was specified to be up to 1.5 g/s. Steam control is implemented through a pneumatically operated automatic control valve, and

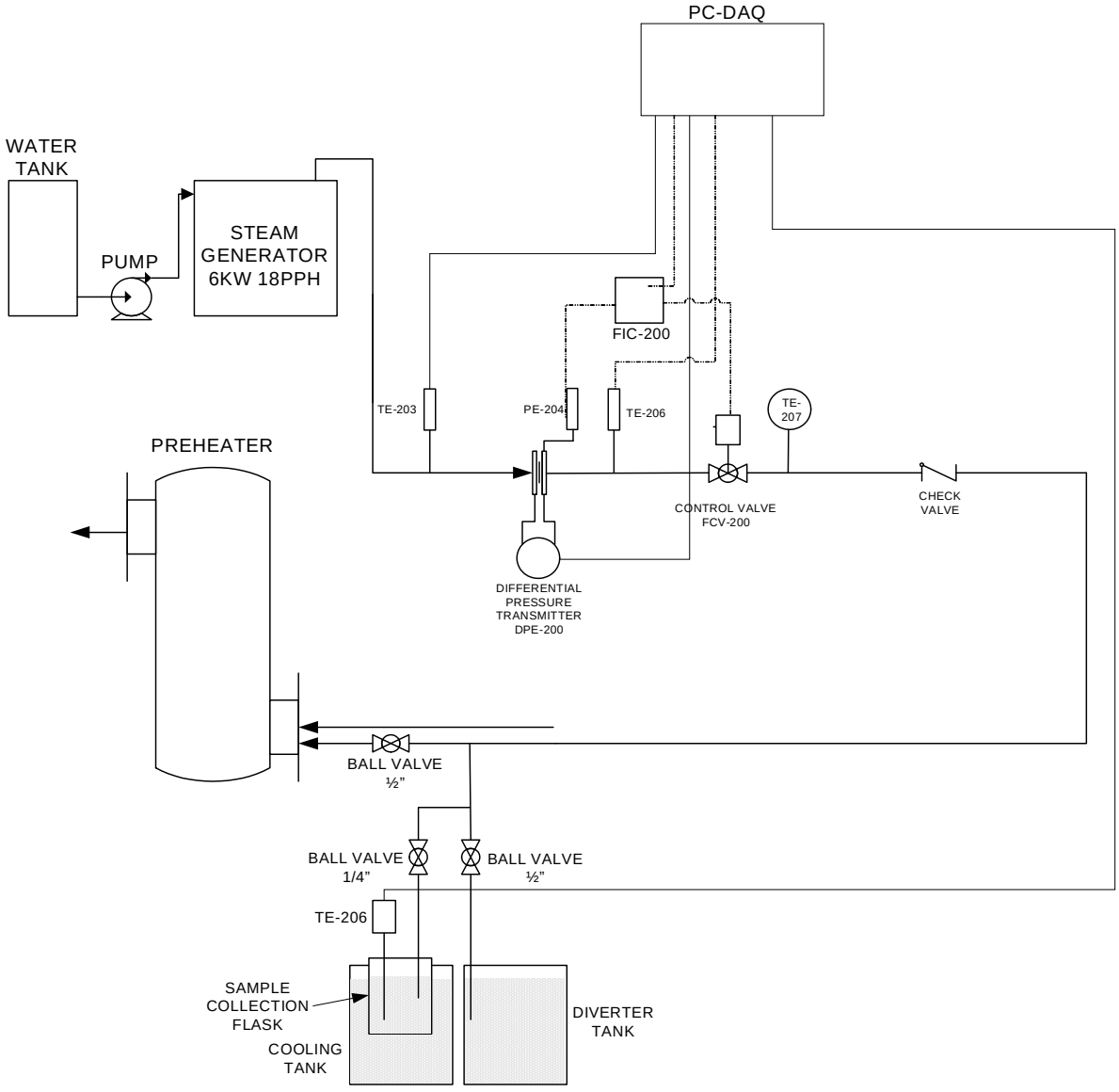

Figure 55: Steam Flow Measurement and Control Testing Apparatus

measurement via an orifice plate with differential pressure measurement. Both the control valve and differential pressure sensor receive/transmit 4-20mA DC signals, originating from a Red Lion model #PCU11004 Loop Controller. This loop controller communicates back to the data acquisition PC via RS-485, and an RS-485 to RS-232 converter. A Labview subroutine running on the data acquisition PC then communicates with the protocol converter.

Measurement of steam mass-flowrate was implemented via an orifice plate and a differential pressure sensor, which transmits the pressure drop across the orifice plate to the data acquisition system, measured in inches of H_2O (and converted by Labview to Pascals). The relationship (in S.I. units) between this pressure drop (Δp) and the mass flow rate of steam (q_m) are given by Formula 11 from section 2.4.1.

For the pilot plant steam system, both C (discharge coefficient) and ε_2 (expansion factor) will be calculated based on collected data, and optimization of collected data with the formulae given in Section 2.4.1. Because both of these factors are multipliers required for the base flow formula, they will be considered as one ($C*\varepsilon_2$) for the purposes of their experimental calculation. These coefficients would ideally be calculated iteratively by the control system, as they will both vary with the Reynolds number and steam density, both of which will change across the flowrate spectrum being assessed. However, as iterative calculation of the Reynolds number is a difficult and complex endeavor (requiring a dedicated software algorithm), these values will be treated as constant over the flowrate being assessed, such that it can be shown that this assumption is valid for a certain error range in the flow calculation. That is, if coefficient constants for C and ε_2 can be determined which result in flow calculation estimates which differ from the true values by equal or less than 10%, then this assumption will be considered valid for the purposes of this flow calculation within that error range.

Calibration data will be collected by operating the system as follows:

A steam sample will be collected at several different flowrates, as controlled by a valve (FCV-200), and as measured by differential pressure transmitter PDE-200. Several flowrate points

were covered across the range of the transmitter, including a range of rates up to and including the maximum required flowrate of 1.5 g/s steam mass-flow rate.

Steam was collected using a 1000 mL beaker, with ice and distilled water placed in the bottom of the beaker. The beaker was weighed on a Mettler-Toledo digital balance prior to each trial to determine initial mass. Steam was collected via a 6.35 mm (¼") PE tube connected to one of the sample ports, and was discharged through a 6.35 mm (¼") SS tube, which was inserted into the end of the P.E. tube. Steam was discharged from the SS tube into the bottom of the beaker, below the pre-filled quantity of distilled water and ice, which acted to condense the steam, thus capturing the sample. A sample was collected for several minutes, and was timed using a stopwatch (for calculation of mass/time rate). Sampling was discontinued when quantity of ice had melted, or temperature of sample exceeded 50°C (to prevent loss of sample through boiling).

Once collection of steam was discontinued, the sample vessel was weighed again on the digital balance to determine the change in mass from the initial value. This quantity of collected mass represented the steam output of the system over the collection period. The mass value was divided by the time period of the sample to determine the average mass flowrate of the system during the sample period.

Other data that were collected for the sample period by the data acquisition PC included the static gage pressure downstream of the orifice, temperature of the steam upstream and downstream of the orifice, orifice plate pressure drop and control valve position. The orifice plate pressure drop was averaged within MS Excel over the time period of the sample, as were each of the other collected values. Next, the downstream density value was determined from steam tables, using the pressure downstream of the orifice and the steam temperature at the same location.

By using Formula 11 for q_m (steam mass flowrate), the system factors C and ε_2 were back-calculated, using the other known values for: qm (sample period average flowrate), d (orifice diameter), Δp (average orifice pressure drop for sample period), ρ_{f2} (average downstream steam density), and B (ratio of D/d).

Based on this calculation for a single sample, an approximate value of the composite system factor $C^*\varepsilon_2$ is known and can be used as a starting point to calculate an optimal $C^*\varepsilon_2$ value that will work with all sample points.

The process was next repeated a number of times, at different flowrates which encompass the approximate required flowrate range, from 0 to 1.5 g/s (0 to 5.4 kg/hour). Based on the collected samples, an optimal value for $C^*\varepsilon_2$ is calculated, which minimized the error between the corresponding calculated flow rate, and the actual flowrate for all collected samples. This composite system factor was next used by the system computer for real-time calculation of the steam mass-flow rate.

Control of steam flow was initially attempted with a vendor selected ½" 15 degree v-port pneumatically operated automatic control valve, followed by a ½" v-ball valve with a slotted type port (Figure 56). Control functionality of these valves was assessed by increasing the valve setpoint incrementally by 0.5 degrees, or 1 degree, and assessing the change in orifice pressure drop, as that value relates to the mass-flow rate.

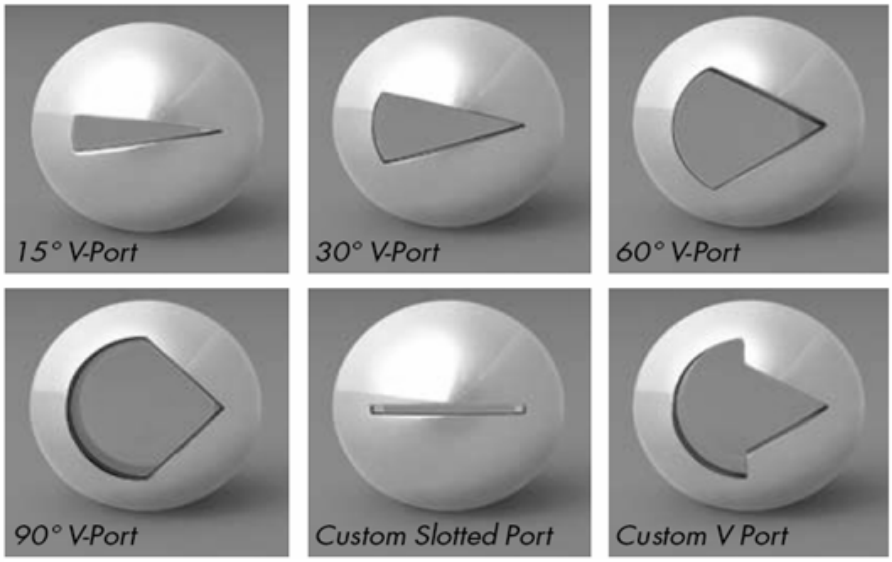

Figure 56: Flow-tek Valve port Styles (Flowtek)

5.2 RESULTS AND DISCUSSION

5.2.1 INITIAL CONTROL AND MEASUREMENT TESTING

The steam flow control system was tested, beginning with an automatic ½" ball valve (with pneumatic actuator and electronic positioner) with a 15 degree v-port as the control element, and with a 3.55 mm (0.14") orifice plate and differential pressure sensor as the primary measuring element. A static pressure sensor was also installed on the downstream tap of the orifice plate. The intent with this system was to calibrate the flow measuring system, then implement automatic PID loop control through the dedicated controller, which would simply receive a flow setpoint from the data acquisition system. However, initial manual operation of the system with this arrangement was unsatisfactory, as it was discovered that the control valve could only change the flowing steam flowrate in relatively large increments, from 3 kPa to 10 kPa in 1 step, with no ability to fine tune this flowrate. As is indicated in Figure 57, the entire range of the differential pressure sensor was encompassed in only 5 step changes in that pressure sensor reading. Many confirmed adjustments to the valve setpoint resulted in no change in differential pressure sensor reading, or flowrate, as also can be inferred by the many small incremental changes in valve position (%) with no corresponding change in pressure drop (orifice).

The entire valve assembly was returned to the manufacturer at this point, to determine what component was at fault, or if the valve itself was incorrectly sized for the application. The vendor determined that the assembly was in working order, and that the port should be changed to a slot-type trim to improve the control range of the valve. Upon receipt of the changed valve, the apparatus was reconfigured such that the valve was downstream of the orifice plate (as in Figure 55). This is the correct orientation for such an apparatus, as it ensures that the pressure drop from generator pressure to reactor pressure occurs after the orifice. At this point testing was repeated, though yielding only slightly improved results, with still very poor control resolution. It was decided at this point that an attempt would be made to calibrate the system for flow measurement, even if control was poor. Any determination towards flowrate calibration should be valid, despite any changes to the control element.

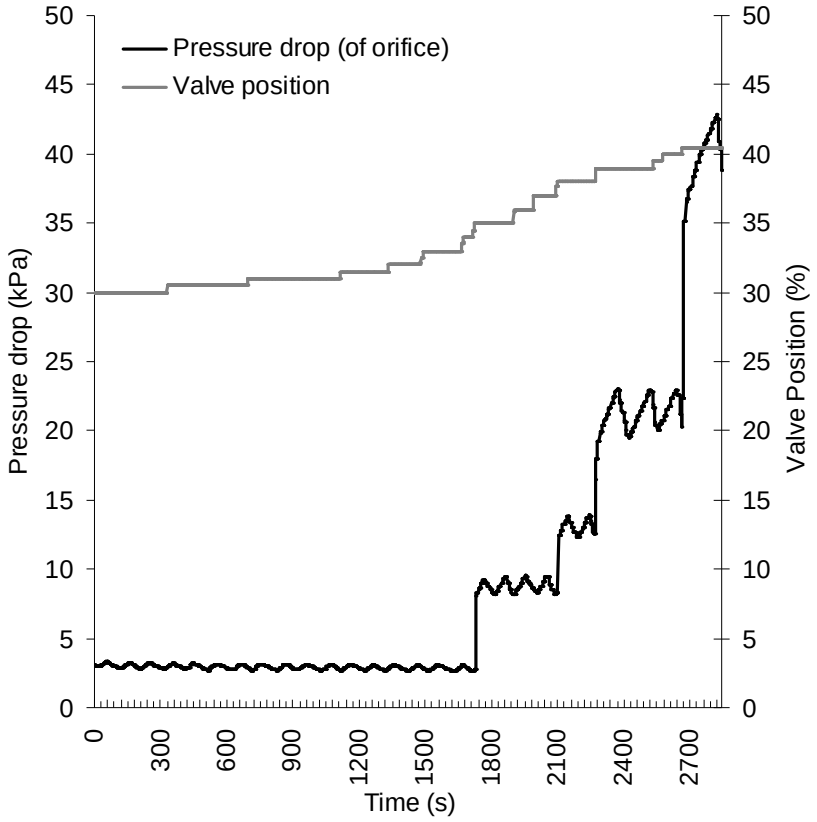

Figure 57: Results of initial control valve operational testing
(15-deg v-port valve - orifice press. drop and valve position vs. time)

Additional control considerations were made, with installation of a manual needle valve in parallel with the automatic valve, to facilitate manual fine control over the steam flow rate. Additionally, a different valve with a lower Cv range was being considered, to replace the poorly functioning automatic valve. This would likely be a globe type pneumatic operated control valve.

5.2.2 300 kPa SUPPLY FLOW MEASUREMENT CALIBRATION

For the initial system calibration, the steam generator was set to operate at a supply pressure of 300 kPa, with approximately 35 kPa differential turn-on pressure.

The control valve, with the new slot-port was set to operate at several operating positions. A typical sample data set for valve position of 31% is shown in Figure 58. At this position, an orifice differential pressure of approximately 4.1 kPa was measured, although this value did fluctuate with the steam generator output pressure, as it cycled from approximately 296 to 331

kPa (top data stream in this figure). For each measured value, the average for that value was calculated for the period of the sample, which lasted from 1.5 to 4 minutes. The sample was collected in a 1000 ml beaker, partially filed with a measured mass of ice and distilled water, used to condense the sample to a liquid. This beaker sat in a cooling tank, also filled with ice, to cool the sample beaker, and maximize the sample duration. The data stream "Sample Temp" is indicative of the sample collection beaker temperature, which started out at -2C approximately, due to the large quantity of ice that was placed in the beaker. As the steam sample was collected, the ice in the beaker melted, and the beaker warmed. As the collection beaker temperature reached 50-60°C, the sample was ended.

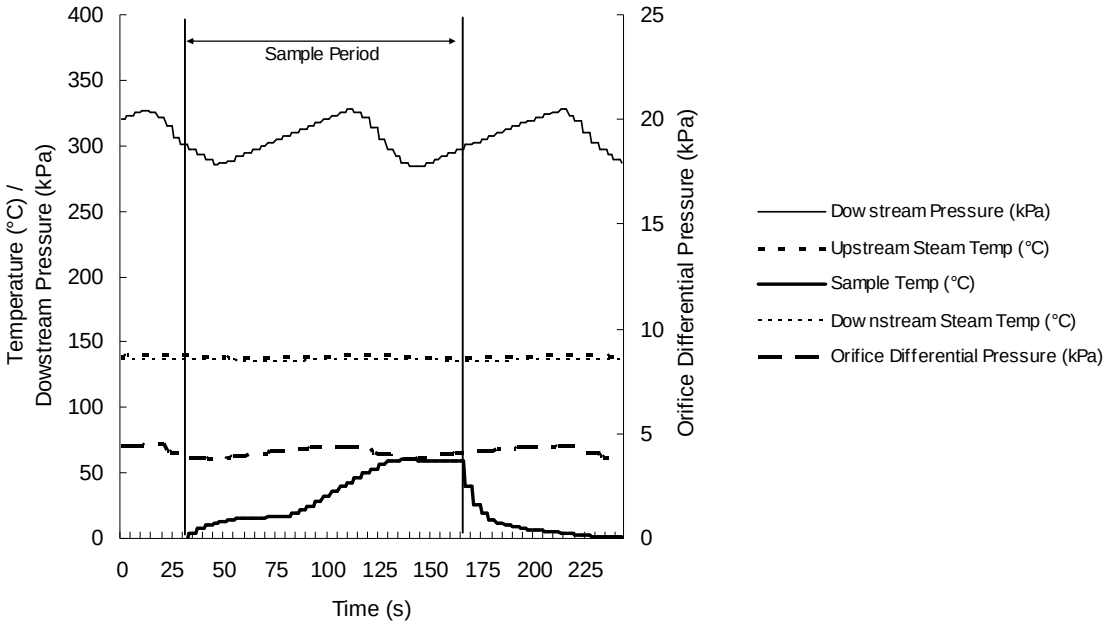

Figure 58: Steam Flow Measurement Calibration test #1 Results Data

By examining the data collected for each sample by the Labview PC (Table 4 illustrates the data from Sample 1), mean values for Δp (orifice pressure drop), P2 (downstream gage pressure), T1 (upstream steam temp), T2 (downstream steam temp) were calculated for the period that the sample was taken. These results are summarized for all samples in Table C-5 (Appendix C).

Table 4: Steam Calibration Test Results #1			
Property	Symbol	Units	Value
orifice diameter	d	meters	0.0036
Orifice Pressure Drop (SI)	Δp	Pa	4080
Steam Density	ρf2	kg/m³	2.19
Diameter Ratio	β	none	0.28
upstream pipe diameter	D	meters	0.0127
Upstream Steam Temp.	T1	°C	139
Dowstream Steam Temp.	T2	°C	136
Final Sample Mass	-	grams	984.7
Initial Sample Mass	-	grams	858.4
Sample Time	t	seconds	101.4
Sample Flowrate	qm	kg/s	0.00125

The results of each sample, including the average steam flow rate (from the sample), vs. the average pressure drop (average measured value) were plotted in Figure 59. Two significant outliers can be observed; one at 0.5 kPa, and one at 4 kPa. Data points at near 0.5 kPa are subject to excess error, as the DP sensor at this range was operating at1% of its full scale capacity, with values at this range having only 10% resolution. The data outlier at 4 kPa was likely due to either a sample timing error or collection error.

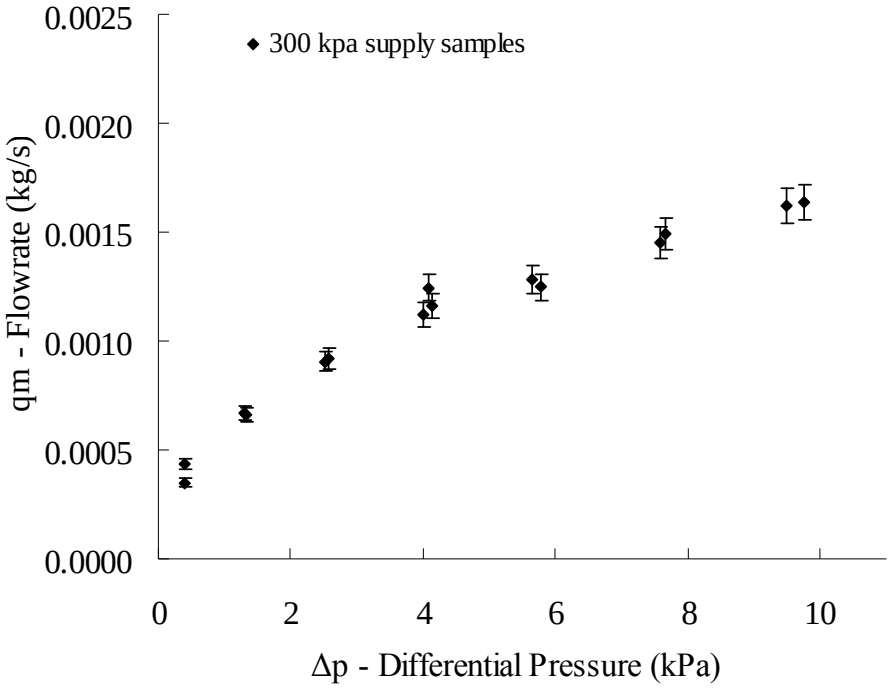

Figure 59: Steam Flow Measurement Calibration Results Flow vs. DP
(Shown with 5% error bars)

Once approximately 15 samples were collected, the calibration factors C (expansion factor) and ε_2 (discharge coefficient) were calculated, based on the data collected. Steam density p_{f2} was also determined, via online saturated steam density calculator (Spiraxsarco.com, 2009), based on the downstream absolute pressure. The factors $C^*\varepsilon_2$ were considered as one factor for the purposes of this calibration, and were calculated such that the average error between the collected samples and the predicted value (based on the steam flow Formula 5.3.1) was minimized.

The error between sample value and theoretical value was minimized to 5.28% by setting the combined factor $C^*\varepsilon_2$ to 0.834. Several data outliers are evident, the largest of which, with over 20% error are found at the lowest end of the calibration curve, with flowrates of less than 0.5 g/s. At this range, the resolution and accuracy of the differential pressure sensor is very limited, as it is operating at below 1% of its operating span, with Δp of 0.25 to 0.5 kPa. Above 1 kPa, or above approximately 0.6 g/s (steam) the error is less than 10% for all samples collected, and the average error is less than 5%. These results are summarized in Figure 49, which illustrates the sample data points, along with the theoretical flowrate curve over the same range, for the calculated values of C, ε_2, and ρ_2.

From this calibration procedure, it has been determined that the most appropriate composite system factor $C^*\varepsilon_2$ was 0.834 (dimensionless). This factor can now be used for any saturated steam flow calculation for this system, where the orifice pressure drop and downstream steam density are known. This system factor, which can be used to predict the relationship between orifice differential pressure (Δp), steam density (ρ_{f2}) - determined from steam tables, and steam flowrate (q_m), is indicated in Formula 28, and plotted in figure 60 for the operating range tested.

$$q_m = 1.408 \times 10^{-5} \times (0.834) \times \sqrt{\Delta p \times \rho_{f2}} \qquad (28)$$

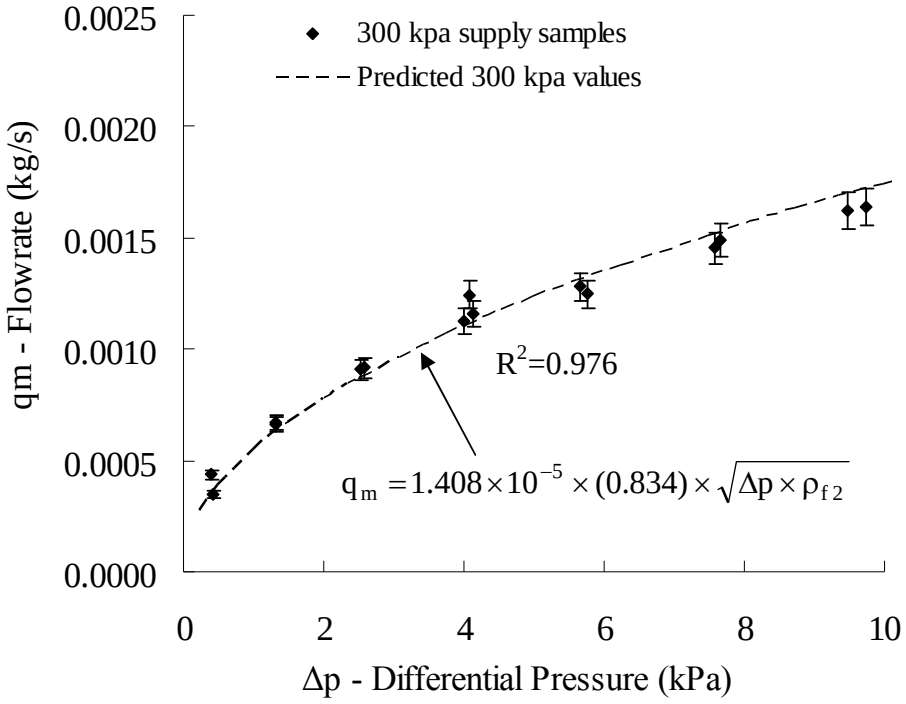

Figure 60: Steam Flow Measurement Calibration Results Flow vs. DP & Theoretical

This factor was tested, by repeating the calibration at a higher supply pressure, resulting in higher steam density.

5.2.3 550 kPa SUPPLY PRESSURE

After completing the calibration curve for the system with 300 kPa steam supply pressure (As set on the Bussman Steam Generator setpoint controller), the steam generator supply pressure was increased to approximately 550 kPa, which will be the supply pressure for use with the FBG as fluidization/oxidation medium. The calibration procedure was repeated for this higher supply pressure, where we see an upward shift in the flowrate values relative to orifice pressure drop, as one would expect for a higher supply pressure, (Figure 61). This figure illustrates the original calibration curve for the lower supply pressure, with the additional 550 kPa calibration sample points superimposed.

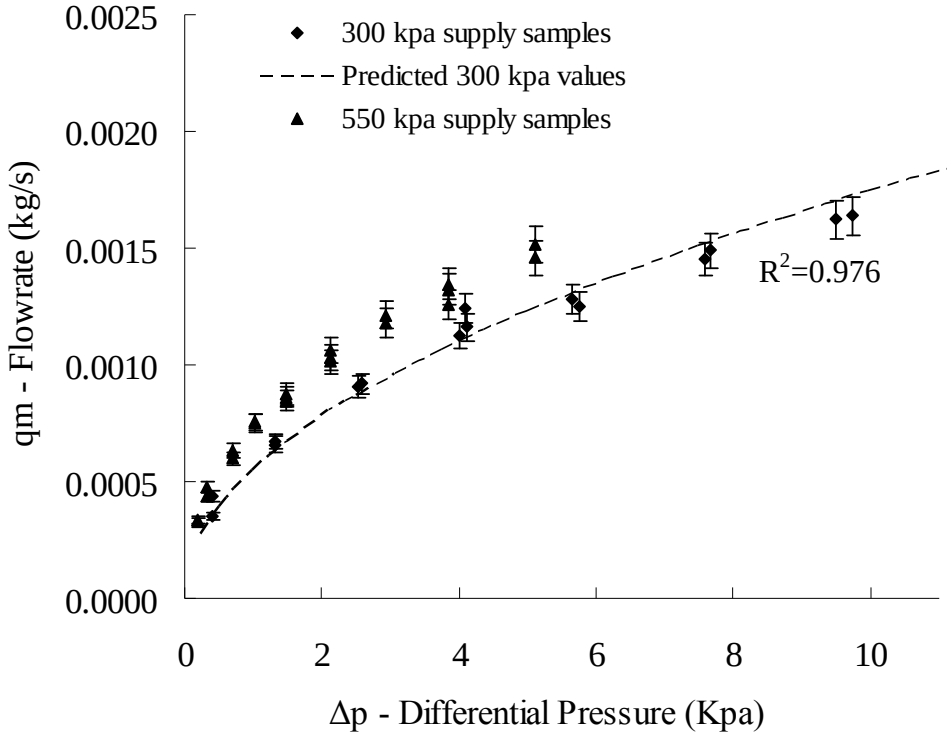

Figure 61: Steam Flow Measurement Calibration Results Flow vs. DP - 310 and 550 kPa Results

The critical adjustment that must be made, with an increase in supply pressure, is to make the corresponding adjustment to the steam density in the flow calculation formula. Figure 62 shows the two sets of data, with two calibration curves, with an average steam density value of 2.19 kg/m^3 for the 310 kPa sample points, and an approximate average steam density value of 3.33 kg/m^3 for the 550 kPa sample points.

Over the range of sample points collected, the steam density varied to a degree, as the steam supply pressure also varied across the range of flowrates.

This second calibration was successful, using the fixed value coefficient value of $C^*\varepsilon_2 = 0.834$, as the average error value between the collected sample points, and the calculated values is less than 10%, and is in fact only 5.28% for the 300 kPa samples, and is 6.24% for the 550 kPa samples. Measurement of steam mass-flowrate for the FBG pilot plant continues using this method.

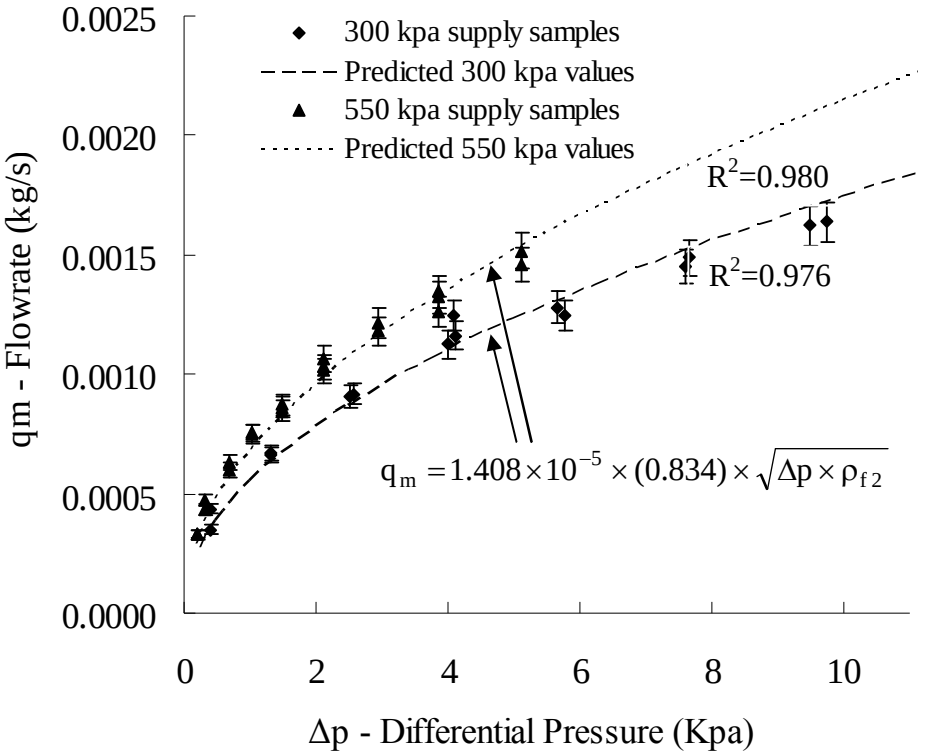

Figure 62: Steam Flow Measurement Calibration Results Flow vs. DP and Theoretical - 310 & 550 kPa Results

6.0 SUMMARY

6.1 FUEL FEEDING SYSTEM

A fuel feeding system was designed, fabricated and commissioned for the U of S FBG pilot plant for injecting biomass-type solid powder fuels such as MBM. This system included a 150 mm screw conveyor for control of the solid fuel flowrate, with a 0.150m^3 storage hopper and load-cell based mass-flow measurement system. This component of the system (Assembly 1) was experimentally tested, and characterized by Formula 23, repeated here:

$$FR = 0.1973 \times S - 0.17$$

Where FR is the fuel output mass flow rate in g/s, and S is the VFD setpoint, in percent. This relation is valid for metering conveyor VFD % speeds from 5 to 100%. The offset component (-0.17) is likely the result of some mismatch between the % value sent by the data acquisition system, and the output rate transmitted by the VFD to the motor. Operating the conveyor at 25%, (the theoretical maximum rate required by the FBG) yielded a mean output rate of 4.8 g/s, with a standard deviation of 2.22, a very high deviation which is the result of the very pulsed nature of operating this conveyor at such low rotational rates (< 1 rpm).

Addition of a 150 mm rotary airlock and 50 mm injection conveyor to the fuel feeding system (Assembly 2) significantly decreased the standard deviation of the output fuel flow rate to 0.21 for 25% conveyor speeds, with a mean flowrate of 5.37 g/s. This improvement was due to the accumulation of some material in the injection screw conveyor hopper, allowing the pulses from the metering conveyor to disappear, as well as the higher rotational rate, open flighting, and smaller diameter of the injection screw conveyor. Additional modifications that were necessary to the injection conveyor system included the addition of air sparging ports to the injection hopper, which actively prevent the bridging and plugging of MBM in this hopper. The addition of the plexiglass observation port that was added to the side of this hopper improved operator awareness as well, and allowed for optimization of the sparging system frequency, and duration. Once these modifications were in place, the system was again operated in order to examine the fuel feed rate range of 1-5 g/s, or approx 5-25% metering conveyor speed range. It was

determined through testing of various speed ratios for Metering conveyor: Injection conveyor that the optimum speed relationship for these conveyors was 1:1 (% of full speed). In other words, if the metering conveyor is operated at 10% of full speed, then the injection conveyor is also operated at 10%.

Finally, the pneumatic injection port was added to the conveyor system and tested, again improving the output stability of the conveyor system, decreasing the range of the flowrate value for the test to 0.78, and decreasing the standard deviation to 0.16. The system output rate was characterized for Assembly 3 for the conveyor speed range of 5-25% by Formula 25, repeated here:

$$FS = 0.219 \times S - 0.42$$

An attempt to pressurize the injection conveyor system made it clear that the rotary airlock would be unable to contain a substantial pressure in the injection system, due to excess air flow across the airlock. The airlock was therefore sealed mechanically to the 150 mm metering conveyor using a rubber hose coupling and clamps, which allowed pressurization of the entire fuel conveying system.

Comparison of the calculated mean flowrate (Table 5) for 25% metering conveyor operation from each Assembly illustrates the incremental improvement in the output rate stability. Improvement in the stability can be observed through the progressive decrease in the signal standard deviation, from 2.22 for Assembly 1, to 0.21 for Assembly 2, and then to 0.16 for Assembly 3.

The fuel feeding system, when coupled to the FBG reactor, works well up to working temperatures of 700°C. Beyond this temperature, fuel char plugs air injection ports for the fuel injection port at the reactor. When the pneumatic injection nozzle was removed, the fuel feeding system was found to work well without it, although reliable pressurization of the fuel feeding system becomes more important with this type of installation.

Table 5: Statistical Analysis of FBG Feeding Apparatus' (feed rate data (grams/second) for 25% conveyor speed)

	ASSEMBLY 1	ASSEMBLY 2	ASSEMBLY 3
Mean	4.80	5.37	5.44
Standard Error	0.06	0.01	0.01
Median	3.96	5.43	5.44
Standard Deviation	2.22	0.21	0.16
Range	7.66	1.34	0.78
Minimum	1.88	4.46	5.04
Maximum	9.54	5.80	5.82
Count	1351	886	801

6.2 FBG PRESSURE MEASUREMENT

Two techniques for pressure measurement of hot, dusty gases were examined, in order to determine their effect upon measurement delay. These techniques included the use of capillary tubing for fluid cooling, and porous plate filters for blocking the flow and ingress of solid particles. For 6.35 mm (1/4") PE tubing, the delay effect for up to 30 meters of length is minimal, with a maximum of 0.303 second delay for a pressure fluctuation of 1.5 to 2.6 kPa/s. The 3 meter PE impulse tubing has even less delay, with a 0.052 second delay for a pressure fluctuation in the 2.67 kPa/s range. A significant aberration was found with a pressure fluctuation of 0.52 kPa/s for this 3 m impulse tubing, where a delay of 0.129 seconds was calculated, much higher than when the faster fluctuations were assessed. Generally, these are all relatively insignificant delays, ranging from 0.05 seconds to 0.303 seconds, all less than the sample period for the FBG pilot plant system. They may be significant, however, if faster response is required, or if accurate frequency analysis is required, as system pressure fluctuations of varying intensity may also have varying delay with this type of measurement, resulting in significant signal degradation.

Combining PE impulse tubing with a media grade 10 porous plate filter, however, increases this measuring delay significantly, up to 1.9 seconds average for pressure fluctuations of 1.9 to 2.3 kPa/second using the 30 m impulse tube. When 3 meters of tubing is combined with the porous plate filter, this delay is only a maximum of 0.221 seconds. This is again, not significant for a system such as the FBG pilot plant, which has a sample frequency of 1 Hz for process

measurements. The filter alone, mounted directly to the manifold, results in a maximum 0.084 seconds delay. The 30 m tube, though much longer than would typically be used in such an application, does illustrate the effect that the combined devices have upon this measurement delay. The addition of the porous plate impedes the flow of fluid between the active side (pressure tank), and the measuring side (impulse tube). This dramatically increases the delay in measurement for each tubing length, when compared to the same impulse tubing length without the filter. A logical assessment of these results would be that a less restrictive filter would reduce this "fill" time and thus the measurement delay of any connected pressure sensor. Additionally, the use of larger diameter tubing, such as 9.53 mm (3/8") instead of 6.35 mm (1/4") would reduce the compression restoring force, and increase the driving pressure force of the measuring system, perhaps improving the pressure system response (Fignola and Beasley, 2000).

6.3 STEAM METERING AND CALIBRATION

Steam mass flow measurement was successfully implemented, using an orifice plate and differential pressure sensor, whereby the following formula can be implemented to calculate the mass-flow rate of steam.

$$q_m = 1.408 \times 10^{-5} \times (0.834) \times \sqrt{\Delta p \times \rho_{f2}}$$

where:

Δp = pressure drop as measured across orifice plate (Pascals)

ρ_{f2} = gas density from steam Tables for saturated steam, using P_2 (downstream pressure) (kg/m^3)

This formula combines the standard formula for gas mass-flow measurement with the experimentally determined composite value for discharge coefficient (C) and expansion factor (ε_2), as well as known values for pipe I.D. and orifice diameter. The stated assumption that the discharge coefficient and expansion factor could be treated as constant for the required flow-rate range was experimentally verified, with the determined composite value of 0.834 resulting in an average error of 5.28% for a flow-rate range of 0.5-1.5 g/s of steam (for steam generator supply pressure of 310 kPa), when the collected sample values are compared with the theoretical calculations. Further, when samples are collected for a higher supply pressure of 550 kPa, and the steam density value is increased to the corresponding correct value, the flow calculation maintains its validity, with an average error of only 6.24%.

Automatic control of steam flowrate is thus far unsuccessful, due to improperly sized flow control valve ports for the procured Flowtek v-ball automatic control valve, which was found to have very poor controllability and very narrow operating range, and thus a Cv which was too high. Currently, a manual needle valve with a very low Cv-range is used to fine-tune the steam flowrate, although a correctly sized low-Cv globe valve is planned to be added to this system.

6.4 RESEARCH AREAS AS PART OF FBG PILOT PLANT CONSTRUCTION

The sum of this completed work now allows for the successful operation of this FBG pilot plant, with a fuel feeding system that operates reliably, without plugging, and with a controllable, predictable and verifiable fuel output rate for MBM fuel. Steam can be added to the reaction for increasing H_2 production, with a flow rate that can be calculated with a 5-6% margin of error. Control over this steam flowrate is still only manual, but plans are in place to automate this as well. Finally, the pressure within the FBG windbox, fluid bed and freeboard can all be measured using filters and lengths of PE tubing, from 2-5 meters. The pressure measurements can be taken without risk of heat-induced damage to the sensors, without solid particles plugging the measuring tubes, and with a measurement delay that is predictable and acceptable, given the operating requirements of this pilot plant.

7.0 CONCLUSIONS AND RECOMMENDATIONS

7.1 FUEL FLOW CONTROL AND MEASUREMENT

7.1.1 CONCLUSIONS

Conveying fuel into FBG is greatly improved by multi-stage conveying, using a primary metering conveyor, and secondary injection conveyor. Addition of injection conveyor, and then injection nozzle, reduces standard deviation for 25% operation of metering conveyor from 2.22 to 0.21, and then to 0.16. An airlock can be used to isolate these conveyors, allow pressurization of injection conveyor while metering conveyor remains at atmospheric pressure, but only if airlock seals with minimal leakage. This was not achieved in the stated experimentation.

When conveying meat and bone meal (MBM), specific measures are required due to tendency of this material to be sticky and have a high angle of repose. These measures include air sparging and high-angled hopper slopes. A pneumatic injection nozzle tested for injecting MBM into FBG from injection screw conveyor. This nozzle works well in standalone testing with injection air rates as low as 50 lpm, and in hot FBG tests up to 700°C.

Above 700°C the injection nozzle plugs due to MBM burning and plugging air injection ports. The nozzle was removed for further tests and this system works well during hot operation without the nozzle. Measurement of fuel mass-flow rate through system was only partially successful using metering conveyor load cell-based weight meter. Flow measurement using the weight meter and load cells was found to have a significant positive offset and mechanical noise due to mechanical coupling of downstream equipment to metering conveyor.

Metering conveyor and injection conveyor should be operated at speed ratio of 1:110 (rotational rate) for minimal system output rate deviation. The system output was characterized by flow testing at various speeds. The complete system has flowrate (FS) to conveyor speed (S) relationship of FS=0.219S-0.420 for conveyor speed range of 5-25%, and for the system without injection nozzle, FS=0.220S-0.355. This relationship is currently used in operation of the pilot plant, in order to predict the flowrate of the fuel feeding system, and is found to predict this

flowrate with approximately 10% error, based on comparison to static weight meter readings, recorded before and after system operation (thus without system noise effects). This relationship is an adequate predictor of fuel flowrate, but a continuous reading should provide an improvement, and less error.

7.1.2 RECOMENDATIONS

A superior airlock should be investigated, which can seal injection conveyor and hopper with minimal air leakage. If superior airlock can be found, the metering conveyor may be decoupled mechanically. This would allow calibration of the weight meter with Labview interface to calculate continuous fuel mass flow rate.

Metering conveyor screw end flighting could be changed to reduce flow irregularity, a change such as toothed flighting for the end flighting section may reduce this irregularity (standard deviation). The data acquisition system analog output card output to the motor control VFD's should be recalibrated to ensure correct value is being transmitted to VFD as set on Labview interface. The, the flow characteristic for system could be recalibrated as well, which should reduce or eliminate offset value in this characteristic.

7.2 FBG PRESSURE MEASUREMENT

7.2.1 CONCLUSIONS

Pressure measurement of hot gases can be accomplished using impulse tubing to isolate pressure sensors from potentially destructive temperatures, reducing the fluid temperature from 850°C to less than 100°C with tubing lengths of 0.2 to 0.3 m. This isolation also allows sensors to be located in much safer locations for maintenance access. Line filters can also be installed to prevent solid particles, such as are found in fluidized beds, from entering and plugging pressure sensing lines.

The combination of porous plate filtering with impulse tubing can result in long sensing delays, due to flow restriction caused by filters, especially when long impulse lines (> 10 m) are used. P.E. impulse tubing of 6.38 mm (1/4") diameter, 30 meter length will have a sensing delay of as

high as 0.303 s for pressure fluctuations of 1.5 kPa/s, low as 0.265 s for pressure fluctuations of 2.6 kPa/s. Combining P.E. impulse tubing of 30 meter length with porous plate media grade 10 filter will result in sensing delay of as high as 1.915 s for pressure fluctuations of 2.24 kPa/s. Pressure fluctuations which have a low rate of increase will often be delayed significantly more, and those which have a high rate of increase will be delayed less.

7.2.2 RECOMMENDATIONS

Filters for pressure sensing should be as unrestrictive as possible (to gas flow), to reduce delay effect. Less restrictive filters should be tested to evaluate the relative delays for different filter grades. Investigate the use of different diameters of impulse tubing, such as 3/8", 1/8" to quantify the effect of tubing diameter as relates to the system response, due to fluid shear and compression effect.

Minimize length of impulse tubing as well, especially when using filters with dusty fluid media. Impulse tubing should not exceed 5-10 m. Investigate pressure delay effect of complex pressure fluctuations, which include high and low frequency components, to assess potential distortion effect of remote sensing method. Calculate frequency response of measuring system with different tubing lengths, effect on predicted agglomeration signal.

7.3 STEAM FLOWRATE MEASUREMENT AND CONTROL

7.3.1 CONCLUSIONS

Steam mass flow rate can be measured using an orifice plate and differential pressure sensor, in addition to a downstream gage pressure sensor. A steam mass flow measuring system of this type can be calibrated to within 5-6% error, by taking manual mass samples of steam, logging system data, and using this data to calculate a combined system characteristic for the flow coefficient and expansion factor.

The mass flow rate as determined by the collected sample was used to determine the composite system factor $C^*\varepsilon_2$, to be 0.834. This factor can be used within equation 27 to calculate flows across the flow rate range of 0.5 to 1.5 g/s. Steam flow calculations using this method have an

average error of 5.28% for 300 kPa supply pressure, and 6.24% for 550 kPa supply pressure. This error is higher for lower flows, below approximately 0.5 g/s, as in this range the differential pressure sensor is operating within about 0.25% of its range, resulting in a resolution (error) of approximately 25% of the measured value or greater.

Steam flow control, for low flows such as from 0.1 to 2.5 g/s, and steam supply pressures of 300 to 550 kPa will have very small Cv factors (less than 0.1), and as such, only a very narrow range of control valves, including globe and needle valves will work successfully. Ball valves generally are inappropriate for steam flow control for such low flow rates.

7.3.2 RECOMMENDATIONS

An automatic globe valve should be procured with Cv value in the range of 0.01 to 0.1 for steam flow control in this application. Generally steam flow control valve sizing should be learned in advance, and performed by the end user as vendors will often make incorrect assumptions in specifying valves for these applications. Ensure control element is always installed downstream of the primary (flow measuring) element, which will insure flow measuring element is always full of flowing fluid - necessary for most flow measurements to work properly

Integrate steam tables with Labview program, to ensure accuracy in steam density used for flow calculations. Re-calibrate system on a twice annual basis, to compensate for shifting system constants and calibration drift.

7.4 OVERALL RECOMMENDATIONS AND POTENTIAL RESEARCH AREAS

The pilot plant fuel feeding system, and the pilot plant in general should be evaluated using other potential fuel materials, with some locally available examples being sawdust/wood waste and wheat straw. This would allow for evaluation of the feeding system with respect to less sticky and less dense fuels.

Analysis of the pressure sensors that are used on the hot working FBG system should be performed, to evaluate how the delay effect observed during the tests described here relates to the actual delay in full operation. Additionally, tests should be performed on the sensors at

intervals of operation to evaluate changes in the observed delays over time and exposure to operating conditions. The frequency response of the pressure measuring apparatus should be investigated as well, to determine its effect upon agglomeration detection systems.

8 REFERENCES

AARI (Alberta Agricultural Research Institute). 2005. Draft paper - TSE Inactivation and Management of Bovine Specified Risk Material.

Albietz, B., T.A. Fonstad, 2007. Unpublished testing results for feeding of MBM into a fluid bed gasifier. Dept. of Agricultural and Bioresource Engineering – University of Saskatchewan

Anderson, R.M., C. A. Donnelly, N. M. Ferguson, M. E. J. Woolhouse, C. J. Watt, H. J. Udy, S. MaWhinney, S. P. Dunstan, T. R. E. Southwood, J. W. Wilesmith, J. B. M. Ryan, L. J. Hoinville, J. E. Hillerton, A. R. Austin, G. A. H. Wells. 1996. Transmission dynamics and epidemiology of BSE in British cattle. *Nature.* 382: 779-788.

ASME. 1990. Measurement of Fluid Flow in Pipes Using Orifice Nozzle. The American Society of Mechanical Engineers. 345 East 47th Street, New York, N.Y. 10017

Basu, P. 2006. Combustion and Gasification in Fluidized Beds. CRC Press – Taylor & Francis Group. Boca Raton, FL.

BLH. 1997. *8-1 Rate-By-Weight*. LCp-200 operators manual.

CFIA. 2009. CFIA position on change over to specified risk material (SRM) removed meat and bone meal (MBM) production in rendering plant operations - Webpage. Accessed 6 Nov 2009. *http://www.inspection.gc.ca/english/anima/feebet/pol/rendeque.shtml*

CFIA [2]. 2007. Bovine Spongiform Encephalopathy Manual of Procedures. Section 4.6 – Incineration.

Cummins, E. J., K. P. McDonnel, S. M. Ward. 2005. Dispersion modeling and measurement of emissions from the co-combustion of meat and bone meal with peat in a fluidized bed. *Bioresource Technology*. 97: 903-913

Dalai, A., T.A. Fonstad, M. Kulkarni, T. Pugsley, Z. Wang. 2006. Gasification of MBM in a Fixed Bed Reactor. Unpublished research paper. Department of Chemical Engineering, University of Saskatchewan, Saskatoon, SK.

DOE. 2009. Gasification Technology R&D. (Website) Accessed Nov 6, 2009 Available from: http://www.fossil.energy.gov/programs/powersystems/gasification/index.html

Dorin H., P. Demmin, D.L. Gabriel. 1987. Chemistry-The Study of Matter 4thEdition. Needham, Massachusetts. Englewood Cliff, New Jersey. Prentice Hall, Inc.

Eastern Instruments. 2009. Centriflow Meter Webpage. Accessed 5 Nov 2009. http://easterninstruments.com/products/centriflow.html

Energy Centre of the Netherlands (website). 2010. http://www.ecn.nl/phyllis/DataTable.asp

Engineering Toolbox (website). 2009. Flow Coefficient - Cv - Formulas for Liquids, Steam and Gases - Online Calculators. Accessed 6 Nov. 2009. http://www.engineeringtoolbox.com/flow-coefficients-d_277.html

Engineering Toolbox [2] (website). 2010. Heating Value. Accessed 13 March 2009. http://www.engineeringtoolbox.com/gross-net-heating-value-d_824.html

EPA. 1995. Meat Rendering Plants. *AP 42*. 1(5): 9.5.3-1 – 9.5.3-8

Fignola, R. S., D. E. Beasley. 2000. Theory and Design for Mechanical Measurements Third Edition. John Wiley & Sons, Inc. New York

Forge, F**.** 2005. Canadian feed policy and BSE. *Library of Parliament.* PRB 05-06E

Fryda, L., K. Panopoulos, P. Vourliotis, E. Pavlidou, E. Kakaras. 2006. Experimental investigation of fluidized bed co-combustion of meat and bone meal with coals and olive bagasse. *Fuel*. 85: 1685-1699

Garcia, R.A., R.A. Flores, C.E. Mazenko. 2005. Factors contributing to the poor bulk behavior of meat and bone meal and methods for improving these behaviors. 2005 ASAE Annual International Meeting Presentation Paper # 056170.

Garcia, R.A., K.A. Rosentrater, R.A. Flores. 2006. Characteristics of North American meat and bone meal relevant to the development of non-feed applications. *Applied Engineering in Agriculture* 22(5): 729-736.

Gomez-Barea, A., M. Campoy, P. Ollero, C. Femandez-Pereira. 2006. Pilot plant experiences with fluidized bed gasification of orujillo and MBM. Proceedings of the 19th International Conference of Fluidized Bed Combustion. Vienna, 20-24 May 2006. Paper 66.

Goransson, K., U. Soderlind, W. Zhang. 2008. BTL Laboratory at Mid Sweden University. Proceedings of the 16th European Biomass Conference & Exhibition. Valencia, Spain. 2-6 June 2008: 1041-1045.

Joliet Technologies. 2009. What is a Variable Frequency Drive Webpage. Accessed 25 Oct. 2009. www.joliettech.com/what_is_a_variable_frequency_drive.htm

Kane, A. 2002 Kulite Application Note #AN 84/01 “Pressure Transducer Temperature Isolation Using Tubing (Steady State Condition)”

Korbee, R., J. R. van Ommen, J. Lensselink, J. Nijenhuis, J. H. A. Kiel, C. M. van den Bleek. 2006. Early Agglomeration Recognition System (EARS). *Journal of Energy Resources Technology*. 128: 143-149

Klimantos, P., N. Koukouzas, A. Katsiadakis, E. Kakaras. 2009. Air-blown biomass gasification combined cycles (BGCC): System analysis and economic assessment. *Energy*. 34: 708-714

Kunstler J.H. 2005. The Long Emergency. Grove Press – New York, NY.

Maxwell, T. T., J. D. Nevill, A. Ertas. 2005. Biomass feed system flow control using a weigh belt Table. *Journal of Energy Resources Technology*. 127: 71-82

Mckendry, P. 2002. Energy production from biomass (part 3): gasification technologies. Bioresource Technology. 83: 55-63.

Nijenhuis, J., R. Korbee,, J. Lensselin, J.H.A. Kiel, J.R. van Ommen. 2007. A method for agglomeration detection and control in full-scale biomass fired fluidized beds. *Chemical Engineering Science* 62: 644 – 654

Omega. 2009. Force, Acceleration & Torque - Webpage. Accessed Nov 5, 2009 http://www.omega.com/literature/transactions/volume3/force.html

Omega [2]. 2009. Load Cells - an Introduction - Webpage. Accessed Nov. 6 2009. http://www.omega.ca/prodinfo/loadcells.html

Omega [3]. 2009. Pressures Gauges and Switches - Webpage. Accessed Nov 6, 2009. http://www.omega.com/Literature/Transactions/volume3/pressure.html#trantype

Omega [4]. 2010. Low-Cost Transducers for Vacuum/Absolute/Differential/Measurements (Web Document). Accessed March 15, 2010. http://www.omega.com/Pressure/pdf/PX140.pdf

PCB Piezotronics. 2010. Model 116B03 Pressure Transducer – Webpage. Accessed Feb 2, 2010. http://www.pcb.com/spec_sheet.asp?model=116B03&item_id=11070

Prenma. 2008. Modular Fluidized Bed Gasification. Accessed April, 2008. (Web Document) Available from: http://www.pr-en-ma.com/DossierEnergie/PEM_SGHC_Web_Decr.pdf

Prusiner, S.B. 1997. Prion diseases and the BSE crisis. *Science*. 278*(*5336): 245-251.

Rhodes, M. 2007. Fluidization of Particles by Fluids. Accessed 2007. *Department of Chemical Engineering - Monash University, Melbourne, Australia*. http://www.erpt.org/012Q/rhod-00.htm

Smeenk, J., R. C. Brown. 2009. Experience with atmospheric fluidized bed gasification of switchgrass. Centre for coal and the environment – Iowa State University. (available from http://www.iowaswitchgrass.com/resources~reports.html)

Spirac. 2009. Horizontal and Inclined shaftless screw conveyor. Accessed Nov 5, 2009. http://www.spirac.com/en/14_horizontal_conveyor/index.asp

Spirax Sarco (website). 2010. Superheated Steam. Accessed March 14, 2010. http://www.spiraxsarco.com/resources/steam-engineering-tutorials/steam-engineering-principles-and-heat-transfer/superheated-steam.asp

The BSE Inquiry (UK). 2000. Chapter 6 - Rendering. *BSE Inquiry Report*. 13(6): 67-69

Thermo Scientific. 2009. Ramsey Series 20 Webpage. Accessed 5 Nov 2009. http://www.thermo.com/com/cda/product/detail/0,1055,14354,00.html (2009)

The Weather Network. 2009. Statistics: Saskatoon Webpage. Accessed 4 Nov 2009. http://www.theweathernetwork.com/statistics/C02075/cask0276

Turblex. 2009. Atmospheric pressure - Webpage. Accessed 6 Nov 2009. http://www.turblex.com/altitude/index.cfm

Ulrich, G.D., P.T. Vasudevan. 2004. Chemical Engineering Process Design and Economics: A Practical Guide, 2nd ed. Process Publishing Durhan, NH.

U.S. Air Filtration Inc. 2009. Rotary Airlock Valves / Rotary Airlock Feeders - Webpage. Accessed Nov 5, 2009. http://www.usairfiltration.com/parts/rotary_valves.htm

Wang, L., C. L. Weller, D. D. Jones, M. A. Hanna. 2008. Contemporary issues in thermal gasification of biomass and its application to electricity and fuel production. *Biomass and Bioenergy. 32(7): 573-581 (July 2008).*

Whitty, K. 2005. Investigation of Fuel Chemistry and Bed Performance in a Fluid Bed Black Liquor Steam Reformer. Annual Topical Report – Year 2. University of Utah. June 2005.

Wika. 2009. Datasheet F-20. Accesssed online 5 Nov, 2009. http://www.wika.com/WIKAWeb/Product/pdf/F-20.pdf.

Woodgas. Webpage. 2010. Fuel Densities. Accessed May 2, 2010. http://www.woodgas.com/fuel_densities.htm

APPENDIX A - Supplementary Diagrams

Diagrams illustrated in this appendix are included to better convey the scope of work that was performed by the author on the pilot plant project, and the relationship of that scope to the research.

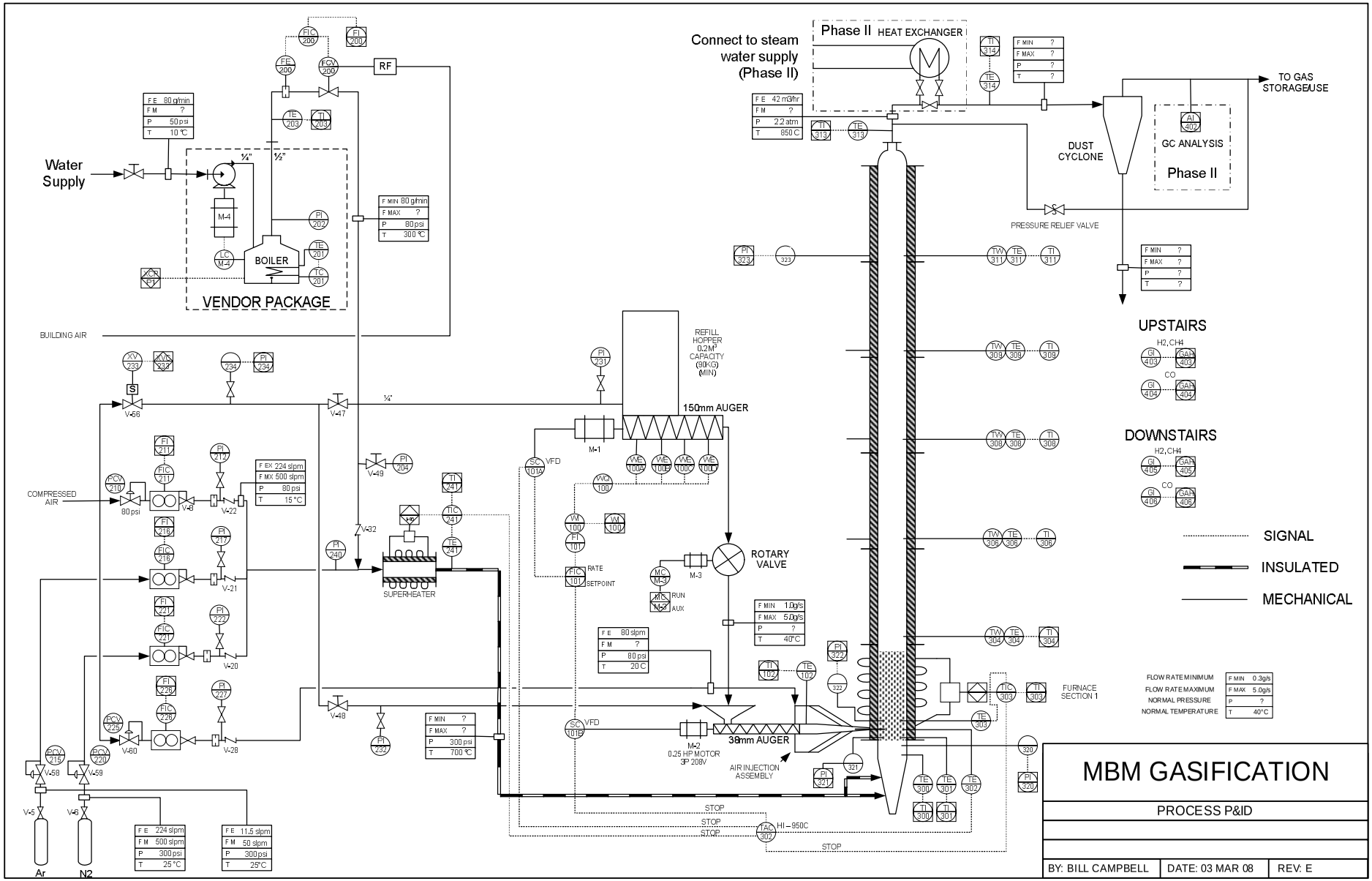

Figure A-1: U of S FBG Pilot Plant P&ID Diagram

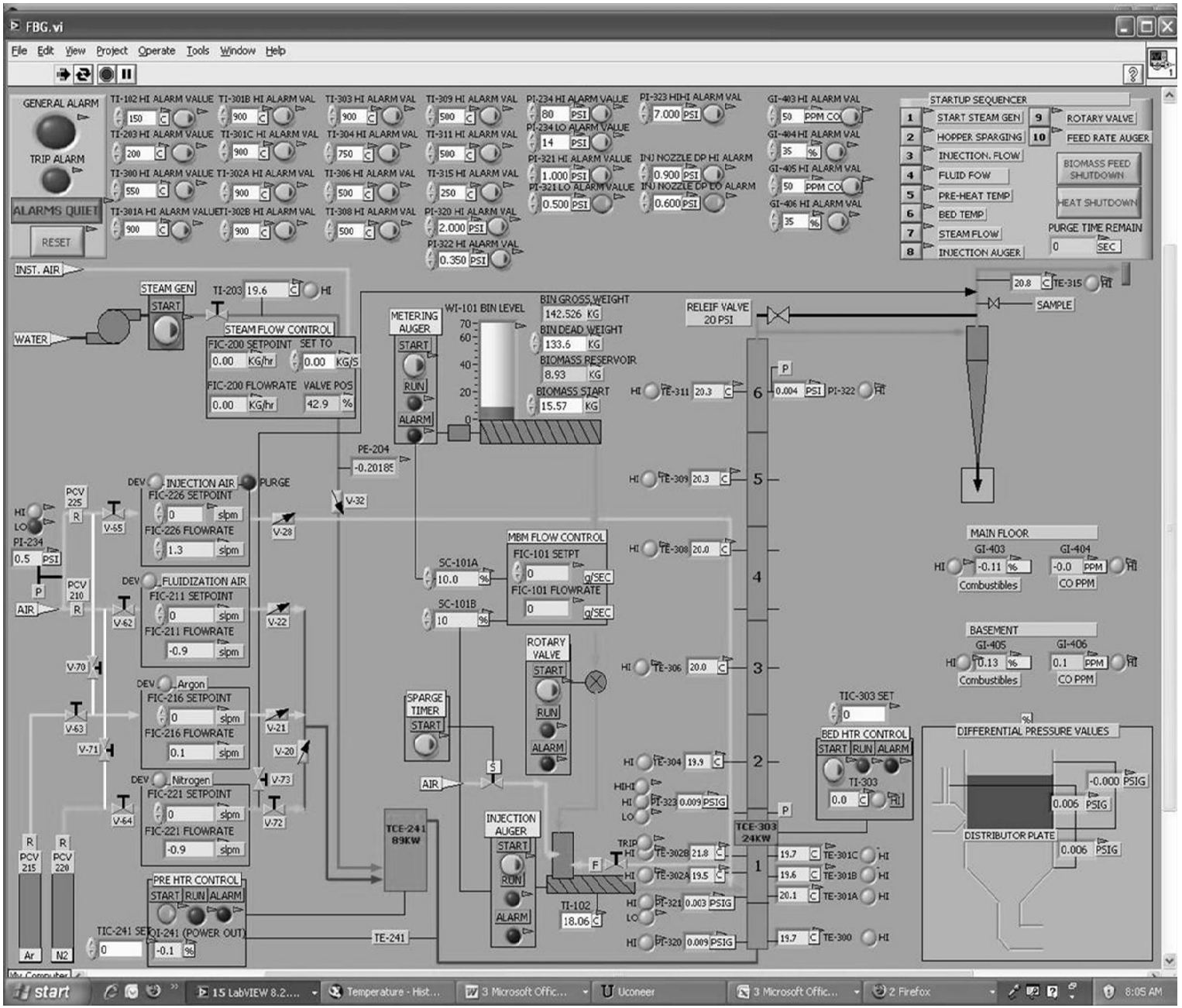

Figure A-2: FBG Pilot Plant Main Interface Labview Screen

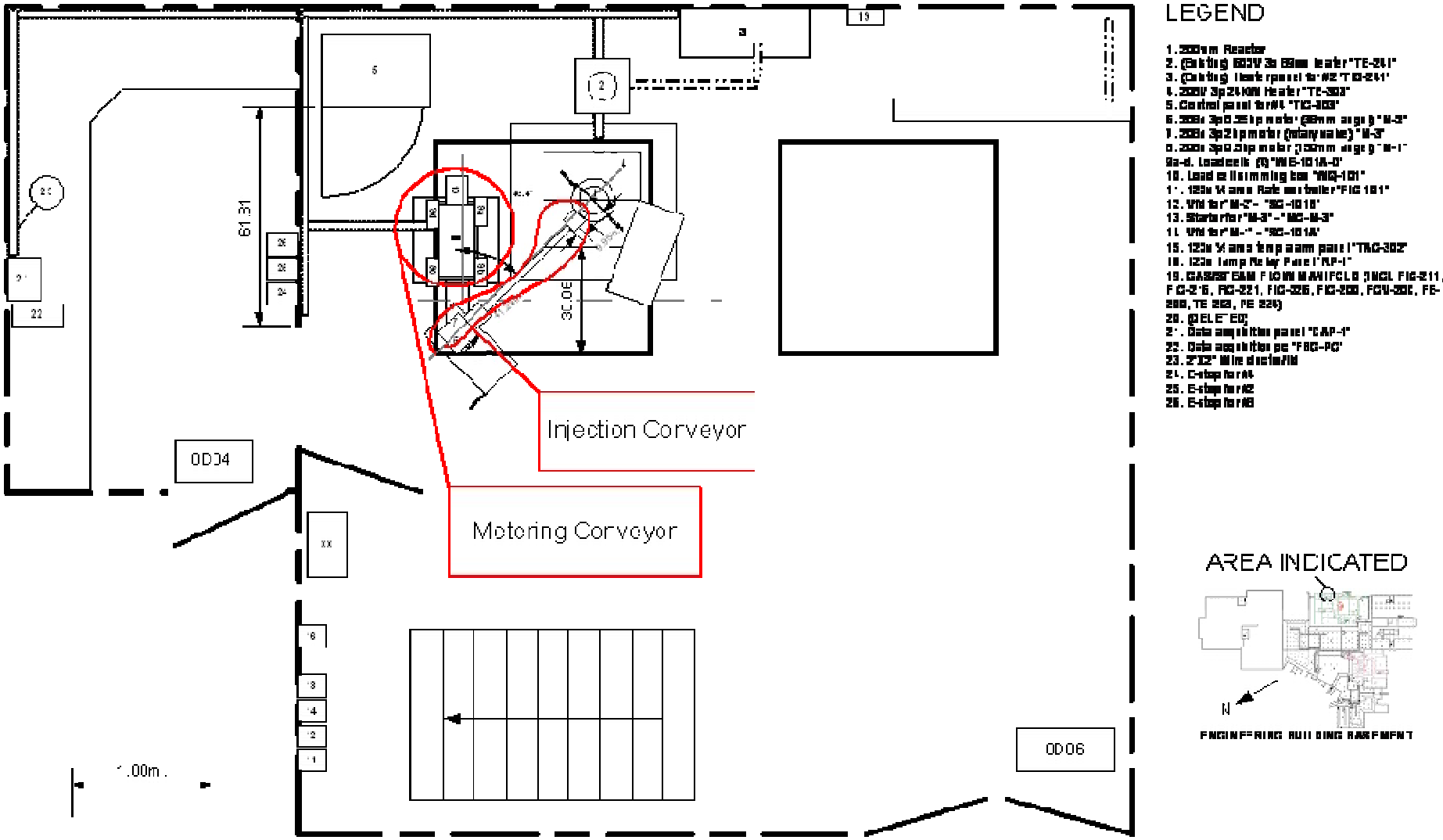

Figure A-3. FBG Pilot Plant Plan View

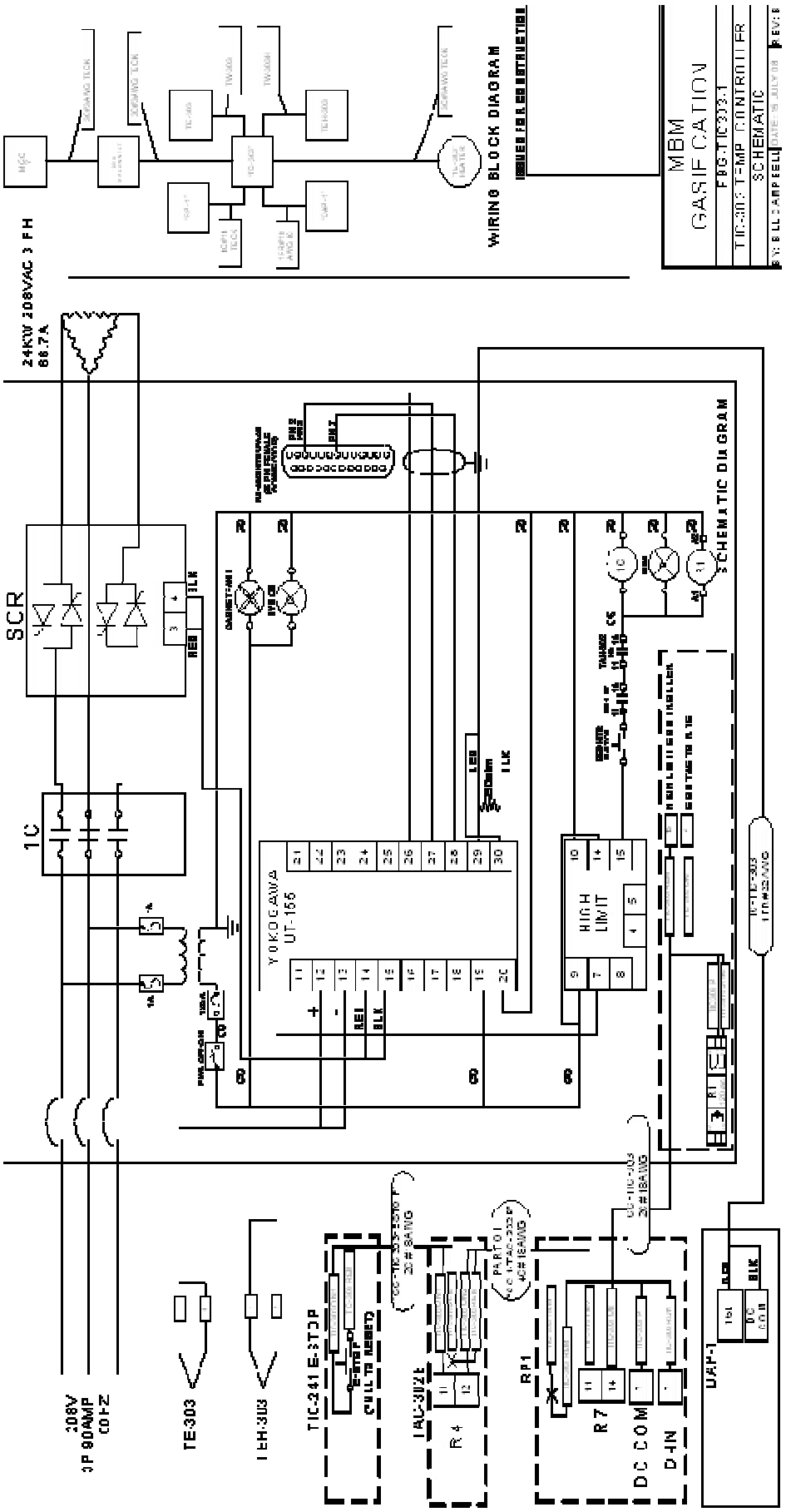

Figure A-4 Schematic and Wiring Diagram for Pilot Plant Bed Heater

APPENDIX B - EXPERIMENTAL DATA

Comprehensive inclusion of all experimental data, as relates to the analysis and conclusions of each research area.

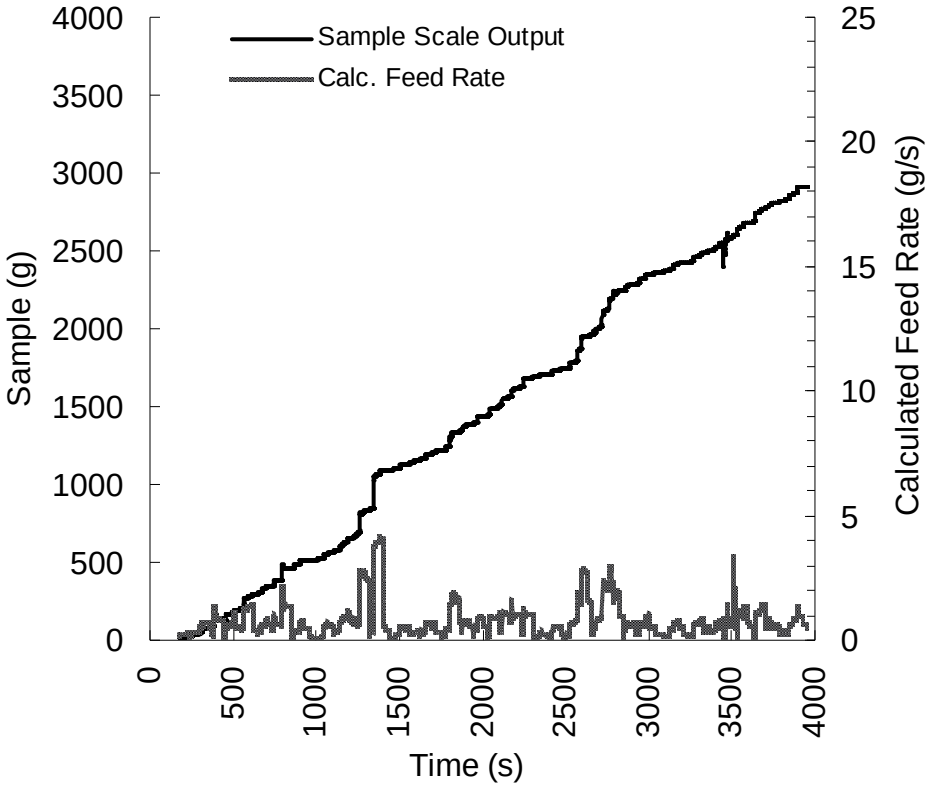

Fig. B-1: Assembly 1 Rate Testing, 5%

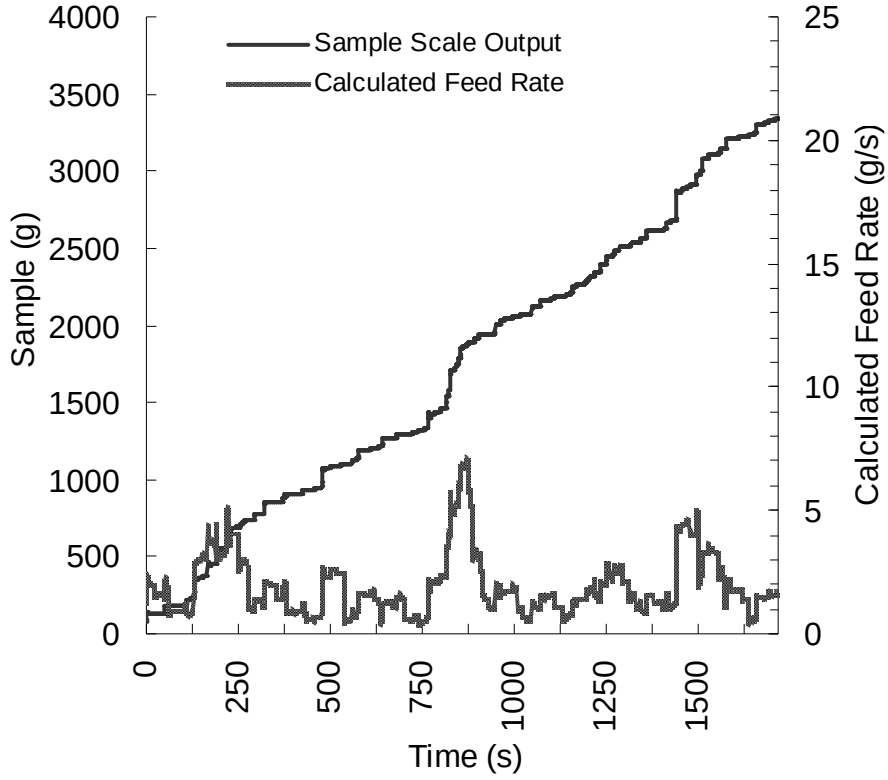

Fig B-2: Assembly 1 Rate Testing, 10%

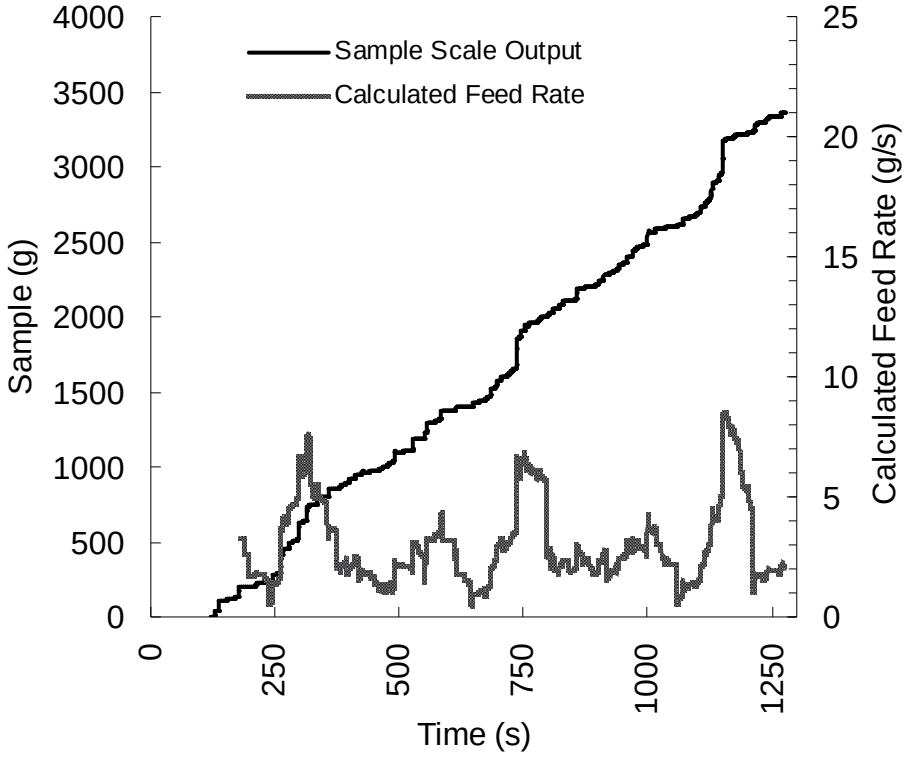

Fig B-3: Assembly 1 Rate Testing, 15%

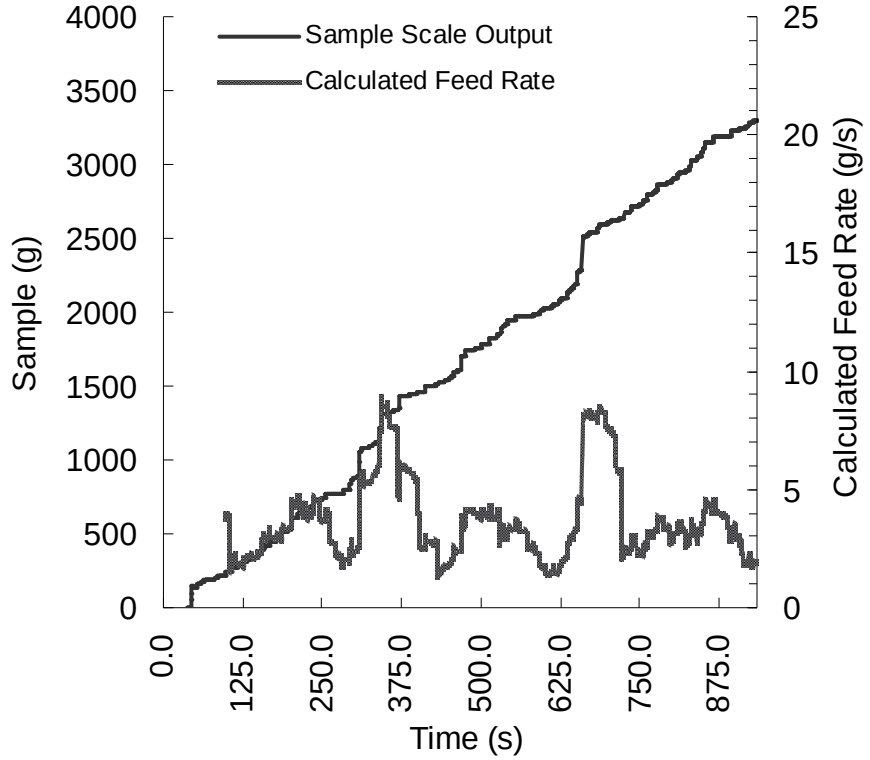

Fig B-4: Assembly 1 Rate Testing, 20%

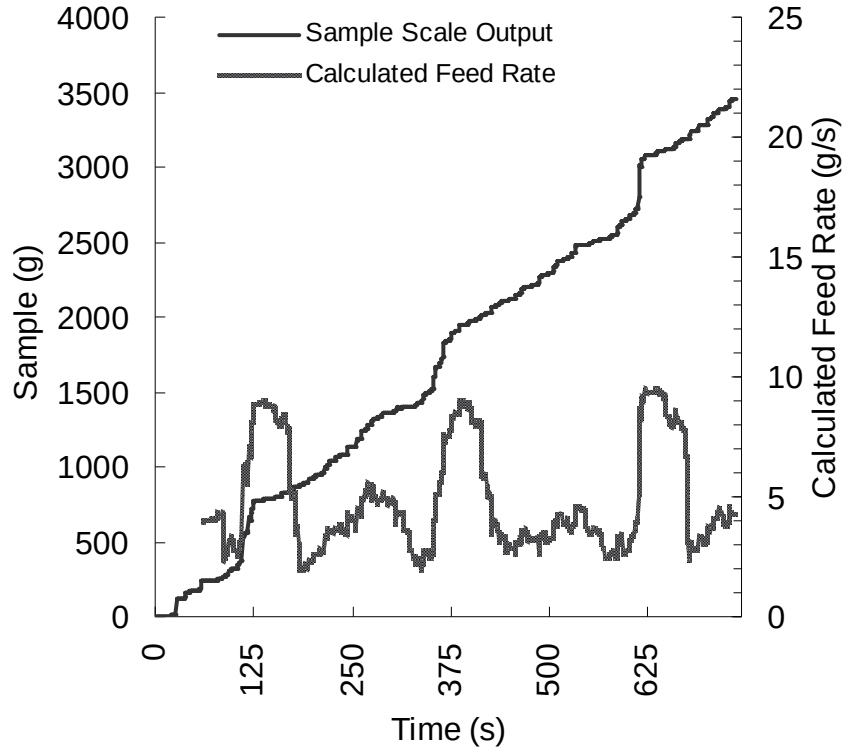

Fig. B-5: Assembly 1 Rate Testing, 25%

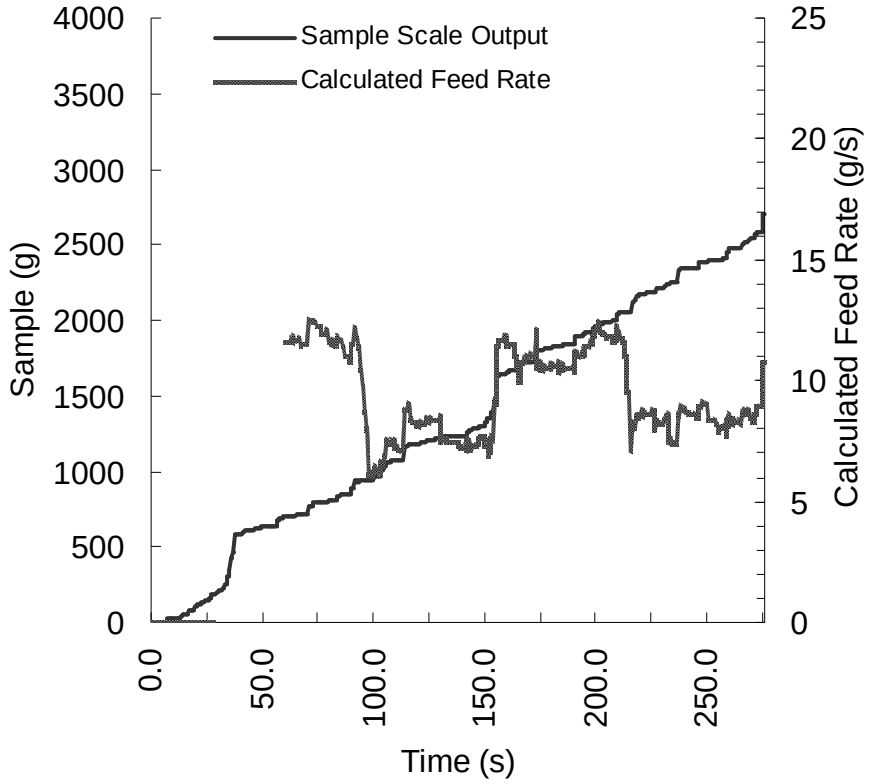

Fig B-6: Assembly 1 Rate Testing, 50%

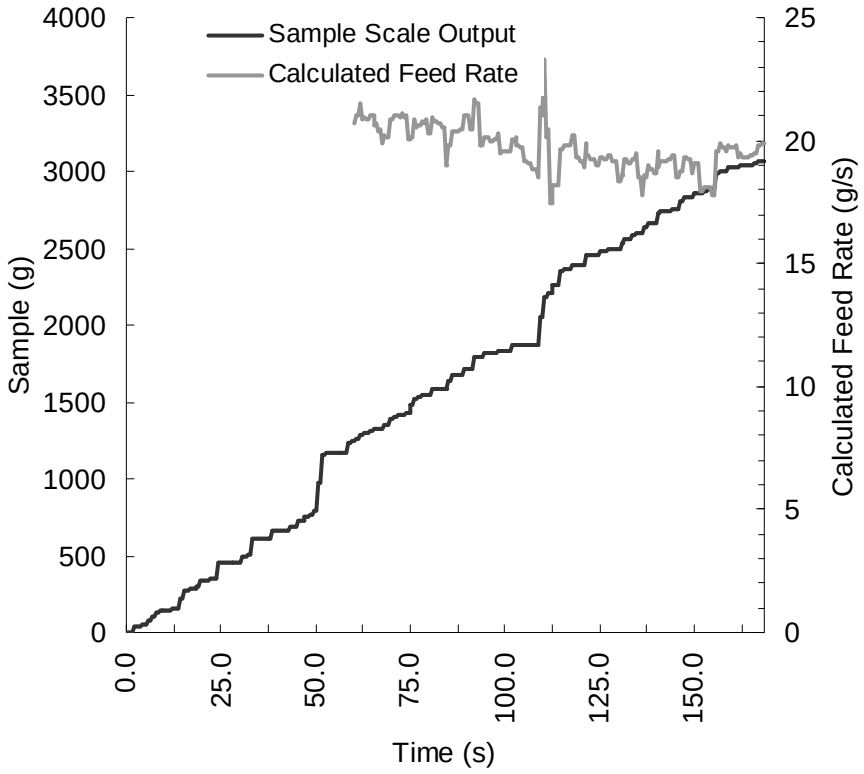

Fig. B-7: Assembly 1 Rate Testing, 100%

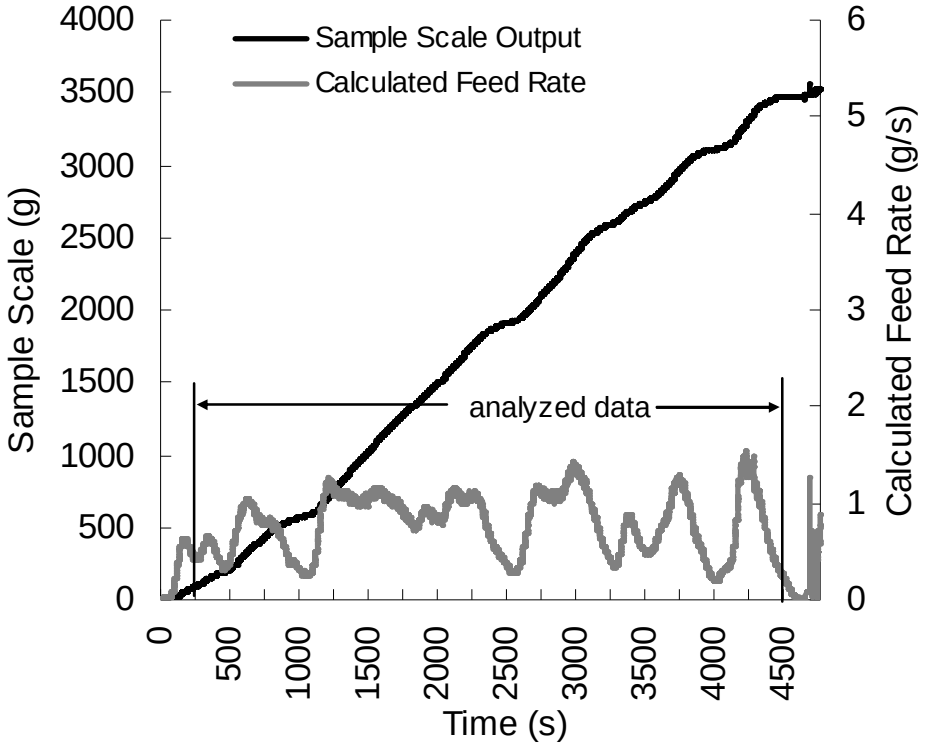

Fig. B-8: Assembly 2 Rate Testing, 5%/5%

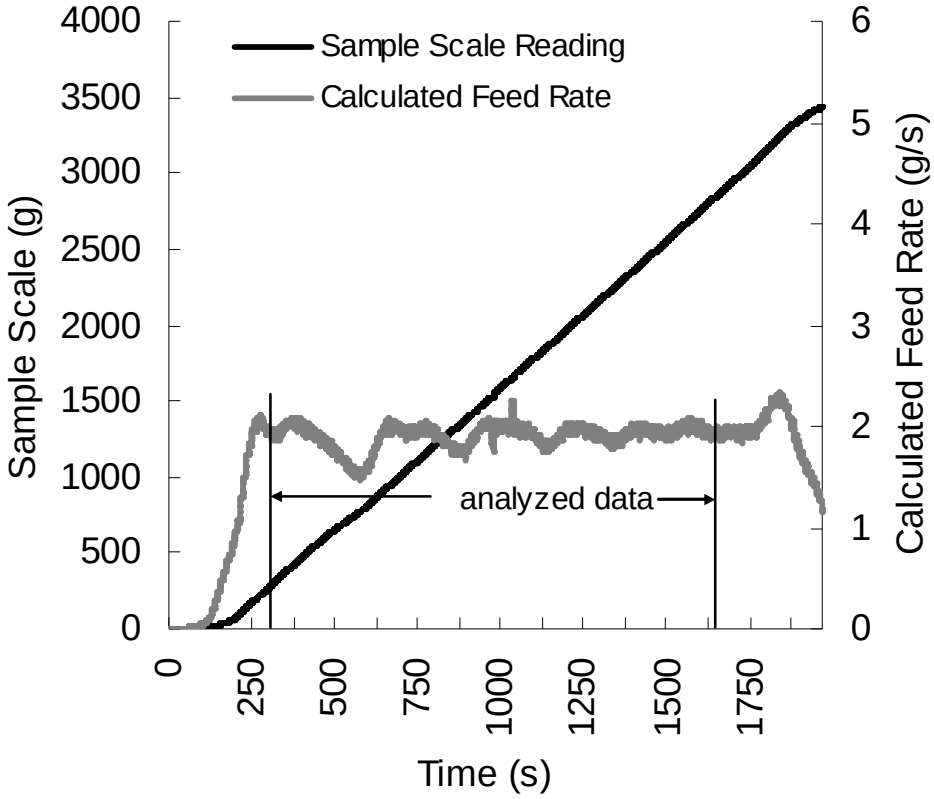

Fig. B-9: Assembly 2 Rate Testing, 10%/10%

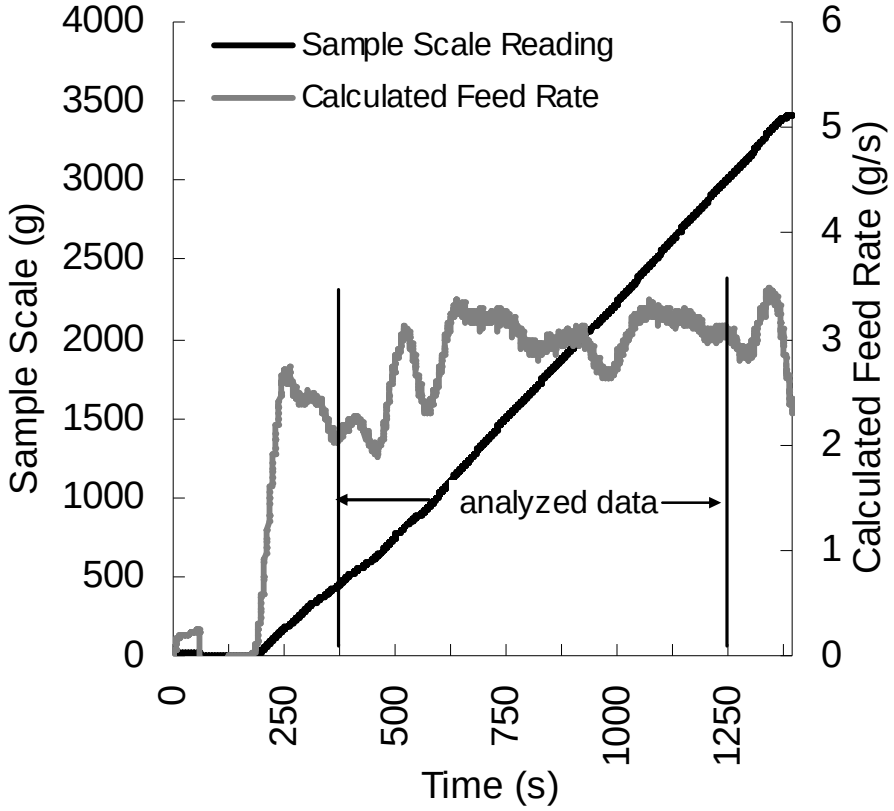

Fig. B-10: Assembly 2 Rate Testing 15%/15%

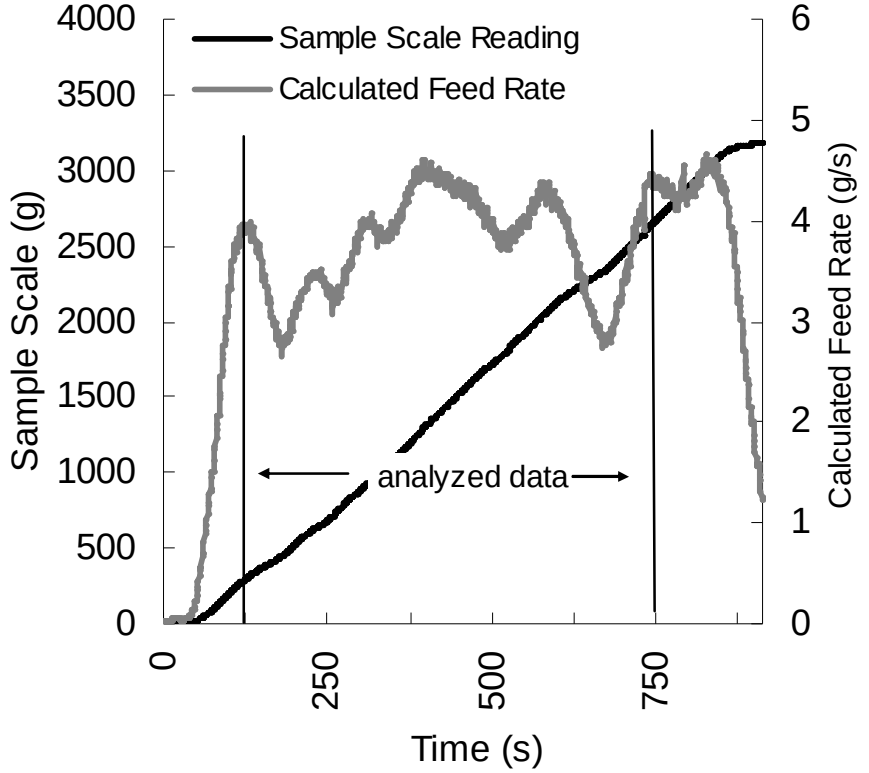

Fig. B-11: Assembly 2 Rate Testing 20%/20%

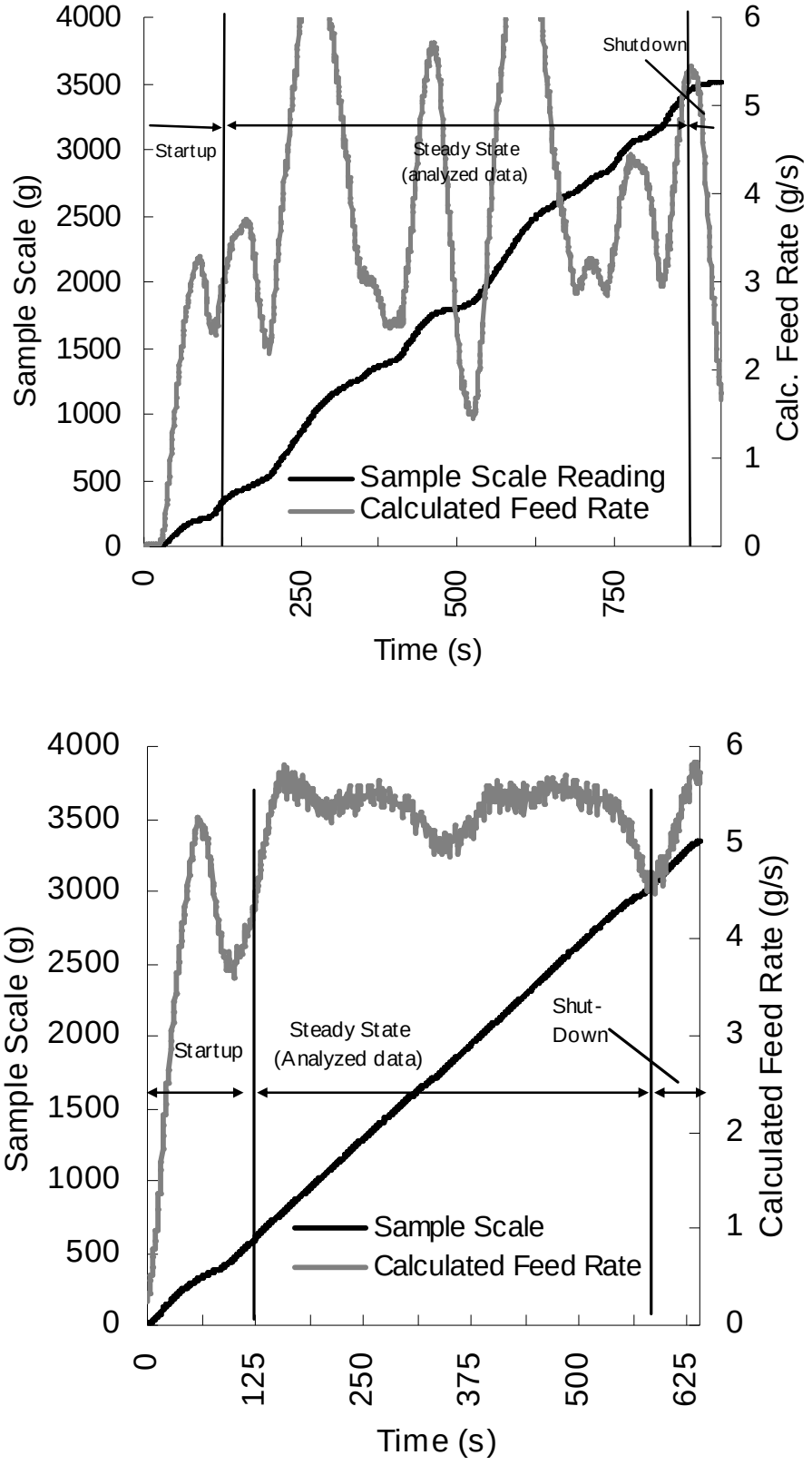

Fig B-13: Assembly 2 Rate Testing, 25%/25%

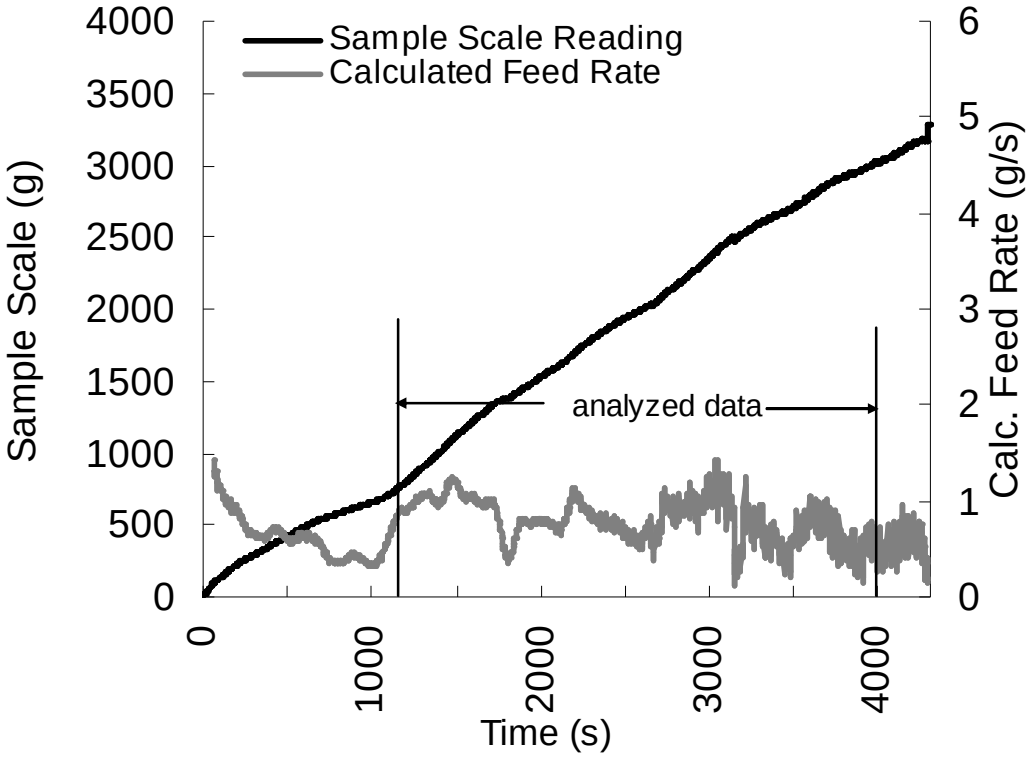

Fig. B-14: Assembly 3 Rate Testing 5%/5%/50 lpm

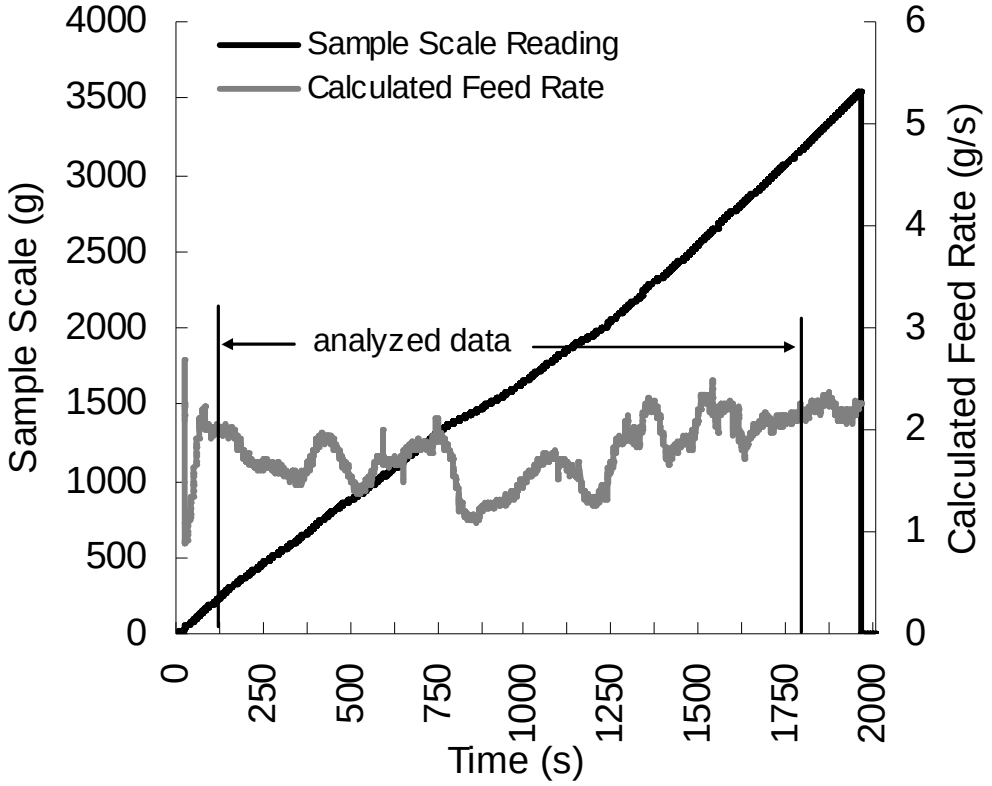

B-15: Assembly 3 Rate Testing: 10%/10%/50 lpm

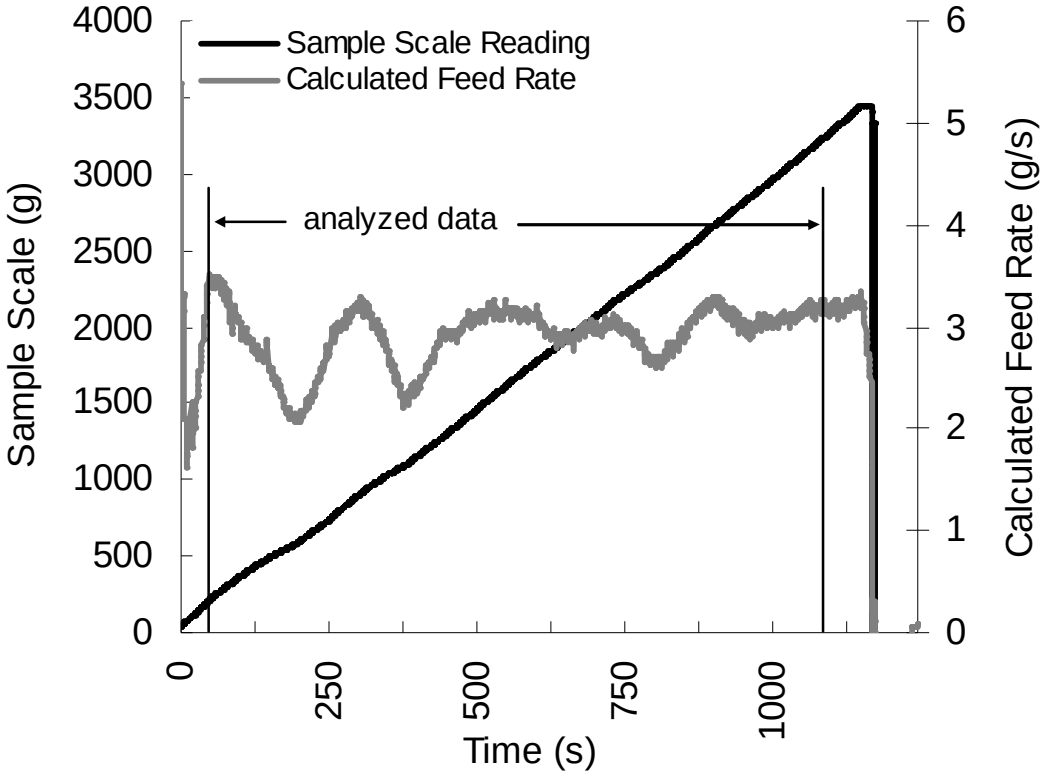

Fig. B-16 Assembly 3 Rate Testing, 15%/15%/50 lpm

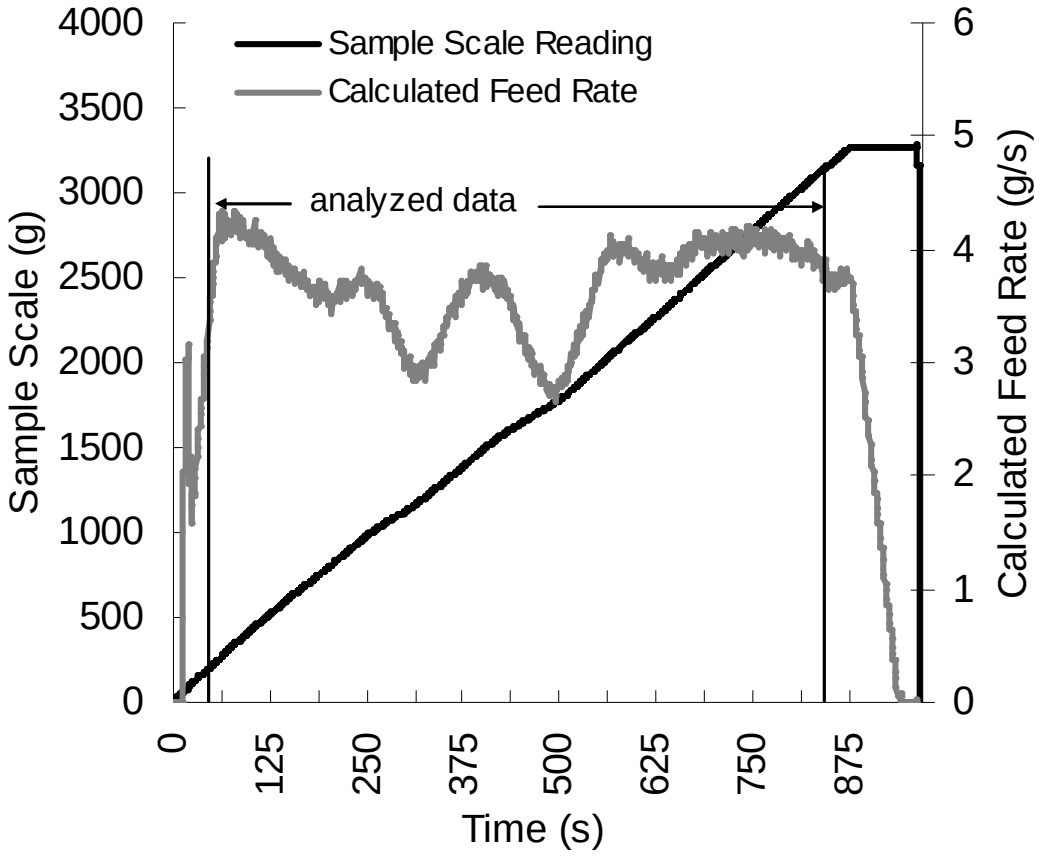

Fig B-17: Assembly 3 Rate Testing 20%/20%/50 lpm

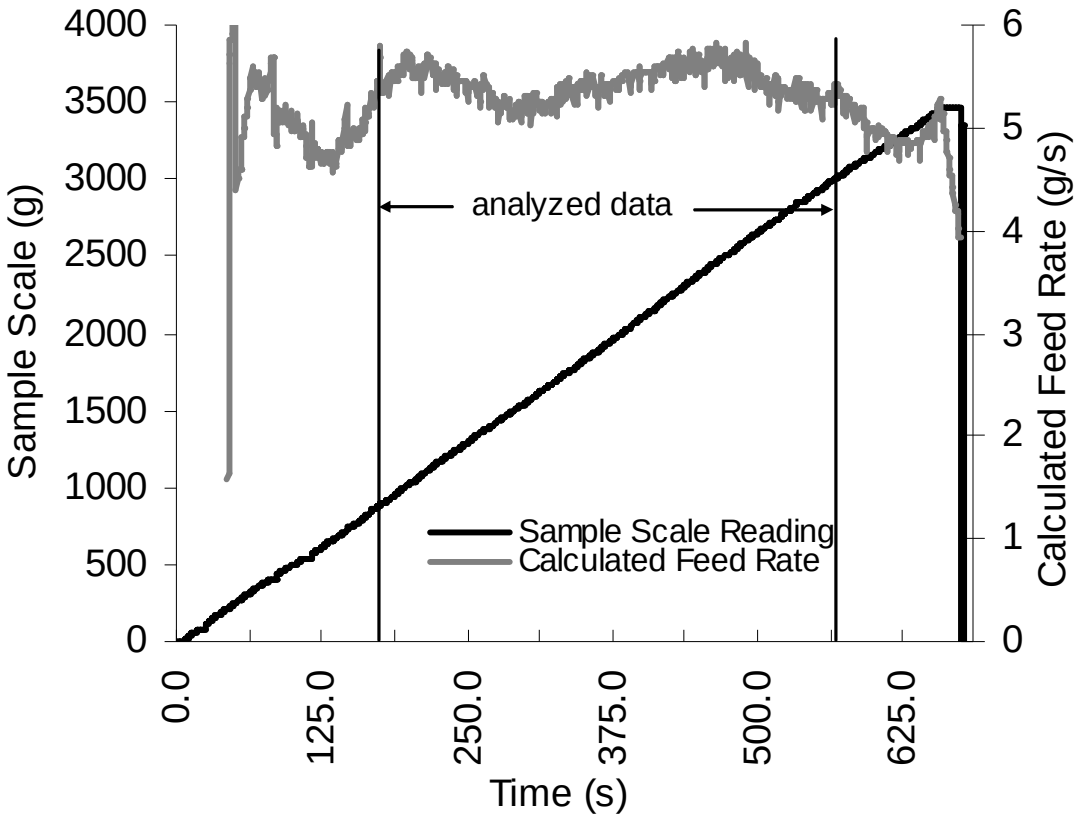

Fig B-18: Assembly 3 Rate Testing, 25%/25%/50 lpm

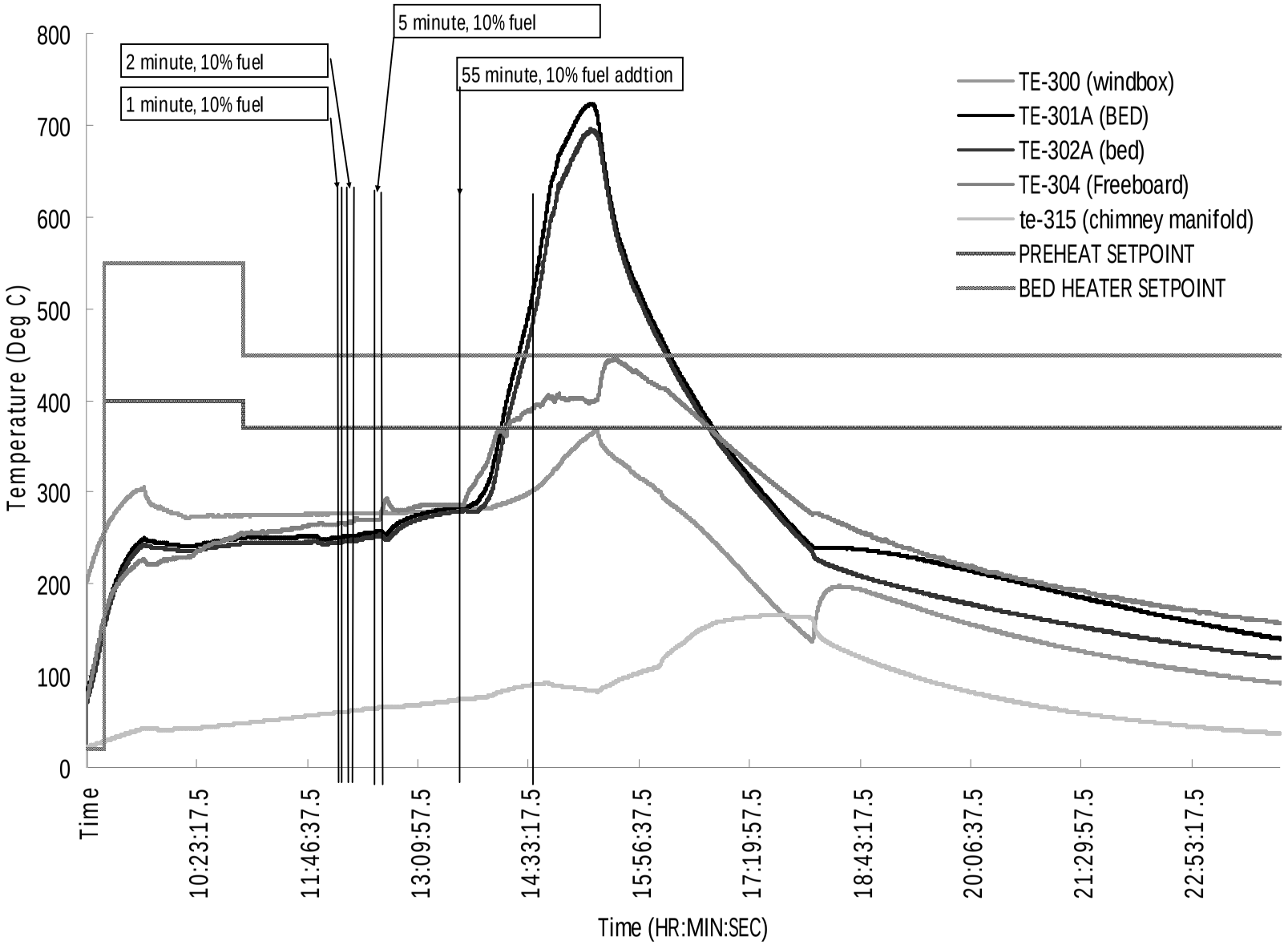

Fig. B-19: FBG Hot Commissioning Reactor Temperature vs. Time

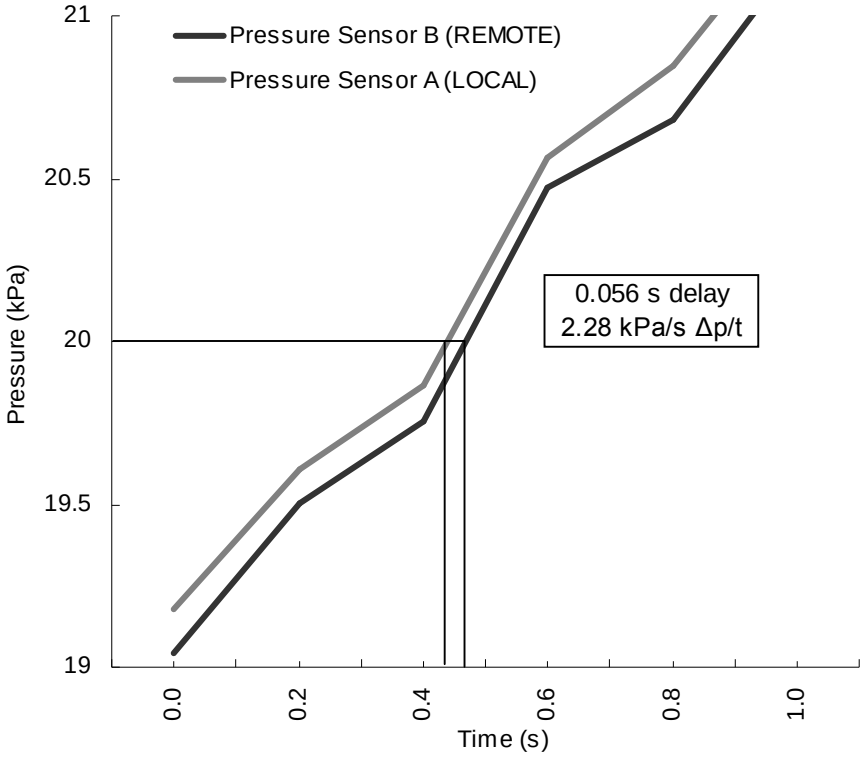

Figure B-20: Pressure sensor reading comparison - local vs. 3 m impulse tube (Trial 1)

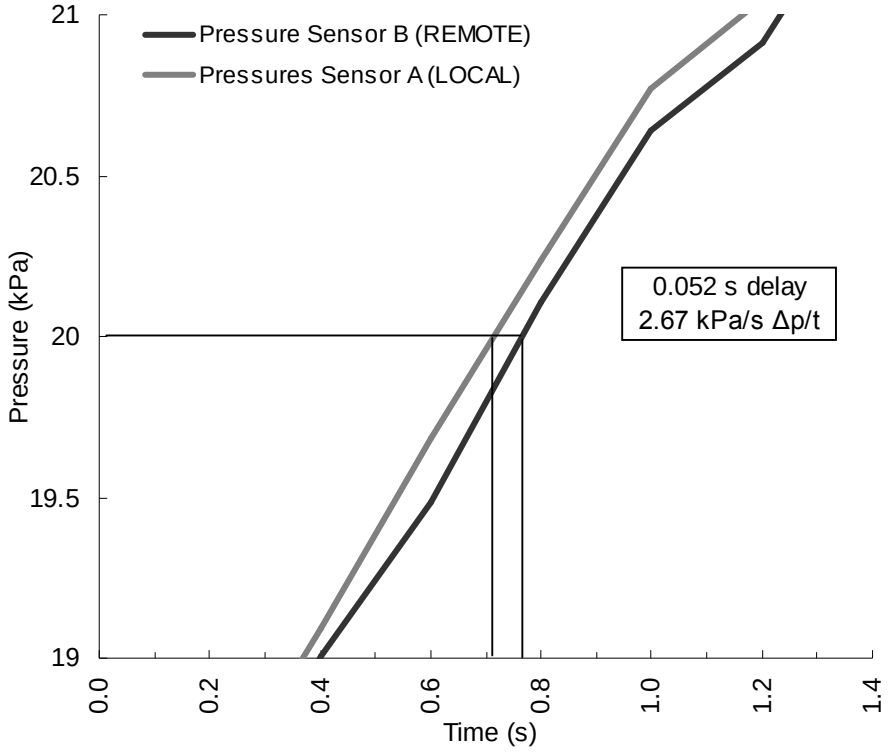

Figure B-21: Pressure sensor reading comparison - local vs. 3 m impulse tube (Trial 2)

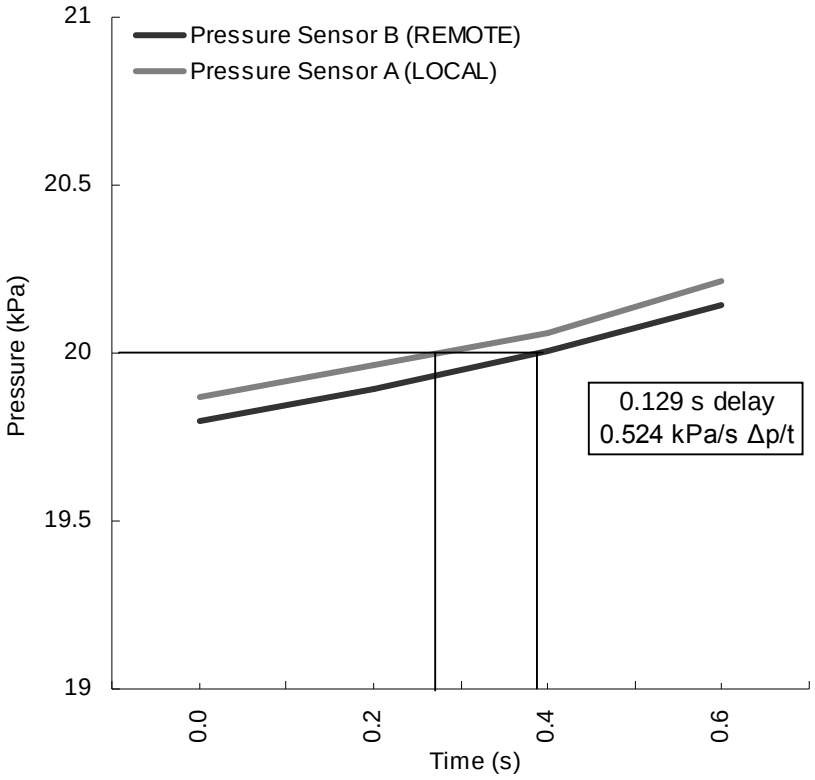

Figure B-22: Pressure sensor reading comparison - local vs. 3 m impulse tube (Trial 3)

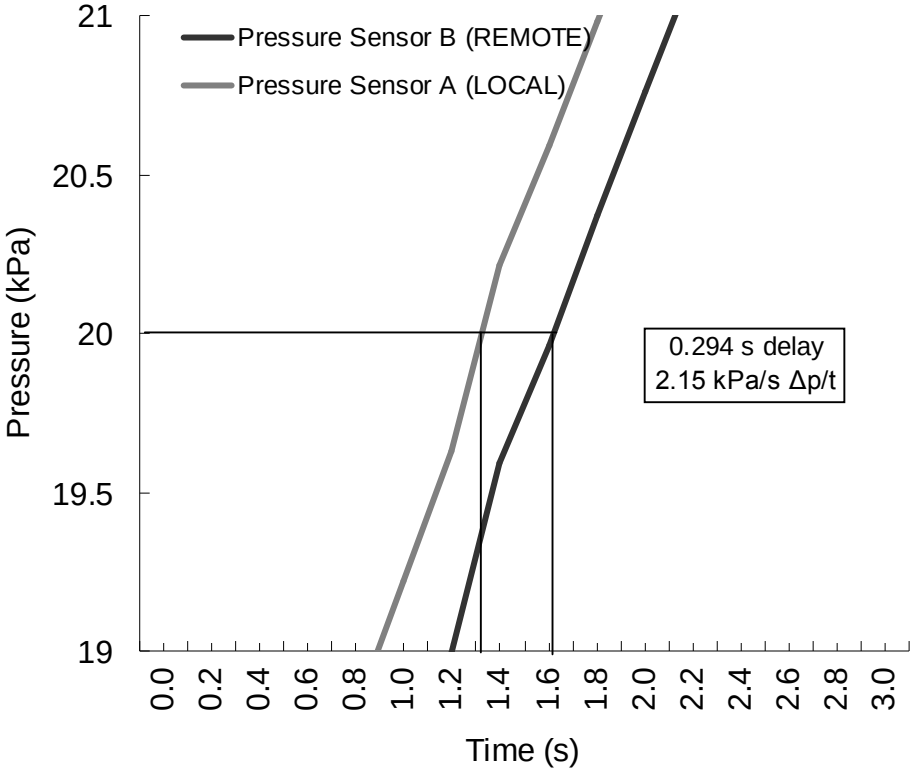

Figure B-23: Pressure sensor reading comparison - local vs. 30 m impulse tube (Trial 1)

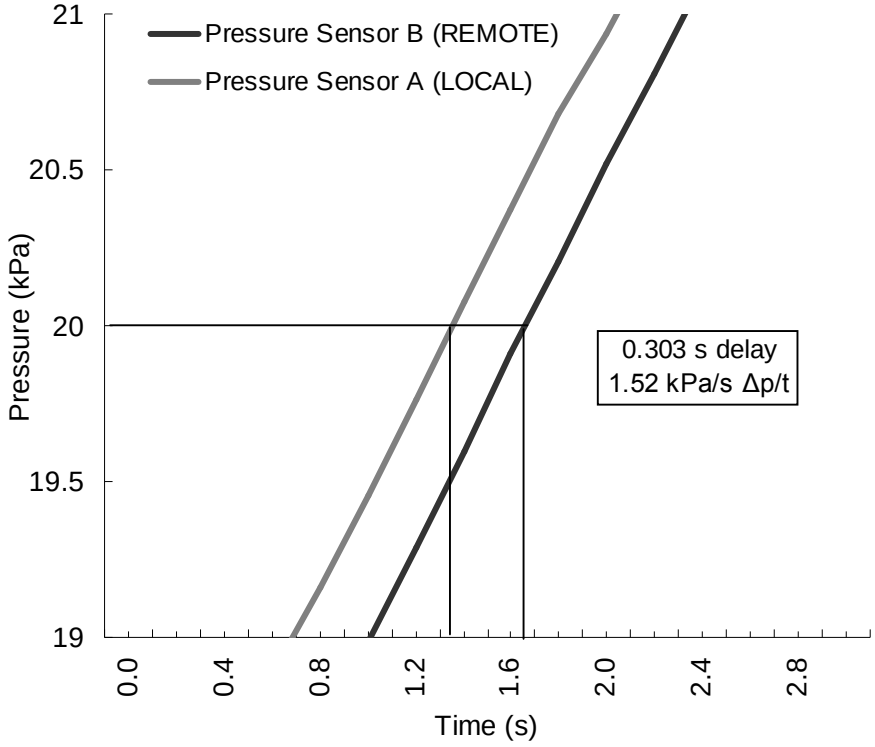

Figure B-24: Pressure sensor reading comparison - local vs. 30 m impulse tube (Trial 2)

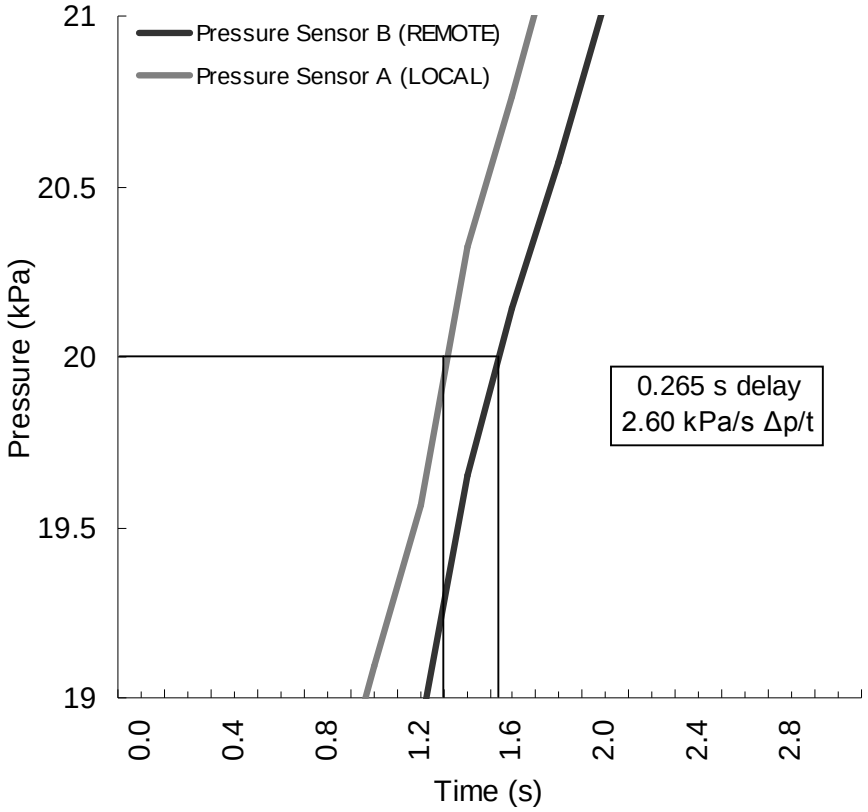

Fig.B-25. Pressure sensor reading comparison - local vs. 30 m impulse tube (Trial 3)

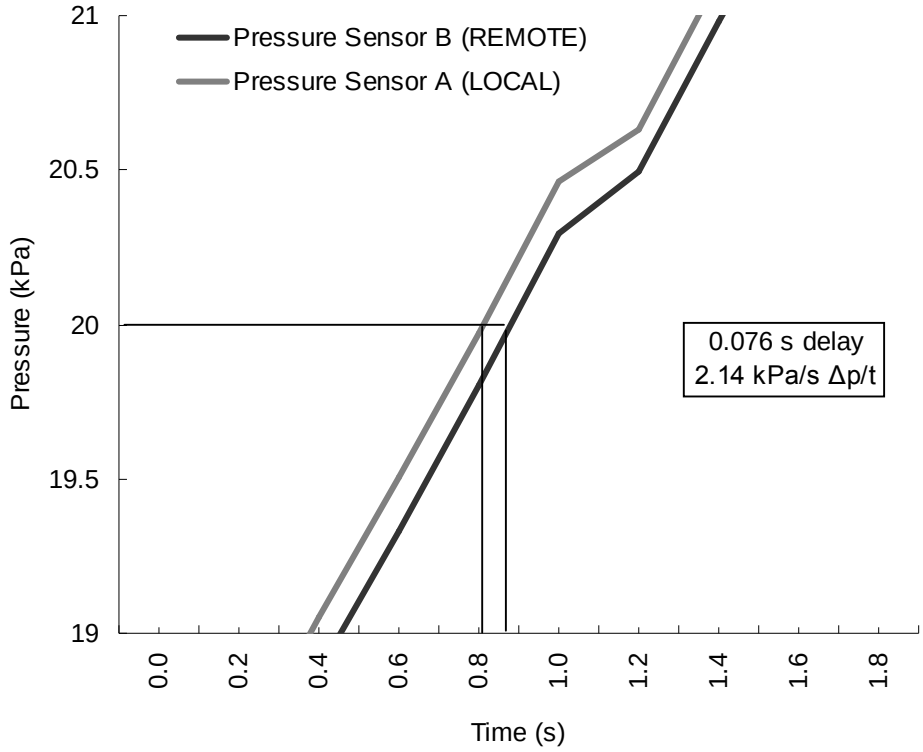

Figure B-26. Pressure sensor reading comparison - local vs. 0 m impulse tube and filter (Trial 1)

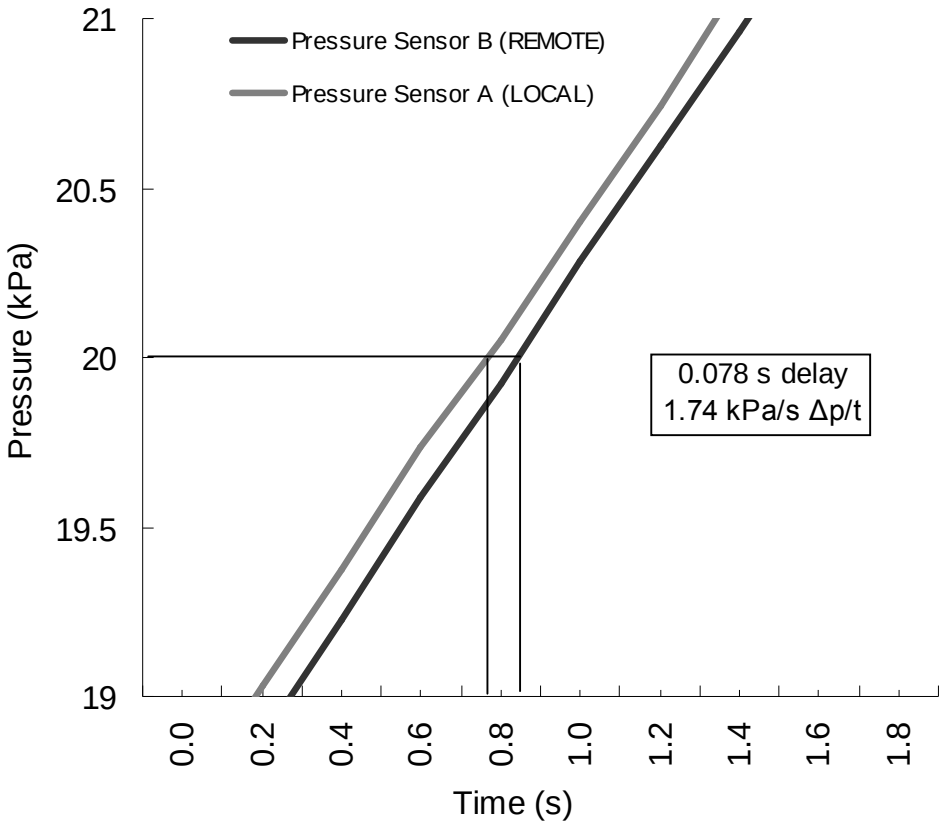

Figure B-27. Pressure sensor reading comparison - local vs. 0 m impulse tube and filter (Trial 2)

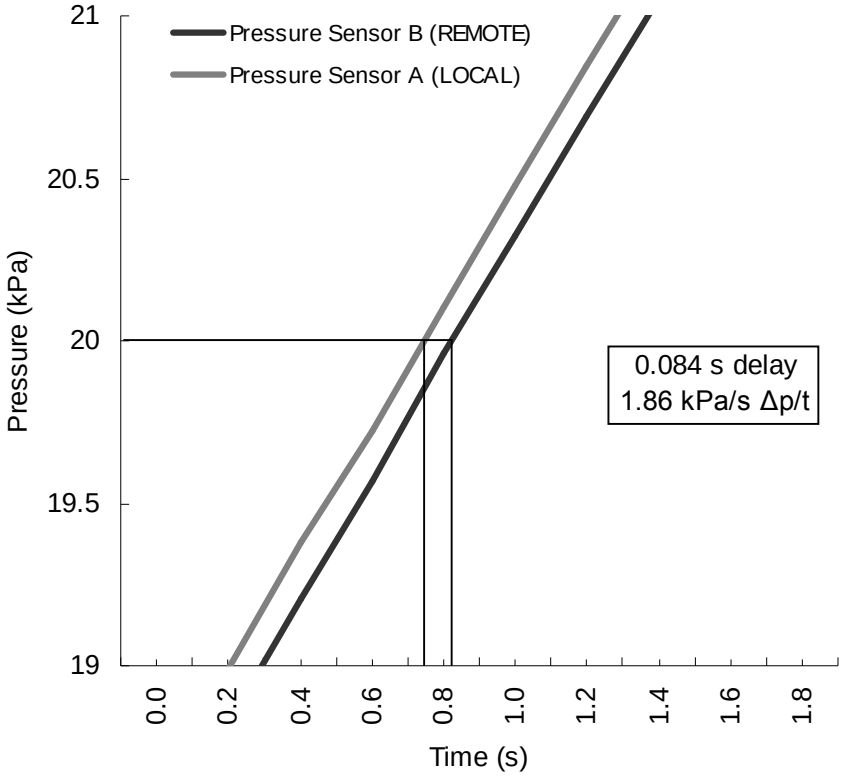

Figure B-26. Pressure sensor reading comparison - local vs. 0 m impulse tube and filter (Trial 3)

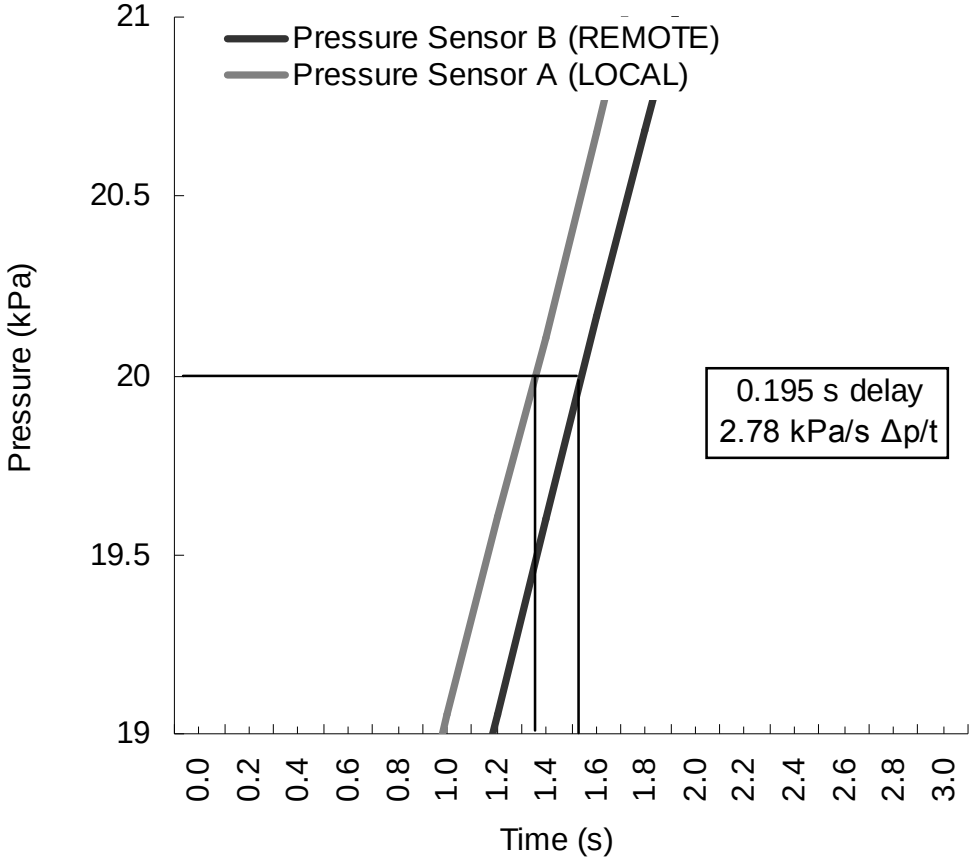

Fig. B-29. Pressure sensor reading comparison - local vs. 3 m impulse tube and filter (Trial 1)

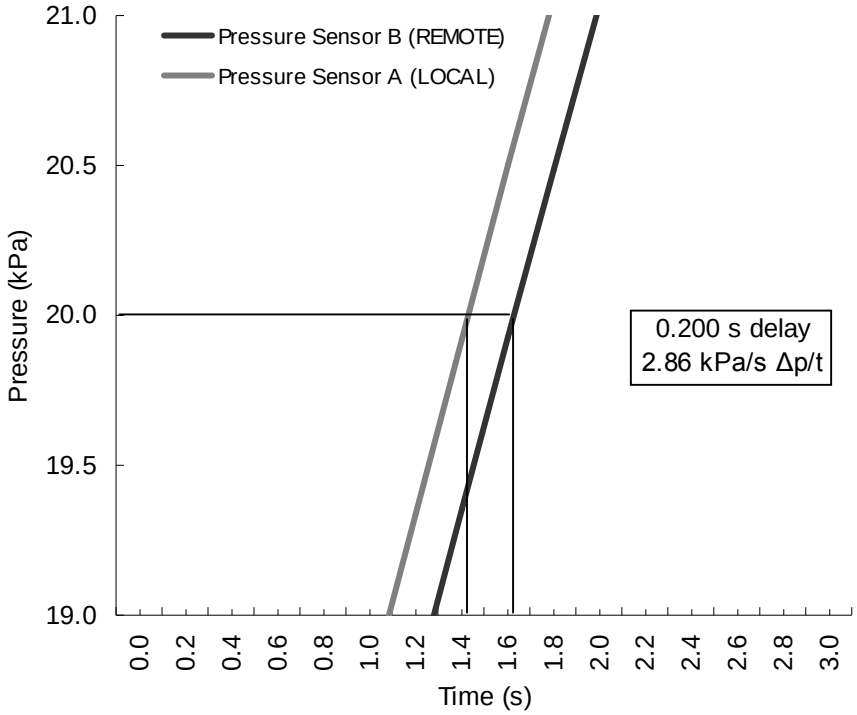

Figure B-30. Pressure sensor reading comparison - local vs. 3 m impulse tube and filter (Trial 2)

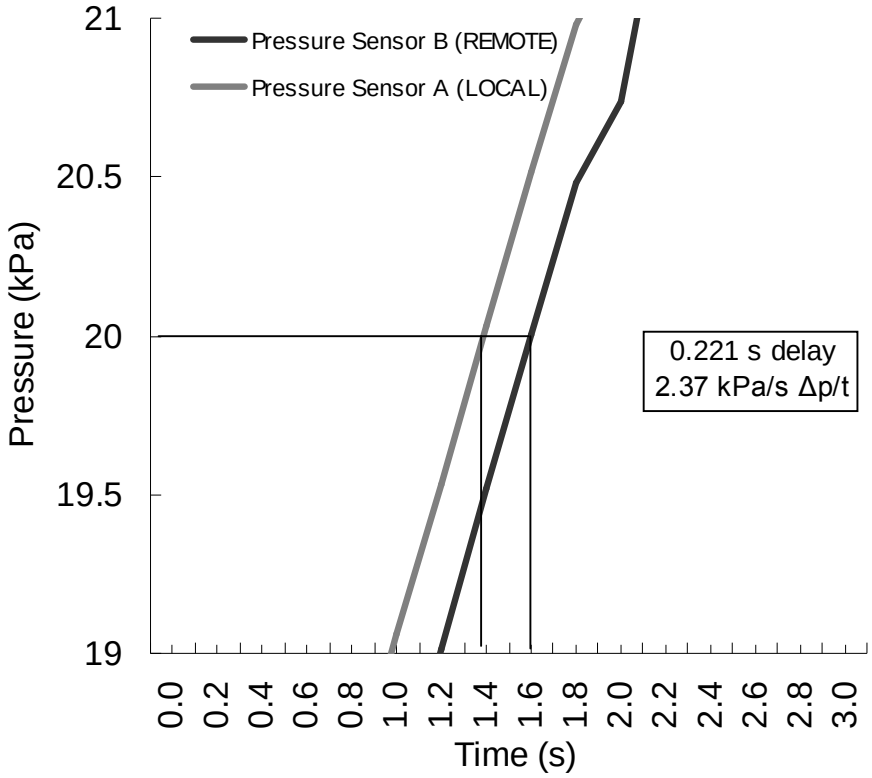

Fig. B-31. Pressure sensor reading comparison - local vs. 3 m impulse tube and filter (Trial 3)

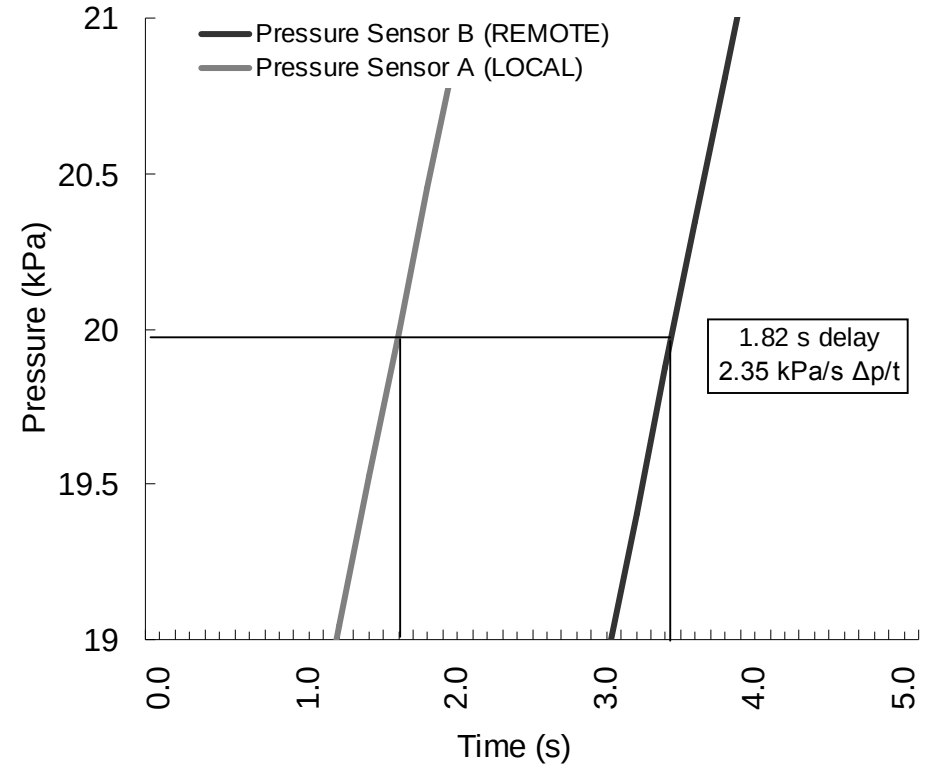

Figure B-32. Pressure sensor reading comparison - local vs. 30 m impulse tube and filter (Trial 1)

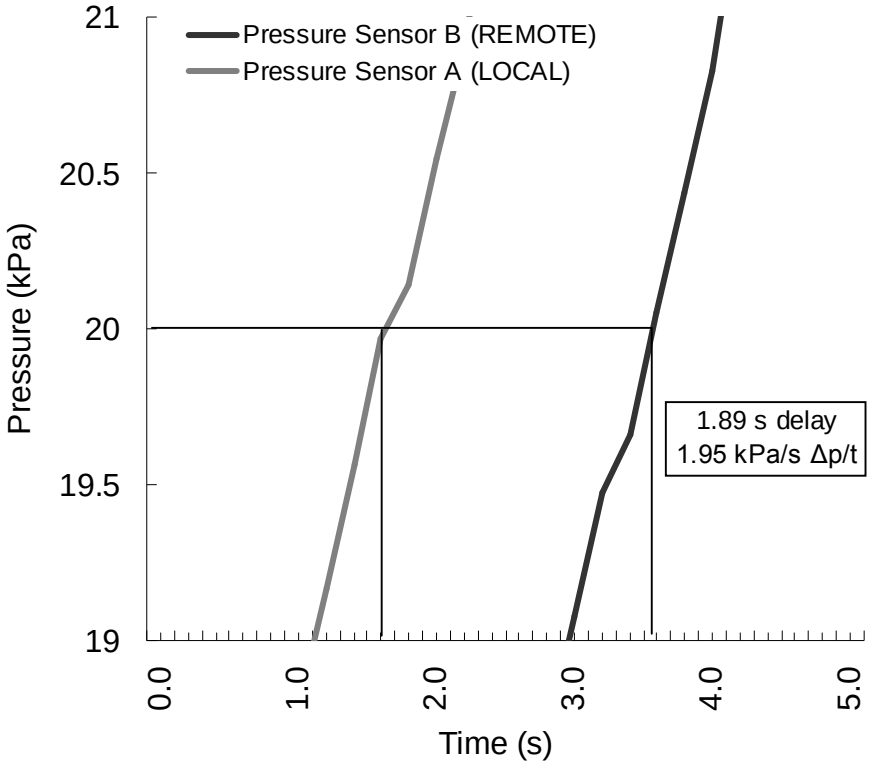

Fig. B-33. Pressure sensor reading comparison - local vs 30 m impulse tube and filter (Trial 2)

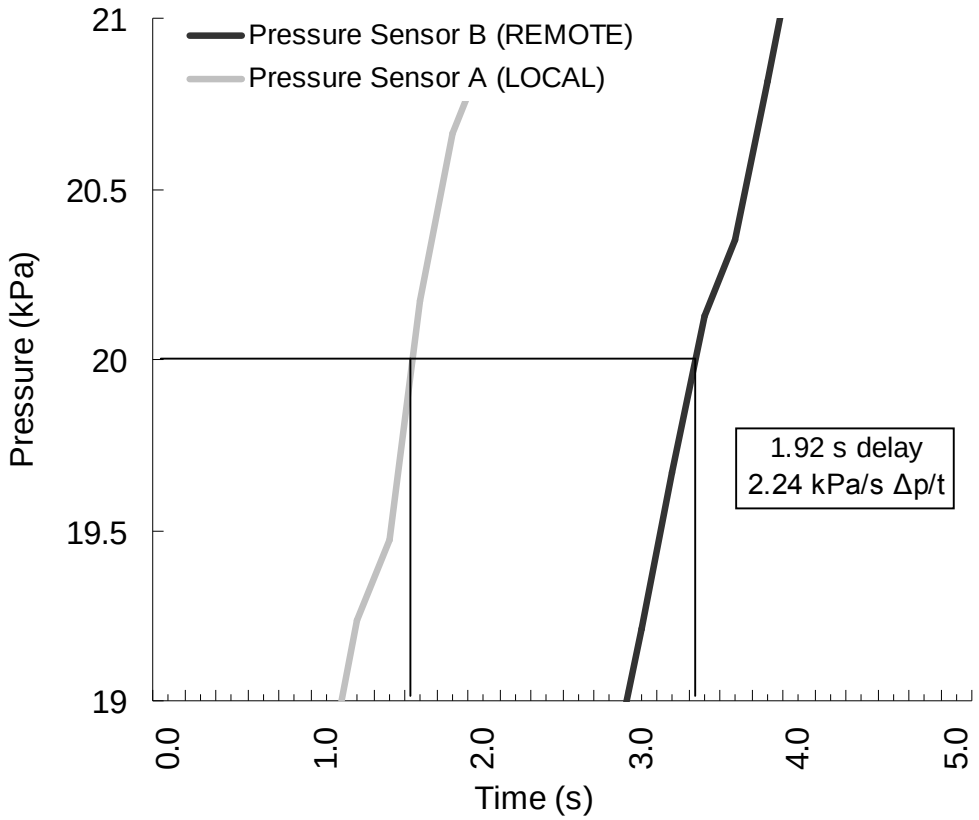

Fig. B-34. Pressure sensor reading comparison - local vs. 30 m impulse tube and filter (Trial 3)

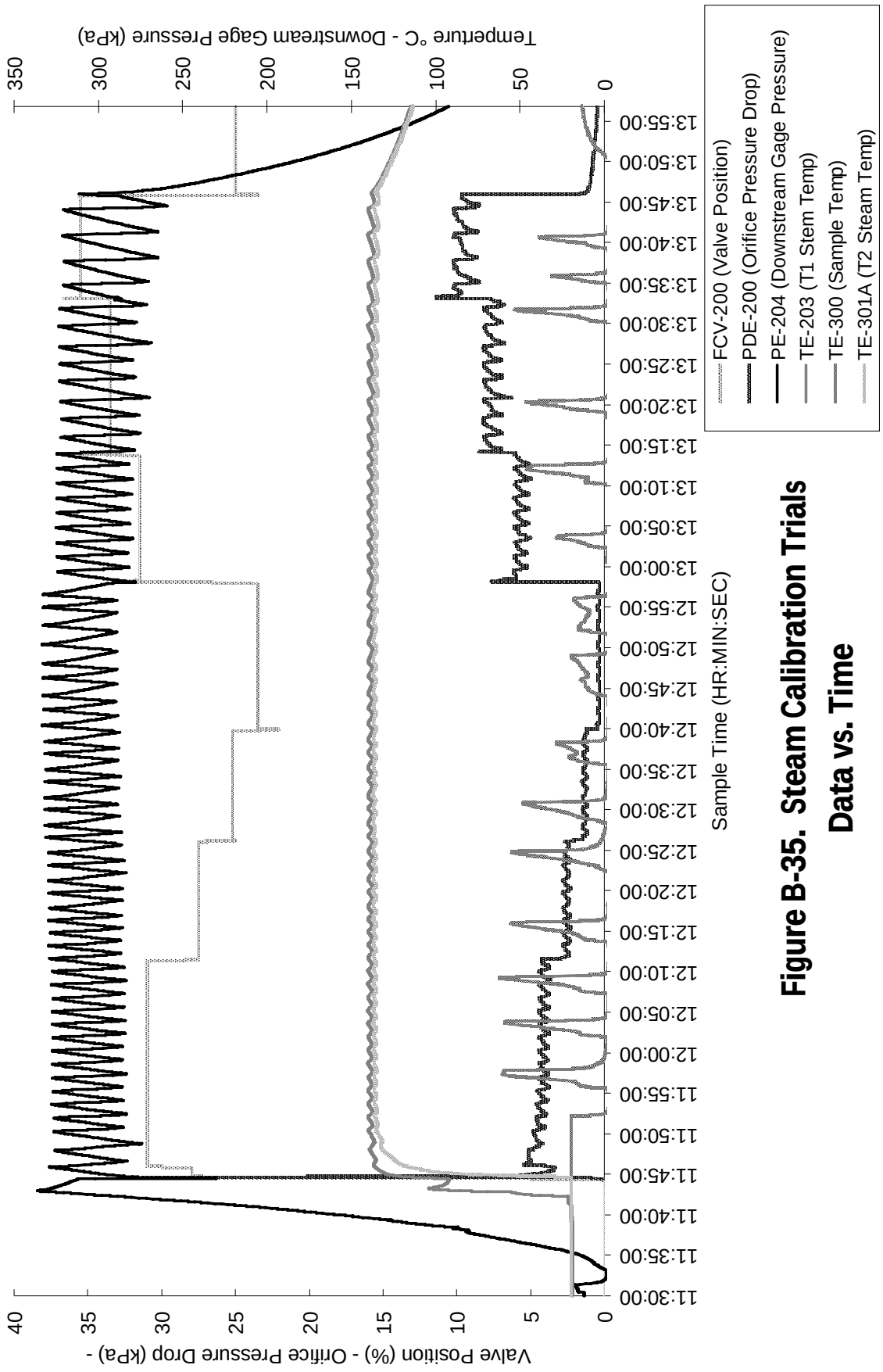

Figure B-35. Steam Calibration Trials Data vs. Time

APPENDIX C - TABULATED DATA RESULTS

Tabulated data including statistical analysis provided to substantiate conclusions and assessments of statistical data. Steam calibration data provided to illustrate complexity of optimization procedure, and substantiate validity of optimized system constants.

Table C-1: Feed System Assembly 1 TestingStatistical Analysis							
Conveyor Speed	5%	10%	15%	20%	25%	50%	100%
Mean Flowrate	0.77	1.92	2.94	3.67	4.80	9.48	19.67
Standard Error	0.01	0.02	0.04	0.04	0.06	0.09	0.06
Median	0.60	1.56	2.37	3.23	3.96	8.79	19.60
Standard Deviation	0.69	1.25	1.71	1.76	2.22	1.78	0.94
Range	5.98	6.76	8.03	7.64	7.66	6.48	6.16
Minimum	-1.79	0.29	0.44	1.28	1.88	6.06	17.18
Maximum	4.18	7.05	8.47	8.93	9.54	12.54	23.33
Count	7554	3434	2191	1674	1351	432	220

Table C-2: Feed System Assembly 2 Testing/Statistical Analysis					
Speed in %FS (150mm conveyor)	5	10	15	20	25
Speed in %FS (50mm conveyor)	5	10	15	20	25
Mean	0.80	1.91	2.90	3.78	5.37
Standard Error	0.00	0.00	0.01	0.01	0.01
Median	0.84	1.94	3.01	3.89	5.43
Mode	1.05	1.92	2.13	4.43	5.49
Standard Deviation	0.32	0.12	0.36	0.49	0.21
Skewness	-0.15	-1.38	-1.16	-0.42	-1.27
Range	1.36	0.77	1.49	1.94	1.34
Minimum	0.18	1.48	1.88	2.65	4.46
Maximum	1.55	2.25	3.37	4.60	5.80
Sum	6773	5256	5076	4728	4762
Count	8495	2751	1751	1251	886

Table C-3: Feed System Assembly 2 Speed Ratio Comparison Statistical Analysis		
Speed in %FS (150mm conveyor)	20	20
Speed in %FS (50mm conveyor)	20	30
Speed Ratio(50mm%:150mm%)	1	1.5
Mean	3.78	4.10
Standard Error	0.01	0.04
Median	3.89	3.78
Mode	4.43	3.67
Standard Deviation	0.49	1.40
Skewness	-0.42	1.95
Range	1.94	5.73
Minimum	2.65	1.46
Maximum	4.60	7.19
Sum	4728	6161
Count	1251	1501

Table 3: Assembly 3 Test Results Statistical Analysis					
Conveyor Speed	5	10	15	20	25
Mean	0.80	1.75	2.92	3.70	5.44
Standard Error	0.01	0.00	0.01	0.01	0.01
Median	0.80	1.75	3.00	3.79	5.44
Mode	0.79	1.42	2.96	4.02	5.50
Standard Deviation	0.22	0.29	0.29	0.39	0.16
Sample Variance	0.05	0.08	0.08	0.15	0.02
Range	1.31	1.41	1.44	1.68	0.78
Minimum	0.12	1.07	2.05	2.65	5.04
Maximum	1.43	2.48	3.49	4.33	5.82
Sum	1116	5968	6142	5925	4354
Count	1401	3401	2101	1601	801

Table C-5: Steam Calibration Tests Data and Results

			trial1	trial2	trial3	trial4	trial5	trial6	trial7	trial8	trial9	trial10	trial 11	trial 12	trial 13	trial 14	trial 15
Property	Symbol	Units															
orifice diameter	d	meters	0.003556	0.003556	0.003556	0.003556	0.003556	0.003556	0.003556	0.003556	0.003556	0.003556	0.003556	0.003556	0.003556	0.003556	0.003556
Orifice Pressure Drop (SI)	Δp	Pa	4080	4122	4013	2528	2576	1310	1313	396	409	5769	5647	7662	7587	9481	9745
Steam Density	ρf2	kg/m3	2.195	2.195	2.195	2.195	2.195	2.195	2.195	2.195	2.195	2.195	2.195	2.195	2.195	2.195	2.195
Diameter Ratio	β	none	0.28	0.28	0.28	0.28	0.28	0.28	0.28	0.28	0.28	0.28	0.28	0.28	0.28	0.28	0.28
upstream pipe diameter	D	meters	0.0127	0.0127	0.0127	0.0127	0.0127	0.0127	0.0127	0.0127	0.0127	0.0127	0.0127	0.0127	0.0127	0.0127	0.0127
Discharge Coefficient*Expansion Factor	C*ε2	none	0.834	0.834	0.834	0.834	0.834	0.834	0.834	0.834	0.834	0.834	0.834	0.834	0.834	0.834	0.834
Upstream Steam Temp.	T1	degC	139	139	139	139	139	139	139	139	139	139	139	138	139	139	139
Dowstream Steam Temp.	T2	degC	136	136	136	136	136	137	136	136	136	136	136	136	136	136	135
Calculated Flowrate	qm	kg/sec	0.00111	0.00112	0.00110	0.00088	0.00088	0.00063	0.00063	0.00035	0.00035	0.00132	0.00131	0.00152	0.00152	0.00169	0.00172
Final Sample Mass	-	grams	984.7	1100.9	1044.8	1109.8	1028.9	1080.9	1207.3	1252.4	1180.5	1195.7	1230.6	1212.5	1187.3	1475.5	1444.7
Initial Sample Mass	-	grams	858.4	963.3	913.5	973.9	899.5	962.5	1085.6	1123.6	1087.9	1101.6	1090.4	1072.8	1050.7	1340.0	1294.5
Sample Time	t	Seconds	101.4	118.5	116.8	149.8	140.9	176.6	184.4	295.3	264.2	75.4	109.4	93.8	94.0	83.5	91.7
Sample Flowrate	qms	kg/sec	0.00125	0.00116	0.00112	0.00091	0.00092	0.00067	0.00066	0.00044	0.00035	0.00125	0.00128	0.00149	0.00145	0.00162	0.00164
Calibration Error		%	10.8%	3.8%	1.9%	3.5%	3.8%	6.0%	4.4%	20.6%	0.4%	5.9%	2.1%	2.3%	4.4%	4.4%	4.9%

APPENDIX D - SAMPLE CALCULATIONS

Sample calculations are provided to back up statements regarding typical results, indicated in the body text.

[D-1] Flow Coefficient and Expansion Factor calculation:

$$q_m = \frac{\pi}{4} \times C \times \varepsilon_2 \times d^2 \times \sqrt{\frac{2 \times \Delta p \times \rho_{f2}}{1 - \beta^4}}$$

Where:

q_m	Mass Flow Rate	(kg/second)
C	Discharge Coefficient	(dimensionless)
ε_2	Expansion Factor (downstream)	(dimensionless)
D	Upstream Pipe Diameter	(meters)
Δp	Orifice Pressure Drop	(Pascals)
ρ_{f2}	Fluid Density after Orifice	(kg/m^3)
β	Ratio of diameters d/D	(dimensionless)
d	Orifice Diameter	(meters)

ρ_{f2} being derived from standard steam Tables using P2, and T_2, where:

P_2	Static (Downstream of orifice) Pressure of Fluid	(Pascals)
T_2	Temperature of Fluid (Downstream of orifice)	(degrees Kelvin)

Trial 1:

1. Calculate discharge coefficient (C) and expansion factor (ε_2) based on known system constants and measured values.

Orifice diameter (d) = 0.0036 m

Pipe I.D. (D) = 0.012675 m

$$\beta = \frac{d}{D} = \frac{0.0036}{0.012675} = 0.28$$

mean pressure drop across orifice during trial period (Δp) = 4080 Pa

Sample Collected = 0.126 kg

Sample time = 101.4 seconds

$$qm = \frac{samplemass(kg)}{sampletime(\sec)} = \frac{0.126kg}{101.4\sec} = 0.00125kg/\sec$$

Local Atmospheric Pressure = 95.6 kPaa

Downstream steam pressure = 303.23 kPag = 303.2+95.6 (kPaa) = 398.8 kPaa

Steam Density (From steam Tables for saturated steam using 398.8 kPaa) = ρ=2.156 kg/m3

Rearranging equation above:

$$C \times \varepsilon_2 = qm \times \frac{4}{\pi} \times \frac{1}{d^2} \times \sqrt{\frac{1-\beta^4}{2 \times \Delta p \times \rho_{f2}}} = 0.00125 \times \frac{4}{\pi} \times \frac{1}{(0.0036)^2} \times \sqrt{\frac{1-(0.28)^4}{2 \times 4080 \times 2.156}} = 0.923$$

2. The next step in the calibration procedure is to use this composite factor to recalculate the flow for each additional sample.

3. Next the error between the calculated value and the measured value is determined.

4. Finally, the composite system factor is adjusted (optimized) to achieve the absolute minimum error between calculated and measured values.

[D-2] Valve Coefficient Calculation

Steam flow = 4.5 kg/hour, p_i = 300 – 900 kPaa (use 480 kPaa), po = 107 kPaa (~10 kPag + ~97 kPaa (atmospheric pressure)

$$C = \frac{7.21 \times 4.5 kg/hour}{\sqrt{(480 kPaa - 107 kPaa) \times 107 kPaa}}$$, Cv = 0.16

[D-3] VFD Full Speed Range Calculations

$$0.05 \times FS_{\max}.for.low.end.of.VFD = 0.05 RPM.low.conveyor.output.range \Rightarrow FS_{\max} = 1 RPM$$

$$2.00 \times FS_{\min}.for.high.end.of.VFD = 0.25 RPM.high.conveyor.output.range \Rightarrow FS_{\min} = 0.125 RPM$$

[D-4] Temperature abatement using air filled impulse tubing

$$\frac{(T - T_\infty)}{(T_o - T_\infty)} = \frac{1}{\cosh\left(\sqrt{\frac{4 \times h \times D_1}{12 \times K \times (D_1^{\,2} - D_2^{\,2})}} \times L \times 6.26\right)}$$

where:

T = temperature of point of interest on tubing (°C)

T_∞ = temperature of ambient air (°C)

T_o = temperature of pressurized (hot) fluid (°C)

L = length of tubing (m)

h = heat transfer rate from tube to still air (assumed to be 8.18 W/m^2*K)

K = coefficient of heat transfer in W/m^2*K

D_1 = outside diameter of tube (m)

D_2 = inside diameter of tube (m)

For Inconel 625, K = 31.8, and for 316 SS, K = 53.4

(From Kane, 2002, converted to S.I. units by Author)

Restating formula according to T:

$$T = \frac{(T_o - T_\infty)}{\cosh\left(\sqrt{\frac{4 \times h \times D_1}{12 \times K \times (D_1^{\,2} - D_2^{\,2})}} \times L \times 6.26\right)} + T_\infty$$

Now, using the following criteria:

T_∞ = 20°C

T_o = 850°C

L = 0.1m

h = 8.18 W/m^2*K

K = 53.4 W/m^2*K

D_1 = 0.009525m

D_2 = 0.00635m

$$T = \frac{(850 - 20)}{\cosh\left(\sqrt{\frac{4 \times 8.18 \times 0.009525}{12 \times 53.4 \times ((0.009525)^2 - (0.00635)^2)}} \times 0.1 \times 6.26\right)} + 20 = 252.7^\circ C$$